Reviewer Comments

A.J.B. Smith (Referee) bertuss@uj.ac.za Received and published: 5 December 2017

Dear Editor – Solid Earth This letter serves to summarize my review of the manuscript entitled "Sedimentary mechanisms of a modern banded iron formation on Milos Island, Greece", submitted by E Chi Fru et al. for possible publication in Solid Earth.

Reviewer: The manuscript documents Quaternary Fe-rich chemical sediments from the Cape Vani sedimentary basin (CVSB) on Milos Island, Greece. The Fe-rich units show a close associated with Mn-rich units and two subtypes were identified: i) microfossil rich iron formation (IF); and ii) non-fossiliferous IF. The IFs also occur over a limited lateral extent. Geochemical and mineralogical data suggest that these units are very similar to Precambrian IFs and could potentially be proxies to the latter. Depositional conditions are also proposed by the authors, which include tectonics, biological activity, changing redox and abiotic Si precipitation. Although there is some overlap with their previous publications in Nature Communications (2013) and Geobiology (2015), the authors state that a major new addition is presenting plausible mechanisms for the temporal and spatial separation between Fe and Mn deposition in the CVSB.

It must be noted upfront that this manuscript covers a fascinating and important geological occurrence, namely a Quaternary, spatially limited IF. With the majority of IF deposited during the Precambrian and, more specifically, prior to 2 Ga, this occurrence shows how unique and isolated conditions can drastically influence localized geology. Further documentation and more field descriptions of this occurrence is therefore always welcome in the literature. The authors should also be commended on the level into which they attempt to present a depositional model for the units, something which is often not even attempted in manuscripts on IFs. The inclusions of the importance of faulting and tectonics is also a great addition into the model, something which often cannot be done in detail on older, Precambrian IF occurrences. The authors also take special care to address a multitude of possible paleoenvironmental conditions, looking at the past and comparing it to the present, and should be complimented on such an even-handed approach. The conclusion on the cause for the banding (main conclusion 5) being caused by episodic hydrothermal intensification is also an important one, and one that I believe is also supported by evidence from Precambrian IFs.

Response: We thank the reviewer (Dr A.J.B Smith) immensely for the enormous time and effort put in reviewing our manuscript. His attention to detail has transformed both the quality of the complex interpretations, better bringing out the remarkable similarities the enigmatic Milos IF share with the Precambrian BIFs and their implications for understanding the past. Below we address his critical comments point by point. Attached to this document is a PDF file named, supplement, containing the manuscript with the changes requested by the reviews in red.

Point 1

Reviewer: There is inconsistent use of element names and symbols in the manuscript (e.g. line 233 uses "iron" and "Mn" in the same line). The authors should be consistent in their use of either

names or symbols for elements. Also, the use of hyphens are also inconsistent and should carefully be revised and updated to ensure format and spelling consistency across the manuscript.

Response: We have amended the text accordingly.

Point 2

Reviewer: It is important that the authors include, even if briefly, the detail on how the age constraints of the CVSB were determined somewhere in the geological setting of the manuscript.

Response: Age constraints and accompanying references are now given in the introductory paragraph in section 1.1, under the geological setting.

Point 3

Reviewer: The results section on geochemistry (section 3.3; line 461 onwards) contains a lot of interspersed petrography and mineralogy, which I believe is inappropriate. I strongly recommend that the two sets of results be clearly separated and presented in their own result sections. This will also require some reshuffling and/or re-editing of figures to properly fit the order and flow of the revised sections.

Response: We agree that this might be confusing to the reader and have therefore divided section 3.3 into four independent subsections entitled:

3.3.1 Geochemistry of the individual Fe-rich and Si-rich bands
3.3.2 Mineralogy of the individual Fe-rich and Si-rich bands
3.3.3 Hydrothermal versus continental weathering
3.3.4 Redox reconstruction

Point 4

Reviewer: The use of North American Shale Composite (NASC) to normalize the REE data is strange and a bit dated. Most new publications on IFs from the mid-1990s onwards use Post-Archean Australian Shale (PAAS) for IF REE normalization. I would recommend the authors rather use this standard as it would make the data more comparable to other IF publications. In addition, the assessment of true Ce anomalies presented in this paper is also based on Bau and Dulski (1996), wherein they used PAAS as the shale standard for normalization. The Ce anomalies therefore need to be recalculated and replotted using PAAS. I do realize this might not make much of a difference, but for comparative purposes and for accuracy relating to the original publication this should be done.

Response: We agree that some recent papers have used PAAS (Post Archean Australian Shale-Taylor and Mclennan 1985) instead of NASC (North American Shale Composite-Gromet et al., 1984) while others use UCC (Multi Element Normalisation- Taylor and Mclennan 1985) and Chondrite-Normalised REE-Thomson 1982), which are all scientifically valid standards. In the case of our study, NASC was used for two main reasons:

1. The NASC normalization maintains data consistency with the REE data published in our previous papers on the Milos IF ((1) Chi Fru, E., Ivarsson, M., Kilias, S.P., Bengtson, S., Belivanova, V., Marone, F., Fortin, D., Broman, C., and Stampanoni, M.: Fossilized iron bacteria reveal a pathway to the origin banded iron formations. Nat. Comm., 4, 2050 DOI: 10.1038/ncomms3050, 2013. (2) Chi Fru, E., Ivarsson, M., Kilias, S.P., Frings, P.J., Hemmingsson, C., Broman, C., Bengtson, S. and Chatzitheodoridis, E.: Biogenicity of an Early Quaternary iron formation, Milos Island, Greece. Geobiology, 13, 225–44, 2015.

2. There are no scientifically demonstrated discrepancies between the PAAS and NASC.

3. Following the instructions given here, data was normalized to PAAS for comparison with the NASC normalized trends. The results produced the same trend as observed when data are normalized to NASC. See new Figure 14 in the manuscript text, accessible in the attached supplement PDF file. Further explanations are also provided under sections 2.6-2.6.1 in the manuscript supplement text.

Reviewer: To make the REE assessment in this paper even more complete, the authors should also plot Y_{SN} in the REE diagram between Dy and Ho (REY plots) as proposed by Bau and Dulski (1996) to get a more complete pattern and assessment of the REE trends.

Response: Unlike the paper by Bau and Dulski that was focused on REE analysis, the REE analysis performed in this study was conducted specifically to answer specific questions that we had posed, relevant to our study. These include:

1. **What are the redox depositional conditions?** In this revision, we have instead included a new Figure 13C-D, which provides independent support from iron extraction for the reducing depositional conditions displayed by the lack of Ce anomaly, which is critical to this paper than the REY plots.
2. **What was the source of sediments to the basin?** By using the Eu anomaly, coupled to the relationship between LREE and HREE, which produces a unique graphical shape for hydrothermal deposits, we could predict the hydrothermal/volcanic source of sediments, supported by the strong presence of volcanic ash in the Fe-rich bands. This information is further supported by other methods such as the chemical index of alternation (CIA), which shows negligible contribution of land-derived weathered sediments to the deposit.
3. In future work we will strive to give more thought to REY plots, especially if they can help resolve pertinent hypotheses for how the Milos IF formed.

Point 5

Reviewer: The conclusion that the IFs were deposited in reducing conditions in a redox stratified sea/ocean, as indicated in figure 16 and stated in lines 685 to 687, is not currently convincing for the following reasons: 1) The lack of a Ce anomaly is not a definite indicator of reducing conditions. This can be buffered by excess Fe(II) in the system (see classic Eh-Ph diagrams by Brookins as well as Smith et al., 2013, Economic Geology, v. 108: 111-134). 2) The Ce anomaly calculations appear to have been done using NASC-normalized REE data instead of PAAS-normalized data. Proposed mechanisms for deeper water anoxia is left for very late in the manuscript, hinging on modern analogues (section 4.2.5), making the lead up at times unconvincing. Some of these arguments are also based on the interpretation of geochemical evidence to suggest

anoxia, when micro-oxic conditions, in my opinion, cannot be completely ruled out. A more even handed approach regarding the Eh conditions throughout the manuscript, and taking into account the redox buffering effect between Fe2+ and Mn2+, is likely required throughout. Micro-aerophilic bacteria also likely played a larger role than currently suggested by the authors when considering how recently deposition occurred and how deep the water could have been (well below wave base). I do believe the authors have generally done a good job regarding Eh conditions in their depositional model and that all the necessary information is throughout the manuscript, but in my opinion they are only 70% there in making it convincing and even handed.

Response: We appreciate the detailed insights and agree that although widely used, Ce anomalies have to be interpreted with caution. For this reason, we have analysed the same set of samples by the sequential iron extraction approach; a widely applied proxy for reconstructing Paleo-redox. These data presented in the new Figure 13C-D and supported by the references below and several others in the public literature, confirm the inferred anoxic depositional conditions indicate by the Ce anomalies. Comparative normaliztion with either the PAAS or NASC standards, produced the same outcome, in agreement with the interchageable use of both standards. More information on the analysis can be found under sections 2.6-2.6.1 and in Figure 14.

1. Poulton, S.W., and Canfield, D.E.: Development of a sequential iron extraction procedure for iron: implications for iron partitioning in continentally derived particles. Chem. Geol. 2014, 209–221, 2005.
2. Poulton, S.W. and Canfield, D.E.: Ferruginous conditions: A dominant feature of the ocean through Earth's history. Elements. 7, 107–112, 2011.

Point 6

Reviewer: The formation of the granular Fe-rich beds (lines 456-459) is not satisfactorily addressed. There has to be morphological evidence within the granules for the authors to be able to commit to either a sedimentary or supergene formational mechanism.

Response: This statement resonates with the opinion provided the anonymous reviewer. We have therefore deleted the paragraph regarding GIF.

Point 7

Reviewer: To me, there is some confusion regarding deep ocean anoxia relative to hydrothermal venting in the depositional model (lines 995-999). This needs to be clarified in the discussion and lead up. Was deep water anoxia semi-permanent or did the venting play a role in establishing it? Here it appears that anoxia was semi-permanent, but the motivation needs to be better conveyed in the lead-up.

Response: The new Figure 13C-D, which reports on redox reconstruction by sequential iron extraction, has been discussed extensively in the manuscript. This proxy is perhaps the most widely accepted tool for reconstructing paleoredox depositional conditions (i.e., oxic, anoxic but ferruginous and anoxic but euxinic environments. See references given under point 5 above. The proxy works on the basis that it is capable of delineating the

redox conditions in the water column beneath which sediments form. We have discussed a number of procedures in the paper by which this anoxia could have developed in the CVSB. The understanding is that there is a combination of the basin being cut off, either in a crater environment like in the adjacent Kolombo volcano and a combination of hydrothermal activity and CO_2 accumulation, creating permanent bottom water anoxia. We have explored all these different pathways in the manuscript. However, what has become more certain with the sequential iron extraction data is that deposition occurred under severe anoxic conditions, which could have been the results of numerous processes. These processes will gradually become evident as our work on this formation expands and as other researchers become genuinely interested in sampling and exploring its formation mechanisms.

Geochemical REE evidence has shown that Fe was sourced from hydrothermal fluids, and deposition took place beneath anoxic waters (see above). This combined with geological and mineralogical evidence for example the presence of tridymite etc, in Fe-rich layers of the NFIF), indicate that oxidation of Fe(II) in the NFIF corresponded closely in time with major Basin 3-scale intense, possibly episodic, submarine volcanism and hydrothermal activity. We suggest that submarine volcanism/hydrothermalism were responsible for generating a dynamic Basin 3-scale chemocline separating anoxic/suboxic ferruginous deep waters from oxic shallow waters. This is explained by the notion that seawater redox state in a basin with restricted circulation and intense submarine volcanism/hydrothermalism like Basin 3, may be lowered by an enhanced flux of hydrothermally derived reductants, like reduced Fe and Mn, H_2 and even CO_2-induced stratification, as discussed extensively for various hydrothermal vent fields in the Hellenic Volcanic Arc. These processes would have overpowered the oxidizing potential of seawater (Bekker et al., 2014).

The oxidation of Fe(II) at and below the chemocline, by microaerophilic chemolithoautotrophs and strict anaerobic photoautotrophic Fe(II) oxidation are favored as potential modes of Fe(III)(oxyhydr)oxide precipitation in the NFIF. However, at the current time, such evidence is lacking for the NFIF. We therefore choose not to delve into speculation. One approach had been to use fossil lipid biomarkers, but consistent with the poor organic content of iron formations, this approach proved not to be very successful. Moreover, unlike the MFIF, the NFIF is microfossil-poor, leaving the question of microbial contribution to the deposition of the NFIF wide-opened. On-going stable Fe isotope analysis may help solve this problem. However, Fe isotopes may not be able to differentiate biological activity from abiological processes, because in some cases both can fractionate Fe equally. Nonetheless, our paper provides an intriguing scenario where Precambrian type-rocks are formed in firmly reconstructed anoxic bottom waters under the modern atmosphere. This is unprecedented. We use a multitude of techniques from REEs, carbon isotopes, Raman analysis, TEM, lipid biomarkers, sequential iron extraction, etc, at a comprehensive scale that is hardly ever seen in one paper, to arrive our conclusions.

Point 8

Reviewer: In the final conclusion (lines 1013-1017) the authors state that "Whether the rocks described here are analogues of Precambrian BIFs or not, and whether the proposed formation mechanisms match those that formed the ancient rocks, is opened to debate." The work here have many similarities to proposed Precambrian BIF depositional models (e.g. Smith et al., 2013; Bekker et al., 2010 and depositional models by Klein and Beukes, Beukes and Gutzmer). The authors should comment on this briefly.

Response: Your comment has been included in the conclusion.

References

1. Bekker, A., Planavsky, N., Rasmussen, B., Krapez, B., Hofmann, A., Slack, J., Rouxel, O. and Konhauser, K., 2014. Iron formations: Their origins and implications for ancient seawater chemistry. In Treatise on geochemistry (Vol. 12, pp. 561-628). Elsevier.
2. Brookins, D.G., 1988, Eh-pH diagrams for geochemistry: Berlin, Springer-Verlag, 176 p.
3. Brookins, D.G., 1989, Aqueous geochemistry of rare-earth elements: Reviews in Mineralogy, v. 21, p. 201–225.
4. Konhauser, K., 2007, Introduction to geomicrobiology: Malden, Blackwell, 425 p.
5. Konhauser, K.O., Hamade, T., Raiswell, R., Morris, R.C., Ferris, F.G., Southam, G., and Canfield, D.E., 2002, Could bacteria have formed the Precambrian banded iron formations?: Geology, v. 30, p. 1079–1082.
6. McCollom, T.M., and Shock, E.L., 1997, Geochemical constraints on chemolithoautotrophic metabolism by microorganisms in seafloor hydrothermal systems: Geochimica et Cosmochimica Acta, v. 61, p. 4375–4391.
7. Smith, A.J., Beukes, N.J. and Gutzmer, J., 2013. The composition and depositional environments of Mesoarchean iron formations of the West Rand Group of the Witwatersrand Supergroup, South Africa. Economic Geology, 108(1), pp.111-134.
8. Taylor SR, McLennan SM (1985) The continental crust: its composition and evolution. Blackwell Scientific Publication, Carlton, 312 p.
9. Gromet PL et al., 1984. The "North American shale composite": Its compilation, major and trace element characteristics. Geochim. Cosmo. Acta 48:2469-2482.
10. Thompson, R.N. (1982) Magmatism of the British Tertiary volcanic province. Scott. J. Geol. 18, 49-107.

Specific Comments:

Abstract

Reviewer: The sentence running from lines 37 to 38 should be rephrased. As it is currently written it does not clearly convey the stratigraphic relationship between the Fe- and Mn-rich units. Is the transition to the Mn-rich formation upwards or downwards? I think rephrasing this as two sentences briefly providing the bottom-up stratigraphy would clear this up.

Response: Rephrased as suggested.

Reviewer: The statements in lines 38 to 41 relating to anoxia might not be completely accurate. Refer to point 6 above.

Response: The statement relating to anoxia is strongly supported by new evidence provided in Figure 13C, in agreement with the lack of Ce anomaly, as discussed above. Also see the extensive discussion on how such anoxic conditions might develop in the CVSB, based on, on-going modern processes that form anoxia along the Hellenic Volcanic Arc. Please kindly check the cited references as they contain valuable information.

Reviewer: The summary of depositional conditions in lines 46 to 48 is too vague and brief. The authors need to take a few more lines and properly summarize their proposed depositional model.

Response: This sentence is given in two parts. The first sentence summarizes the basic Si mineralogy of the two deposits, while the concluding sentence sums up the findings in this study, which are indeed too complex (involving a number of processes) to be laid out completely in the abstract. To attempt to explain each process and how they are linked together is beyond the scope of the abstract, given their complexity. The abstract has been reformatted to read as:

An Early Quaternary shallow submarine hydrothermal iron formation (IF) in the Cape Vani sedimentary basin (CVSB) on Milos Island, Greece, displays banded rhythmicity similar to Precambrian banded iron formation (BIF). Sedimentary and stratigraphic reconstruction, coupled to biogeochemical analysis and micro-nanoscale mineralogical characterization, confirm the Milos IF as a modern BIF analogue. Spatial coverage of the BIF-type rocks in relation to the economic grade Mn ore that brought prominence to the CVSB implicates tectonic activity and changing redox in their deposition. Field-wide stratigraphic and biogeochemical reconstruction demonstrate two temporal and spatially isolated iron deposits in the CVSB with distinct sedimentological character. Petrographic screening suggests the previously described photoferrotrophic-like microfossil-rich IF (MFIF), accumulated on basement andesite in a ~150 m wide basin, in the SW margin of the basin. A strongly banded non-fossiliferous IF (NFIF) sits on top the Mn-rich sandstones at the transition to the renowned Mn-rich formation, capping the NFIF unit. Geochemical evidence relates the origin of the NFIF to periodic submarine volcanism and water column oxidation of released Fe(II) in conditions apparently predominated by anoxia, similar to the MFIF. Raman spectroscopy pairs hematite-rich grains in the NFIF with relics of a carbonaceous material carrying an average $\delta^{13}C_{org}$ signature of ~-25‰. However, a similar $\delta^{13}C_{org}$ signature in the MFIF is not directly coupled to hematite by mineralogy. The NFIF, which post dates large-scale Mn deposition in the CVSB, is composed primarily of amorphous Si (opal-$SiO_2{\cdot}nH_2O$) while crystalline quartz (SiO_2) predominates the MFIF. An intricate interaction between tectonic processes, changing redox, biological activity and abiotic Si precipitation are proposed to have collectively formed the unmetamorphosed BIF-type deposits in a shallow submarine volcanic center.

Introduction

Reviewer: The introduction and geological setting is brief, concise and appropriate. Here are some comments/corrections:

Reviewer: The author should start the introduction with a one sentence definition of IFs, mentioning their normal age distribution, and moving the references in line 63 and 64 to the end of the definition sentence. In the current form, the references in the middle of the first sentence clutters it and takes away from the impact of this sentence. If it reads better, the authors can also place the IF definition after the current first sentence

Response: Sentence restructured as suggested.

Reviewer: For line 84, a good reference to add would be Beukes et al., 2016, Episodes v. 39: 285-317. It reviews all the Mn deposits of Africa.

Response: Added as suggested.

Reviewer: More information needs to be provided on how the age range of the CVSB was determined.

Response: The text has been updated to:
K-Ar radiometric dating of biotite and amphiboles belonging to the dacitic/andesitic lava domes flooring the CVSB basin gave an Upper Pliocene age of 2.38±0.1 Ma (Fytikas et al., 1986; Stewart and McPhie, 2006). The fossiliferous sandstones/sandy tuffs hosting the Mn-rich deposit, which contain the gastropod mollusk guide fossil, Haustator biplicatus sp. (Bronn, 1831), indicate an Upper Pliocene-Lower Pleistocene age.

Reviewer: Some minor comments and corrections are noted in the pdf copy. Make sure to address these too**.**

Response. We have made all the corrections suggested in the annotated PDF. The responses are highlighted red in the new text appended in the supplementary document.

Methodology

Reviewer: It should be stated very early on in the methodology section how many samples were taken, what sample types (lithologies) were taken and the approximate localities of the samples

Response: The cardinal points from where samples were collected are given in the paper, such that any individual can follow this direction to the exact location of sampling. This study shows the sawn rocks and discusses how each representative layer was analysed by a variety of methods. The focus of this study is on the fine textures of these rocks, combined with field survey over the entire 1 Km long basin.

Reviewer: The sample preparation subsection (lines 119-125) is insufficient. More detail needs to be provided on how samples were taken, and how they were prepared for the different analyses. The type of mill used is not even mentioned. To refer to previous papers in the manner done here for sample preparation is not sufficient.

Response: Samples were sawn to remove weathered surfaces, and chips of rocks were sent to GeoTech Labs, which is a certified commercial laboratory for preparing thin sections. We are not sure what can be said about sawing a rock to remove weathered surfaces, which is why that part of the sentence has been left unchanged. Usually, it is enough to provide information on commercial providers, since they are accredited and certified. The rock polishing is a service provided by GeoTech Labs and can be requested at a fix rate, the details of which are not needed for this paper. Thirdly, the manuscript is over 15000 words. It is correct scientific practice to reference methods that can be obtained from previous publications. This is the practice advised by some of the most influential scientific journals. We have beefed parts of the acid digestion and removed parts as requested. However, the mechanism by which the rocks were pulverized is inconsequential because any mechanism would work as long as it enables the final dissolution of the powder into a liquid phase whose chemical analysis can be analyzed which is where focus is put. XRD analysis was performed directly on the pulverized samples as discussed in the manuscript.

Reviewer: Lines 120-121: I am not sure how this fits under the subheading of sample preparation. This will need to be moved and better explained. So yes, it does form the basis for facies analysis, but what was actually done and how?

Response. Line120-Line 121 has been removed as advised to Section 3.1, as an introductory sentence under Lithostratigraphy, where the methodology for facies analysis is described in detail.

Reviewer: Raman spectroscopy (lines 132-138 should not be included under the XRD subsection heading (section 2.2.1).

Response: Corrected.

Reviewer: Line 172: The abbreviations ICP-ES/MS and XRD have not been defined. Also, AcmeLabs has had its name changed to Bureau Veritas. Where is the lab situated?

Response: Corrected.

Reviewer: Lines 226 to 227: To use North American Shale Composite (NASC) for normalization of BIF data is an older way of doing it. Most of the newer publications use Post-Archean Australian Shale (PAAS). The authors should consider rather normalizing to PAAS for better comparison to recent literature.

Response: We have provided justification above

Results

Reviewer: Lines 266 to 268 contains repetition from what was stated in line 264. The authors should combine and clean this up to remove the repetition.

Response: Lines 266 to 268 have been deleted.

Reviewer: Line 292: The term "Sh beds" has not been previously defined. What does it mean?

Response: It has been removed and named accordingly as explained in the next comment. This abbreviation, like the one below, is an editing oversight.

Line 298: The term "Gcm" has not been previously defined. What does it mean?

Response: All abbreviations relating to lithological successions have been removed and fully spelt out throughout the text. "Sh" has been replaced with "plane-parallel-laminated sandstone/sandy tuff", "Gcm" has been replaced with "clast-supported pebble-to-cobble conglomerate".

Reviewer: Lines 398-400: The bracket started in line 398 is never properly closed. Please do so.

Response: Corrected

Reviewer: Lines 431-434: The phrase "from a relatively shallow and deeper water setting: : : to a relatively deeper quiet water environment" appears to be contradictory at the start. Some rephrasing is required to improve clarity.

Response: The paragraph has been shortened to: The hypothesized deepening of Basin 3 is consistent with the interpretation that active rifting was an important mechanism in the formation of the CVSB (Papanikolaou et al., 1990).

Reviewer: Lines 456-459: The granules associated with supergene formation versus those associated with sedimentary reworking will have very different internal structures. Whole rock geochemistry will also be very different. Why is such data not available? These are two very different formational proposals that should be resolved.

Response: We have not completed the mineralogical and geochemical description of these rocks. Therefore at the moment the sedimentary reworking vs. supergene origin cannot be deciphered. However, resolving this problem is beyond the scope of the present paper, and it is the subject of a future communication. Therefore, we have removed the reference to GIF, leaving the supergene possibility, because to our best judgment this better fits the geological and macroscopic characteristics of these ironstones.

Reviewer: Lines 467-469: The way this sentence is phrased does not read accurately. Why do dramatic fluctuations control the Fe to Si ratio? Seems to be overly obvious and

at the same time not supported by evidence, as if the lines between correlation and causality are being blurred. I would strongly recommend that this statement gets rephrased to more accurately represent what the data is actually showing, namely an inverse correlation between Fe and Si, which is to be expected when the two components are the only two major ones in the rock!

Response: Revised as suggested to read:

The laser ablation ICP-MS data further show that dramatic fluctuations in Fe concentrations control the Si to Fe ratio in both types of rocks, despite the thousands of millions of years gap between them. This inverse correlation between Fe and Si is expected because they are the two major elemental components of the rock.

Reviewer: Lines 520-523: Here the normalization to NASC becomes problematic. The paper that originally presented to calculations and plot to assess true Ce anomalies (Bau and Dulski, 1996), used PAAS as their shale standard. All the calculations in that paper therefore used PAAS-normalized values and NASC. This alone likely justified why the authors should redo the REE data normalized to PAAS

Response: We found no difference by normalizing the data either with NASC or PAAS. However, we maintained the NASC data to maintain consistency with recent publications that have used the NASC standard on the Milos IF. See sections 2.6-2.6.1 in the manuscript. Also see Figure 14.

Reviewer: Lines 522-523: Depending on the journal's citation format, shouldn't "Bau et al." be "Bau and Dulski"?

Response: Corrected.

Discussion

Reviewer: Lines 604-606: I do not believe the conclusion here is completely accurate. One can only state the MFIF deposition preceded the second-stage Mn mineralization. There is no clear evidence that the MFIF and first-stage Mn mineralization was coeval.

Reponse: Deleted

Reviewer: Lines 614-615: Please rephrase this so that the clarity is improved. Lines 615-616: "This uplifting into shallower water event": Which event is this? The discussion preceding this statement in this paragraph has only been referring to a transgressive (i.e. deepening) event. Please rewrite and restructure where necessary to make this paragraph read better and make more sense.

Reponse: This paragraph from line 614-line 619 has been modified to:
The deepening of Basin 3 is reflected in the underlying graded conglomerate bed that exhibits an upward fining trend, and transitions into the NFIF. The conglomerate bed may represent rapid deposition during a high-energy event, i.e. storm or mass flow,

whereas the fining upwards in the bed is better explained by the depositional mechanism losing energy through time. These high-energy conditions apparently must have ceased during the deposition of the overlying NFIF, where we interpret that increased abundance of finely laminated IF and decreased evidence of storm and/or mass flow reworking reflects deepening conditions. The hypothesized deepening of Basin 3 is consistent with the interpretation that active rifting was occurring during CVSB evolution (Papanikolaou et al., 1990).

Reviewer: Lines 651-655: Break this sentence into two shorter ones and do some restructuring that it reads better and the content is clearer.

Response: The sentence split into two as suggested.
However, samples were sawn to remove exposed layers and only the laminated bands for the NFIF were analyzed. Modern sediments from Spathi bay, located Southeast of Milos Island where hydrothermal activity is presently ensuing at 12.5 m below sea level, revealed similar plant lipids as recorded in the Quaternary IF (Fig. 15G).

Reviewer: Lines 663-672: This starting sentence for this paragraph reads like it comes out of nowhere. The authors need to lead into the content of this paragraph much better. Also, I am not convinced that this paragraph belongs in the subsection, as it does not directly relate to mineral paragenesis and also reads like it comes out of nowhere

Response: This paragraph has been deleted.

Reviewer: Lines 685-687: This statement has a few potential problems. Firstly, the lack of a Ce anomaly is not a definite indicator of reducing conditions. This can be buffered by excess Fe2+ in the system. Secondly, the Ce anomaly calculations appear to have been done using NASC-normalized REE data instead of PAAS-normalized data. At the very least the latter issue has to be resolved, and thereafter a more convincing argument need to be provided for reducing conditions.

Response: We have confirmed the redox conditions using another much accepted method as stated above. And as already stated and shown above, whether NASC or PAAS was used, the outcome was the same.

Reviewer: Lines 697-699: This one line is not convincing enough as a mechanism for redox stratified depositional environment. I admit that better and more convincing mechanisms are discussed later in the manuscript, but here the line comes over as unconvincing. Maybe note that possible mechanism for redox stratification are discussed in more details later.

Response: We have provided more supportive evidence for seafloor anoxia during deposition of both the NFIF and the MFIF using amore reliable redox proxy. Given that bottom water anoxia would have existed beneath a permanently oxygenated atmosphere, surficial waters column would have been oxidized.

Reviewer: Lines 722-729: I am not following the argument in point 3 very well. It requires some rephrasing and rewriting to convey the argument more clearly and concisely.

Response: This response is particularly directed at sedimentologists who according to our experience have attacked our conclusions by proposing that anoxic hydrothermal fluids may have penetrated preformed sediments to form the IF-rich bands as a diagenetic product. However this is impossible, given that reduced hydrothermal fluids in anoxic sediments deprived of light and oxygen, would lack oxidizing power to precipitate iron oxides. The new text reads as:

The reducing depositional conditions do not support sediment diagenesis as an alternative model for explaining the origin of the Milos IF. This is because the oxidation of ferrous Fe supplied in reduced hydrothermal fluids, must interact with a sizeable pool of oxygen, enabling microaerophilic bacteria oxidation of ferrous iron to Fe(III)(oxyhydr)oxides (Johnson et al., 2008). Otherwise, light-controlled photoferrotrophy—an extremely rare sediment characteristic—precipitates Fe oxides in the absence of oxygen in sunlight environments Weber et al., 2006).

Lines 722: The authors need to re-evaluate all the statements related to Ce anomalies after recalculating the anomalies to PAAS

Response: See above for justification with links to revision in the text and Figure 14.

Reviewer: Lines 730-738: For point 4 as well, the argument is not coming through clearly. There also appears to be some structuring and grammatical problems in this paragraph. From what I can follow the argument is probably sound, but I cannot be sure as the paragraph is not well written

Response: This is equally a comment that has been raised by sedimentologists. But we believe that the paper is clear enough and have deleted this point.

Reviewer: Lines 806-809: Many authors agree with the statement that the lack of organic carbon is not due to metamorphism, but for a different reason. The organic matter is also likely destroyed in Precambrian BIF in a redox reaction with Fe3+, leading to the formation of 13C-depleted siderite and ankerite. This should be briefly addressed. See, for example, Smith et al. (2013, Economic Geology, v. 108:111-134) and references therein.

Response: The text has been updated to include this information:

Importantly, prokaryotic biomarkers are suggested to poorly preserve in these young BIF analogues. This raises the possibility that this may provide an important explanation for why lipid biomarkers are yet to be extracted from Precambrian BIFs. Moreover, the data are compatible with the low C_{org} recorded in BIFs of all ages, suggesting that the low

C_{org} abundance may not be due to metamorphism as often proposed (Bekker et al., 2010) or to C_{org} oxidation by dissimilatory iron reducing bacteria to form ^{13}C-depleted siderite and ankerite during diagenesis (Johnson et al., 2008; Bekker et al., 2010). The Milos BIF-type rocks are unmetamorphosed and lack iron carbonate, yet have vanishingly low C_{org} levels similar to the ancient metamorphosed BIFs. However, an alternative possibility is that the iron oxides may have been reduced through biological oxidation of organic carbon, but carbonate saturation was not reached (Smith et al., 2013).

Reviewer: Lines 832-838: The tectonic and sea level mechanisms for changing redox conditions seem plausible. However, it only truly works when the motivation and mechanism for anoxia during IF deposition are more convincing. See main comment nr 6 above

Response: We have provided a strong evidence for anoxia by the sequential iron proxy.

Reviewer: Lines 851-853: For interest, also see Smith et al. (2013, Economic Geology, v. 108: 111-134).

Response: According to the anonymous reviewer comments, we felt that it is better to delete lines 851-853.

Reviewer: Lines 857-858: Rephrase and fix the grammar in this sentence.

Response: corrected

Reviewer: Line 876-877: The statement "most likely dependent on prevailing redox conditions" is not yet convincing! The accumulation of Mn could also be buffered by the availability of Fe^{2+}

Response: New evidence has been provided that strongly support reducing depositional conditions of both the NFIF and MFIF.

Conclusions

Reviewer: Lines 990-994: Agreed that this is a feasible mechanism. However, Prevalence of available Fe2+ as a redox buffer should also be considered and addressed.

Response: Redox depositional conditions are firmly established.

Reviewer: Lines 995-999: This needs to be clarified in the discussion and lead up. Was deep water anoxia semi permanent or did the venting play a role in establishing it? Here it appears that anoxia was semi-permanent, but the motivation needs to be better conveyed in the lead-up.

Response: We have provided plausible mechanisms that can explain the anoxia recorded in this basin in extensive review of redox processes along the entire volcanic arc.

However the change from Mn deposition to the NFIF certainly indicates that redox was changing intermittently. This subject has been thoroughly discussed throughout the manuscript and to avoid repetition we have not brought it up again here.

Lines 998-999: What about the chemolithoautotrophs (microaerophilic bacteria)? I am not convinced that one can commit to only the photoferrotrophs with the dataset presented here

Response: Lines 995-999:

We agree and have within the entire text discussed this point, but we have been careful since all endeavours have fallen short to identify their presence in Milos. Any extensive discussion on this topic is highly speculative as stated above. Inasmuch as we want to have this discussion, we feel that it is reasonable to limit it to the available data at hand. However, the similar depositional conditions as MFIF, give us the opportunity to discuss more about photoferrotrophy, as there is some evidence pointing to this. We have searched for characteristic microaerophilic fossils such as the twisted stalks of *Mariprofundus ferrooxydans* but found no evidence. This sentence has been changed to read:

The mechanism of formation of the MFIF and NFIF therefore most likely involved exhalative release of reduced hydrothermal/volcanic fluids into a restricted and deoxygenated seafloor water column where the oxidation of reduced Fe to Fe(III)(oxyhydr)oxides occurred, most likely by the activity of photoferrotrophs (Chi Fru et al., 2013). Microaerophilic oxidation of Fe(II) was likely critical, but that remains to be shown.

Anonymous Referee #2 Received and published: 24 January 2018 Review of: Modern Banded Iron Sedimentary Rocks on Milos Island, Greece.

Comments
The manuscript is well written, though it does suffer from a smattering of grammatical mistakes.

Responses: We extend thankfulness to this reviewer for taking time off to read and comment on our manuscript. His comments have condensed the sedimentology, tightening up loose parts suffering from lack of clarity. To satisfy the comment about a smattering of grammatical errors, we have taken care to minimize errors that might previously have escaped careful editing. Attached to this document is a PDF file named, supplement, containing the manuscript with changes, including those requested by the reviews, in red.

The layers under study do seem somewhat similar to Precambrian BIFs and are thus worth investigation, though it must always be emphasized that Precambrian ocean chemistry was very different than today's seas. I have not directed many comments at the iron deposits themselves as their description and interpretation is reasonable. This review concentrates mostly on the sedimentological aspects of the manuscript, which are problematic. Basically not enough substantiating data is provided for the interpretations given. Many of the interpretations are very specific and the limited exposures available do not provide the types of data necessary to validate the interpretations. The author's interpretations, in general, could be correct, but there are other equally as valid interpretations of the depositional systems possible. This situation is not helped by the inclusion of references after an interpretation is put forward that describe a depositional process or rock unit that was formed in a similar environment to that proposed but appear to bear little in common with the rocks present in this study. This reduces down to the problem that the characteristics of the rocks described in this study are not detailed enough to support specific interpretations. For example: a conglomeratic unit is interpreted as a channelized mass flow deposit in a submarine fan. If it was deposited by a high-density turbidity current it will have certain internal characteristics that are well defined in the literature (see some of Walker and Lowe's older papers). If it was a debris flow it will have other characteristics, such as disorganized clast orientations, matrix support, poor sorting etc. that these conglomerates do not appear to have. However, there is an even bigger problem with this interpretation. Submarine fan channel successions form thick fining upwards successions, commonly over tens of meters vertically. Finally submarine fans are one category of submarine base of slope deposit, a group that also includes ramps and aprons, and no evidence is given why this would not be a ramp or an apron, or simply, and much more likely, a conglomerate bed. I put in the latter as a few conglomerate beds do not make a fan, ramp or apron, which are very much larger features. These are just the problems that exist with one interpretation of depositional environments. Similar problems exist with the others. It would have been beneficial if the authors delegated more discussion to the deposition of the silica-rich layers as the Fe-rich layers forming from hydrothermal fluids are easy to understand but the deposition of the silica layers in BIF is much more difficult to explain. The use of references is perplexing. Most of them do not have direct bearing on what they are referencing in the text. They are on the same general subject, but many do not reinforce the correctness of the preceding statement. I recommend that the

interpretations of the depositional environments of the siliciclastics be eliminated. They are very problematic and greatly distract from the manuscript.

Response: For the sake of clarity, we should indicate that we are not proposing the Milos BIF-type rocks as the exact equivalent of Precambrian BIFs or insinuating that the seawater in which they formed had the exact composition of the Precambrian oceans. But we have found several components of the deposit that have the potential of providing and aiding mechanistic models aimed at understanding how BIFs formed. They may give new insights into the deep past from the present-day seawater biogeochemical perspective. These are some of the challenges we wish to resolve by detailed description of the geological and geochemical processes behind the perplexing deposition of the Milos IF. To enable comparison, we use the simple definition of BIFs as marine sedimentary rocks with alternating layers of Fe-rich and Si-rich bands, containing at least 15% Fe. This definition does not restrict the potential for BIFs to form only in Precambrian oceans, although they are a major feature of this unique period, a time when seawater had extraordinarily high levels of dissolved Fe and Si.

What our data are showing is that these local conditions of elevated and cyclic supply of dissolved Fe and Si and accompanied by strict bottom water anoxic conditions in a localised reservoir cut off from the open ocean, can in principle allow the rare deposition of BIF-type rocks in the modern ocean. The rarity of these types of deposits in the present-day ocean hints that such conditions seldom develop under the existing atmosphere, but that they can indeed occur. Therefore we present these as a rare modern BIF-type facies, different from the Precambrian BIFs, in the same way the rare Neoproterozoic BIFs are different from the widespread Paleoproterozoic Superior BIFs, which are in turn distinct from the mainly Algoma-type Archean BIF deposits that are limited in scale. This paragraph has been edited and included in our conclusions to highlight the importance of distinguishing this deposit from the Precambrian formations.

We strongly agree that sedimentary features can be difficult to interpret with certainty. We have therefore reduced the degree to which these interpretations have been made for the above reasons laid down by this reviewer. We however believe that it is important to keep solid parts of the interpretations that help explain how anoxic conditions could have apparently developed in the CVSB to enable dissolved Fe enrichment and its oxidation to Fe(III). Further, sedimentology must not be interpreted independently from the geochemistry and redox. This has become even more crucial with the new Figure 13C-D that unambiguously supports the contentious anoxic depositional conditions previously illustrated by REEs. This new information has been acquired using the widely accepted iron extraction redox proxy (See *Poulton, S.W. and Canfield, D.E. 2011. Ferruginous conditions: A dominant feature of the ocean through Earth's history. Elements 7, 107–112, for a review)*.

This reviewer indicates that it would have been more helpful to dedicate more time discussing the Si bands. Our data show that band formation was mainly controlled by the activity of Fe, while Si precipitation was a passive process that cannot be explored beyond the fact. As we have shown and discussed, it is the cyclic release and oxidation of ferrous Fe that in fact controls the enrichment of Fe in the Fe-rich bands and Si in the Si bands. This particular observation provides the first independent

modern verification for similar processes suggested to have formed the ancient BIFs (See Bekker et al. 2010 for details and references therein, cited in the main text).

The description and discussion of the IF can stand alone. Its lack of current formed structures implies a low energy environment and that is about all that can be inferred about physical processes from the IF. Thus, the manuscript would need major revisions. A more detailed line by line review follows:

Response: We agree with this reviewer about the low-energy environment in which the IF formed, which is in agreement with our initial conclusions. However, it would appear that the switch from one redox state to the other was often accompanied by tectonic activity that caused deepening and shallowing.

Line 73: Rare Earth Elements should not be capitalized.

Response: Corrected

Line 115: Rhyolite is not intrusive.

Response: Corrected to extrusive

Line 226: It is much more common in work on iron formations to us PAAS to normalize the data.

Response: The rationale for using the NASC is as follows:

1. The NASC normalization maintains data consistency with the REE data published in our previous papers on the Milos IF ((1) Chi Fru, E., Ivarsson, M., Kilias, S.P., Bengtson, S., Belivanova, V., Marone, F., Fortin, D., Broman, C., and Stampanoni, M.: Fossilized iron bacteria reveal a pathway to the origin banded iron formations. Nat. Comm., 4, 2050 DOI: 10.1038/ncomms3050, 2013. (2) Chi Fru, E., Ivarsson, M., Kilias, S.P., Frings, P.J., Hemmingsson, C., Broman, C., Bengtson, S. and Chatzitheodoridis, E.: Biogenicity of an Early Quaternary iron formation, Milos Island, Greece. Geobiology, 13, 225–44, 2015.

2. There are no scientifically demonstrated discrepancies between the PAAS and NASC.

3. Following the above suggestion, data was normalized to PAAS for comparison with the NASC normalized trends. The results produced the same trend as observed when data are normalized to NASC. See new Figure 14 in the manuscript text, accessible in the attached supplement PDF file. Further explanations are also provided under sections 2.6-2.6.1 in the manuscript supplement text.

Line 327: Below storm wave base does not necessarily mean below 100 to 200 meters. At present storm wave penetration is deepest in locations such as southeastern Australia and Atlantic Canada where it reaches 120m. But these are very storm prone open ocean facing areas. It is difficult to give an estimate for paleo-storm wave base in the study area, but I doubt that it could be even close to 100m as more would mean waves with greater than 200 meter wavelengths in a sheltered area compared to the open Atlantic.

Response: We have omitted our attempt at specifying a value in the text for the depth. The new wording has been rephrased to:

The MFIF rests directly on the submarine dacites-andesites that were deposited in a relatively shallow submarine environment (Stewart and McPhie, 2006).

Line 340: Not enough evidence is given to justify the turbidite interpretation. Graded beds just mean they were deposited by powering-down events, which can occur in many different environments. Even if they are turbidites, which I have no idea whether they are or not from the evidence, the setting cannot be termed a fan, ie, why not a ramp or apron or a number of other environments that can have turbidites.

Response: Removed from text.

Line 344: Slump deposits infers an intact or partially intact block that slid. The conglomerates are not slump deposits. They could be debris flows, but again there is not enough evidence given to say this.

Response: Lines 337-361 have been deleted and replaced with this short paragraph:

In the overlying sandstone-conglomerate facies, the presence of sedimentary structures indicative of wave action and currents (e.g. cross-stratification), that signify rapid deposition during a high energy event, are consistent with a switch to a shallow-submarine high energy environment (Stewart and McPhie, 2006; Chi Fru et al., 2015). This shift in depositional environments may have been controlled by a combination of submarine volcano-constructional processes, synvolcanic rifting and volcano-tectonic uplift known to have formed the CVSB (Papanikolaou et al., 1990; Stewart and McPhie, 2006).

Line 347: If a flow is carrying pebbles it is not a low density turbidity current.

Response: Deleted and replaced with the paragraph above.

372: gravel to pebble is not proper terminology. Pebbles are gravel if unconsolidated.

Response: Lines 370-373 have been deleted and replaced with:

The lower sandstone facies represents the host of the main economic grade Mn oxide ores in the CVSB. This constitutes part of a separate study devoted to the Mn ores and will not be dealt with further here.

Line 395: mm-scale layers are not beds, they are laminae.

Response: Deleted and replaced with laminations.

Line 418: Why not below storm wave-base?

Response: Corrected.

Line 422: The only evidence for the interpretation that the conglomerates are " a series of channel deposits in an inner turbidite fan-like setting" appears to be that they are conglomerates. A great deal more evidence is necessary to be so specific about the depositional environment.

Response: Lines 420-434 have been deleted.

Line 424: No evidence has been given for a tidal environment and little evidence for a shoreface.

Response: Lines 420-434 have been deleted.

Line 427: There are also many papers that describe iron formations in other settings.

Response: Lines 420-434 have been deleted.

Line 434: This is an example of a reference that has little bearing on the preceding statement. The Mesoarchean Barberton is not a good analog for the sedimentary environment of the basin described here.

Response: Lines 420-434 have been deleted.

Line 439: The sedimentary structures described could have been formed in the environments proposed, but they are not limited to the environments given the lack of evidence.

Response: Lines 335-340 deleted.

Line 458: The description of these deposits has little in common with GIF. It is also better to reference the originator of the term GIF (Simonson), rather than Bekker, which is just a review article.

Response: References to GIF have been deleted from the text.

Line 481: This is circular reasoning.

Response: We agree and further demonstrate this in the new Figure 13D. These emphases must be highlighted to show some of the similarities these rare deposit shares with true BIFs.

Line 482: Precambrian BIF can be sulfide facies.

Response: We agree. We are trying to make the statement that these are those type of BIF facies that are sulfide rich. We have therefore peplaced with the text:

Lack of association of the framboidal-iron-rich particles with S, following SEM-EDS analysis, rules out a pyrite affiliation and is consistent with the non-sulfidic depositional model suggested by the sequential iron extraction redox proxy (Fig. 13D).

Line 522: This statement is not correct. Planavsky and others (see authors' references to this statement) put forward that the anomaly for Ce must be less than .95 and greater than 1.05 to be significant, not less than or greater than 1.

Response: This has been corrected.

Line 528: They do not have similar enrichment levels; they are light depleted.
Response: Enrichment changed to depleted.

Line 574: The positive Eu anomalies are quite small compared to those associated with oceanic hydrothermal vent sediments. Also, volcanic detritus can carry positive Eu anomalies. A plot of Ti vrs Eu* would be useful to distinguish if the anomaly is related to volcanic detritus in the IF.

Response: We agree, but this effort will not tell us anything more than what we have already shown, since multiple evidence shows that we are dealing with materials being released into the basin intermittently by hydrothermal/volcanic activity as demonstrated by the ash particles in the bands. As we have shown in Figure 13 and from using multiple lines of evidence, the supply of materials from the continent to the basin was not an important source of sediments during the formation of the alternating Fe and Si layers. Our main interpretation is a hydrothermal source, backed by data in our cited publication in Nature Communications and Geobiology, in addition to the present submission.

Line 614: What is described as an upward fining trend appears to me to be simply one single graded bed. The fining upwards in the bed is better explained by the depositional mechanism losing energy through time. Also, conglomeratic beds usually represent rapid deposition during a high energy event, ie. storm or mass flow, rather than the slow pebble on pebble accumulation over years.

Response: This text has been revised as suggested. The new text reads like this:

Geomorphological/chemical reconfiguration orchestrated the deposition of the NFIF in a deeper, small-restricted basin (Fig. 2). The deepening of Basin 3 is reflected in the underlying graded conglomerate bed that exhibits an upward fining trend, followed by transition into the fine-grained NFIF. The conglomerate bed may represent rapid deposition during a high-energy event, i.e. storm or mass flow, whereas the upwards fining in the bed is better explained by the depositional mechanism losing energy through time. These high-energy conditions apparently must have ceased during the deposition of the overlying NFIF, where we interpret that increased abundance of finely laminated IF and decreased evidence of storm and/or mass flow reworking reflects deepening conditions. The hypothesized deepening of Basin 3 is consistent with the interpretation that active rifting was an important mechanism in the formation of the CVSB (Papanikolaou et al., 1990).

Line 682: Comparing the small Eu anomalies present in this study with the larger Precambrian anomalies should include giving the values for the average Precambrian anomalies. Simply stating the values of Eu anomalies of samples in this study are more similar to Archean anomalies is somewhat misleading.

Response: The paragraph has been deleted.

Line 757: If even small amounts of seawater are mixing with the hydrothermal fluid, as previously stated, anoxia could not exist.

Response: See new Figure 13C-D that firmly establishes the anoxic/ferruginous depositional conditions. Moreover the statement made by this reviewer that even if small amounts of seawater are mixing with hydrothermal fluid, anoxia cannot exist, is misleading and a bit perplexing because this argument means that redox gradients should not exist in nature. Following the rules of stoichiometry in chemical reactions, large volumes of highly reduced solutions such as hydrothermal fluids require equally large concentrations of oxidants (especially oxygen) to make the fluid oxidizing. From this reasoning, considerable amounts of oxygen are required to react with the large volumes of the highly reduced chemicals and compounds present in hydrothermal fluids. This argument is given as an explanation for why it took so long for oxygen to rise in the atmosphere (See Lyons et al., 2014. The rise of oxygen in Earth's early ocean and atmosphere. Nature 506:307–315: and the review by Bekker et al. 2010, cited in the manuscript). The reasoning is that reduced hydrothermal fluids that made up a bulk of the early oceans were eventually overwhelmed stoichiometrically by oxygen (meaning more oxygen was being produced than consumed by the reduced fluids), leading to the rise of oxygen in the atmosphere, c. 2.4 billion years. Even after that, although the Paleoproterozoic surface ocean was oxidized for close to two billion years, complete ocean oxygenation only came at the end of the Precambrian despite the fact that reduced deep ocean hydrothermal fluids continuously mixed with the oxygen-rich ocean surface seawater. If we were to follow the argument given by this reviewer, then the whole ocean would have been oxidized following the mixing of the reducing fluids with the thin layer of oxygen-rich seawater on the ocean surface. This indicates that the sedimentology, geochemistry and redox must be jointly interpreted to understand what occurred at Milos.

Line 842: The presence of a conglomeratic bed does not commonly mean deepening of a marine succession. There are literally thousands of papers where the upward transition of sandstones to conglomerates is interpreted as shallowing as energy levels increase with shallowing in a marine setting.

Response: We strongly agree that the paragraph was not well-phrased, leading to the difficulty in understanding the meaning of the sentence. It has now been revised to:

All of this is feasible with the three-basin-fault-bounded hypothesis as a requirement for movement along fault lines in response to temporal tectonic activation. The upward sequence transition from the Mn-rich sandstone facies, through the pebbly conglomerate and the final termination in the overlying mud-grained NFIF (Fig. 8B), reflect sedimentary features formed during multiple changes in seawater levels (Cattaneo & Steel, 2000). This study proposes that the NFIF that overlies the transgressive-type conglomeratic lag along an erosional contact surface was likely deposited during maximum flooding, when the basin became stagnant and stratified, and subsequently was uplifted to emergence.

Line 848: The presence of a transgressive conglomeratic lag implies that the area was emergent prior to this and the conglomerate formed by wave reworking in a shore proximal environment. Evidence has not been given to support this, and if I am not mistaken the conglomerate has previously in this manuscript been interpreted as a mass flow.

Response: Deleted.

Line 853: In these references the maximum regressive surface is overlain by a transgressive lag and then very shallow shoreline deposits affected by wave activity. A very different scenario to what these authors are proposing.

Response: Paragraph and references removed.

Line 855: The referenced BIFs are not deposited in sandstone/grainstone environments, the IFs are grainstone with very low siliciclastic contents and they are interlayered with chemical muds, but the IFs are not banded.

Response: Because this interpretation is not of immediate relevance to the strength of the paper, the paragraph has been deleted.

Line 1004: This process would be expected to produce a sharp bottom contact to the Fe-rich layer, which would then mineralogical grade upwards into the silica-rich layer. Is this the way the layers are organized?

Response: Yes. We show this in supplementary Figures 8 and 9.

Sedimentary mechanisms of a modern banded iron formation on Milos Island, Greece

[1,2]Ernest Chi Fru*, [3]Stephanos Kilias, [4,5]Magnus Ivarsson, [1]Jayne E. Rattray, [3]Katerina Gkika, [2]Iain McDonald, [6]Qian He, [1]Curt Broman

[1]Department of Geological Sciences, 10691, Stockholm University, Sweden.

[2]School of Earth and Ocean Sciences, Cardiff University, Park Place, CF10 3AT, Cardiff, UK.

[3]Department of Economic Geology and Geochemistry, Faculty of Geology and Geoenvironment, National and Kapodistrian University of Athens, Panepistimiopolis, Zographou, 15784, Athens, Greece.

[4]Department of Biology, University of Southern Denmark, Campusvej 55, Odense M, DK5230, Denmark

[5]Department of Palaeobiology, Swedish Museum of Natural History, Box 50007, Stockholm, Sweden.

[6]School of Chemistry, Cardiff University, Park Place, CF10 3AT, Cardiff, UK.

*Corresponding author

Tel: +44(0) 29 208 70058

Email: ChiFruE@cardiff.ac.uk

Short title: A modern banded iron formation

Abstract. An Early Quaternary shallow submarine hydrothermal iron formation (IF) in the Cape Vani sedimentary basin (CVSB) on Milos Island, Greece, displays banded rhythmicity similar to Precambrian banded iron formation (BIF). Sedimentary and stratigraphic reconstruction, coupled to biogeochemical analysis and micro-nanoscale mineralogical characterization, confirm the Milos IF as a modern BIF analogue. Spatial coverage of the BIF-type rocks in relation to the economic grade Mn ore that brought prominence to the CVSB implicates tectonic activity and changing redox in their deposition. Field-wide stratigraphic and biogeochemical reconstruction demonstrate two temporal and spatially isolated iron deposits in the CVSB with distinct sedimentological character. Petrographic screening suggests the previously described photoferrotrophic-like microfossil-rich IF (MFIF), accumulated on basement andesite in a ~150 m wide basin, in the SW margin of the basin. A strongly banded non-fossiliferous IF (NFIF) sits on top the Mn-rich sandstones at the transition to the renowned Mn-rich formation, capping the NFIF unit. Geochemical evidence relates the origin of the NFIF to periodic submarine volcanism and water column oxidation of released Fe(II) in conditions apparently predominated by anoxia, similar to the MFIF. Raman spectroscopy pairs hematite-rich grains in the NFIF with relics of a carbonaceous material carrying an average $\delta^{13}C_{org}$ signature of ~-25‰. However, a similar $\delta^{13}C_{org}$ signature in the MFIF is not directly coupled to hematite by mineralogy. The NFIF, which post dates large-scale Mn deposition in the CVSB, is composed primarily of amorphous Si (opal-$SiO_2 \cdot nH_2O$) while crystalline quartz (SiO_2) predominates the MFIF. An intricate interaction between tectonic processes, changing redox, biological activity and abiotic Si precipitation are proposed to have collectively formed the unmetamorphosed BIF-type deposits in a shallow submarine volcanic center.

Keywords: Banded iron formation; BIF analogue; Hydrothermal activity; Iron cycling; Silica cycling.

1 Introduction

Banded iron formations (BIFs), are marine sedimentary deposits containing at least 15% Fe, marked by Fe-rich bands alternating with Si-rich layers that formed predominantly during the Precambrian (James, 1954; Gross, 1980; Simonson, 1985, 2003; Bekker et al., 2010). Recently, an Early Quaternary iron formation (IF), ~2.0 million years old, displaying banded rhythmicity typical of Precambrian banded iron formations (BIF) was serendipitously discovered in the Cape Vani sedimentary basin (CVSB) on Milos Island, Greece (Chi Fru et al., 2013, 2015). Before this discovery, Cape Vani was long known to host Mn oxide ores of economic potential (Hein et al., 2000; Liakopoulos et al., 2001; Glasby et al., 2005; Kilias et al., 2007). Milos is an emergent volcano on the Hellenic Volcanic Arc (HVA) where arc-volcanism and seafloor hydrothermal activity occur in thinned pre-Alpine to Quaternary continental crust (Kilias et al., 2013b) (Fig. 1). The first reported IF from Cape Vani is unmetamorphosed and contains diverse microfossils encrusted by hematite, with ferrihydrite proposed as a primary precursor mineral (Chi Fru et al., 2013, 2015). Field stratigraphy, rare earth elements (REEs), stable isotopes, petrographic and microfossil studies point to microbial Fe deposition in a semi-enclosed, shallow submarine basin under conditions analogous to those that formed the Precambrian Algoma-type BIFs near volcanic centers (Chi Fru et al., 2015). These earlier reports assumed a one-time basin-wide depositional event and a common origin for all Fe-rich sedimentary rocks in the CVSB.

However, it remains unclear what sedimentary processes caused the distinct deposition of the BIF-type rocks in a basin where Mn precipitation was apparently widespread at various intervals. Moreover, it is not known how the Mn ores relate temporally and spatially to Fe deposition in the ~1 km long CVSB. This knowledge

may provide clues to processes that triggered large-scale deposition of similar Proterozoic Fe-Mn-rich deposits (Roy, 2006; Tsikos et al., 2010; Beukes et al., 2016). Here, new sedimentological, petrological and biogeochemical evidence describes cycles of periodic precipitation of shallow submarine Si and Fe-rich sedimentary rocks and the plausible mechanisms that enabled their temporal and spatial separation from the Mn deposits in the CVSB. The data reveal a much more complex depositional system not only controlled by microbial Fe(II) oxidation as previously proposed (Chi Fru et al., 2013, 2015), but illuminates episodic submarine hydrothermal activity coupled to changing redox conditions as a central mechanism in the formation of the banded iron rocks.

1.1 Geological setting

K-Ar radiometric dating of biotite and amphiboles belonging to the dacitic/andesitic lava domes flooring the CVSB basin gave an Upper Pliocene age of 2.38±0.1 Ma (Fytikas et al., 1986; Stewart and McPhie, 2006). The fossiliferous sandstones/sandy tuffs hosting the Mn-rich deposit, which contain the gastropod mollusk guide fossil, *Haustator biplicatus sp.* (Bronn, 1831), indicate an Upper Pliocene-Lower Pleistocene age. The geology, Fe and Mn mineralization of the CVSB have previously been described in detail (Plimer, 2000; Hein et al., 2000; Liakopoulos et al., 2001; Skarpelis and Koutles, 2004; Glasby et al., 2005; Stewart and McPhie, 2006; Kilias, 2011; Alfieris and Voudouris, 2005; Alfieris, 2006; Alfieris et al., 2013: Chi Fru et al., 2013, 2015; Papavassiliou et al., 2017). Briefly, the Milos IF is part of the CVSB, a recently emergent sedimentary rift basin located NW of Milos Island, along the HVA in the Aegean Sea, Greece (Fig. 1). It hosts a fossil analogue of active shallow-submarine hydrothermal activity on the coast of Milos Island (Dando et al., 1995).

The CVSB developed within a shallow-submarine rhyolitic-dacitic volcanic center, filled up mainly by a ~35-50 m thick stratigraphic succession of volcaniclastic/epiclastic sandstones and sandy tuffs spanning Upper Pliocene to Lower Pleistocene, 35-40% of which is hydrothermally mineralized by Mn oxides and barite (Hein et al., 2000; Liakopoulos et al., 2001; Skarpelis and Koutles, 2004; Papavassiliou et al., 2017). Sedimentologic and ichnologic data, including sedimentary structures, lamellibranch, echinoid and brachiopod fossils, the gastropod mollusk fossil, Haustator biplicatus (Bronn, 1831), and microbially induced sedimentary structures (e.g., Kilias, 2011), suggest that most of the CVSB sandstones/sandy tuffs hosting the Mn-rich deposit, are foreshore to shoreface shallow submarine deposits, formed at a maximum depth of 200 mbsl. Over the last 0.8 Myr, fluctuating water depths due to sea-level change of up to 120 m and volcanic edifice building, has resulted in tectonic uplift of ~250 m (Papanikolaou et al., 1990). The CVSB infill, currently 35 m above sea level, is tectonically bound by extrusive rhyolite to the north, framed by elevated andesitic-dacitic centres, with the Cape Vani and the Katsimoutis dacitic lava domes being the most prominent (Fig. 1).

2 Methodology

2.1 Sample preparation

Prior to mineralogical and geochemical analysis, exposed rock surface layers were sawn and removed. GeoTech Labs (Vancouver, Canada) produced doubly polished thin sections for mineralogical and textural analysis. Trace and rare earth elements analysis was performed on pulverized powders digested with a mixture of HNO_3, HF and heat until a clear solution was obtained (Chi Fru et al., 2013, 2015).

2.2 Mineralogical analysis

2.2.1 X-Ray Diffraction (XRD) analysis

A PANalytical Xpert-pro diffractometer at room temperature, 45 kV, 40 mA and 1.5406 Å wavelength and Cu-Kα radiation and Ni-filter, was used for Powder X-Ray Diffraction (PXRD) analysis. Samples were analyzed between 5-80° in step sizes of 0.017° with continuous mode scanning step time of 50.1650 s while rotating.

2.2.2 Raman spectroscopy

Raman analysis was performed with a confocal laser Raman spectrometer (Horiba instrument LabRAM HR 800), equipped with a multichannel air-cooled (-70°C) 1024 x 256 pixel charge-coupled device (CCD) array detector as previously described (Chi Fru et al. 2013, 2015). Spectral resolution was ~0.3 cm^{-1}/pixel. Accuracy was determined by a repeated silicon wafer calibration standard at a characteristic Raman line of 520.7 cm^{-1}.

2.2.3 Transmission electron microscopy

Specimens for transmission electron microscopy (TEM) were prepared from the crushed rock specimen powder. This was followed by dry-dispersal onto a 300 mesh holey carbon TEM Cu grid. Microscopy was conducted using a JEOL 2100 TEM with a LaB_6 source in the School of Chemistry, Cardiff University, operated at 200kV. The X-EDS analysis was performed with an Oxford Instrument SDD detector X-Max^N 80 T.

2.2.4 Scanning electron microscopy

Scanning Electron Microscopy-Energy Dispersive Spectroscopy (SEM-EDS) analysis was done on a FEI QUANTA FEG 650 ESEM. Images were captured at 5 kV and EDS data collected at 20 kV, using an Oxford T-Max 80 detector (Oxford Instruments, UK). The analyses were performed in low vacuum to minimize surface charging of uncoated samples. EDS elemental maps were collected for 30 min or until the signal had stabilized, indicated by a clear distribution trend. The data were further processed with the Oxford Aztec software.

2.3 Geochemical analysis

2.3.1 Laser ablation ICP-MS and trace element analysis

Laser Ablation-Inductively Coupled Plasma-Mass Spectrometry (LA-ICP-MS) was performed at Cardiff University on polished thin sections. The LA-ICP-MS system comprised a New Wave Research UP213 laser system coupled to a Thermo X Series 2 ICP-MS. The laser was operated using a frequency of 10 Hz at pulse energy of ~5mJ for an 80µm diameter beam using lines drawn perpendicular to the layering and at a movement speed of 26 microns sec^{-1}. Samples were analyzed in time resolved analysis (TRA) mode using acquisition times of between 110 and 250 seconds; comprising a 20 second gas blank, 80-220 second ablation and 10 second washout. Dwell times varied from 2 msec for major elements to 35 msec for low abundance trace elements. Blank subtraction was carried out using the Thermo Plasmalab software before time resolved data were exported to Excel.

Separated and independently pulverized banded layers were digested by lithium borate fusion followed by major, trace and rare earth element (REE) analyses using ICP- Atomic Emission Spectrometry-Mass Spectrometry (ICP-AES-MS) and X-Ray Florescence (XRF) at Bureau Veritas (Ankara). Geochemical data were compared

192 with previously published results for the more widely investigated Mn deposits (Hein
193 et al., 2000; Liakopoulos et al., 2001; Glasby et al., 2005).
194
195 **2.3.2 Isotope analysis**
196 C, N and S isotopic composition for the pulverized samples was determined as
197 previously described (Chi Fru et al., 2013, 2015), following combustion in a Carlo
198 Erba NC2500 analyzer and analyzed in a Finnigan MAT Delta V mass spectrometer,
199 via a split interface to reduce gas volume. Reproducibility was calculated to be better
200 than 0.15‰ for $\delta^{13}C$ and $\delta^{15}N$ and 0.2‰ for $\delta^{34}S$. Total C and N concentrations were
201 determined simultaneously when measuring the isotope ratios. The relative error was
202 <1% for both measurements. For carbon isotopic composition of organic carbon,
203 samples were pre-treated with concentrated HNO_3 prior to analysis.
204
205 **2.4 Organic geochemistry analysis**
206 Lipid biomarker and compound specific $\delta^{13}C$ analyses were executed on powdered
207 samples of sectioned bands from which exposed surface layers had been removed.
208 Modern sediments from Spathi Bay, 36°40'N, 24°31'E, southeast of Milos Island,
209 collected by push coring at 12.5 m below the seafloor were freeze-dried prior to
210 extraction to aid the identification of potential syngenetic biomarkers in the
211 Quaternary rocks. Between 4-6 g of ground samples were ultrasonically extracted
212 using 3×Methanol, 3×(1:1) Methanol:Dichloromethane (DCM), and 3×DCM and
213 extracts were combined and dried under N_2. Samples were subsequently re-dissolved
214 in DCM then methylated following the method of Ichihara and Fukubayashi (2010).
215 The resulting residue was silylated using, 20 µl pyridine and 20 µl (N, O-
216 Bis(trimethylsilyl)trifluoroacetamide) BSTFA and heated at 60˚C for 15 min. Total

lipid extracts were analyzed using a Shimadzu QP 2010 Ultra gas chromatography mass spectrometer (GC/MS). Separation was performed on a Zebron ZB-5HT column (30 m x 0.25 mm x 0.10 µm) with a helium carrier gas flow at 1.5 ml min^{-1}. Samples were injected splitless, onto the column at 40˚C with the subsequent oven temperature program ramped to 180˚C at a rate of 15˚C min^{-1}, followed by ramping to 325˚C at a rate of 4˚C min^{-1} and a final hold for 15 min. The MS was set to scan from 50 to 800 m/z with an event time of 0.70 sec and a scan speed of 1111 u/sec. All peaks were background subtracted and identification confirmed using the NIST GC/MS library and literature spectra. Contamination was not introduced into the samples, as blank samples worked up concurrently with the rock fractions had results comparable to the ethyl acetate instrument blank.

2.5 Chemical weathering analysis

Chemical index of alternation (CIA) was used to determine whether variations in chemical weathering intensities would in addition to hydrothermal activity deliver materials into the depositional basin from the continent, according to the formula: $CIA = Al_2O_3/(Al_2O_3 + CaO + Na_2O + K_2O) \times 100$. Extensively applied, the CIA index reveals subtle changes in weathering fluxes (Nesbit and Young, 1982; Maynard, 1993; Bahlburg & Dobrzinski, 2011), where increasing CIA values generally indicate amplified chemical dissolution of rocks and selective release of dissolvable CaO, Na_2O and K_2O into solution (Nesbit & Young, 1982; Maynard, 1993; Bahlburg & Dobrzinski, 2011). The broken rock particles enriched in the poorly soluble Al_2O_3 fraction, settle to the seafloor as weathered sediments carrying a chemical composition different from the source. In the absence of chemical dissolution, no net chemical change is expected in the composition of sediments

compared to source and thus a low CIA index. CIA indices for detritus of 0-55, 55-75 and >75, are considered unweathered, unweathered to slightly weathered and weathered to highly weathered, respectively (Nesbit & Young, 1982; Maynard, 1993; Bahlburg & Dobrzinski, 2011).

2.6 Redox analysis

Redox depositional conditions were evaluated using the sequential Fe extraction redox proxy (Poulton and Canfield, 2005, 2011), combined with REE composition of the sediment (Planavsky et al., 2010).

2.6.1 REE redox analysis

REE data obtained as described in section 2.3.1 were normalized with the North American Shale Composite (NASC) to maintain consistency with previous studies in which NASC-normalized REE data (SN) were reported for the Milos BIF-type rocks (Chi Fru et al., 2013, 2015). The data were further normalized with the Post Archean Australian Shale (PAAS) (McLennan, 1989) standard for comparative purposes, according to Bau and Dulski (1996). Ce anomalies, calculated from Ce/Ce* ($Ce_{(SN)}/0.5Pr_{(SN)} + 0.5La_{(SN)}$) and Pr/Pr* ($Pr_{(SN)}/0.5Ce_{(SN)} + 0.5Nd_{(SN)}$) values, were considered significant when Ce/Ce* and Pr/Pr* were less than and greater than 1, respectively (Bau and Dulski et al., 1996; Planavsky et al., 2010).

2.6.2 Sequential iron extraction redox analysis

This analysis was performed on three representative MFIF samples and the six sectioned bands of a typical NFIF sample using the method developed by Poulton and Canfield (2005) and data interpreted accordingly (e.g., Canfield and Poulton, 2005,

2011; Guilbaud et al. 2015; Sperling et al. 2015). Reagent blanks and geological standards were used for data calibration.

3 Results

3.1 Lithostratigraphy

Sedimentary structures, grain-size trends, lateral facies variations, vertical stacking trends, and key stratigraphic surfaces form the basis for facies analysis. Field-wide sedimentological and lithostratigraphical mapping of the CVSB in the summer and fall of 2014 enabled the assessment of the lateral and vertical coverage of the Milos iron oxide-rich facies relative to the Mn-rich sandstones that dominate the Early Quaternary sedimentary basin (Fig. 2). Six stratigraphic sections, representing marine siliciclastic lithofacies sequences, were investigated along a ~1 km SW-NE trending portion of the CVSB infill (Supplementary Figs 1-7). Sequence stratigraphy was conducted on outcrops and vertical shafts and tunnels left behind by previous Mn mining activity. Two of those sections; Section A located at 36°44'17.85''N, 24°21'17.72''E and Section B located at 36°44'35.11''N, 24°21'11.25''E, contain stratigraphic units composed of layered, bedded, or laminated rocks that contain ≥15 % Fe, in which the Fe minerals are commonly interlayered with quartz or chert, in agreement with the definition of Precambrian BIFs (James, 1954; Gross, 1980; Bekker et al., 2010). These IFs are descriptively referred to here as microfossiliferous iron formation (MFIF) according to Chi Fru et al. (2013, 2015), and non-microfossiliferous iron formation (NFIF) (this study), respectively (Fig. 2). The MFIF and the NFIF occupy at most ~20% of the entire CVSB infill. The stratigraphy and sedimentary lithofacies are illustrated below, using lithofacies codes modified after

Bouma (1962), Miall (1978, 1985), Lowe (1982), Mutti (1992) and Shanmugam (2016).

Further field stratigraphic survey revealed considerable lithologic variability within three fault-bounded volcanosedimentary sub-basins in the CVSB (Fig. 2), which for the sake of simplicity are referred to as Basin 1—host of the MFIF; Basin 2—host of economic grade Mn ore; and Basin 3—host of the NFIF (Fig. 2). Each section is framed by distinct marginal normal faults that strike in the NW-SE and NE-SW to NNE-SSW directions, distinguishable by distinct lateral sedimentary facies exhibiting unique vertical sequence stratigraphy (Fig. 2; Supplementary Figs 1-7). Faulting in the CVSB is related to major geographical activation of extensional structures at intervals that shaped Milos into a complex mosaic of neotectonic units (Papanikolaou et al., 1990; van Hinsbergen et al., 2004).

3.1.1 Section A (36°44'17.85''N, 24°21'17.72''E)

Informally known as "Little Vani", Section A is the type section containing the MFIF at the base. It crops out in the W-SW edge of the CVSB (Figs 1 & 2) as a ~6-7 m high cliff resting stratigraphically on submarine dacitic and andesitic lavas and domes. This section extends laterally in the N-NE direction for an estimated 300–500 m.

Lithologically, the MFIF comprises laminated and massive fine-grained red and white weathered ferruginous jaspelitic red chert layers (Chi Fru et al., 2013, 2015). The chert layers contain morphologically distinct Fe minerals dispersed in a fine-grained siliceous matrix (Fig. 3), marked by the notable absence of pyrite and an extremely low S content (Chi Fru et al., 2013, 2015). Layers are tabular and typically laterally continuous at scales of several meters, whereas wave and current structures (e.g., cross-lamination) are generally absent from the MFIF. The hematite-rich MFIF

Ernest C 26/2/2018 20:27
Deleted: The MFIF is correlatively interpreted to be in direct stratigraphic contact with Late Pliocene-Early Pleistocene (2.5–1.5 Ma) basement submarine dacitic-andesitic rocks.

laminae (Table 1) are built by massive encrustation of anoxygenic photoferrotrophic-like microbial biofilms by precipitated Fe (Chi Fru et al., 2013). The base of the MFIF outcrop, is visibly mineralized by black diffused bands/veins composed of Mn oxides (Fig. 4 & Table 1).

A markedly ferruginous 2-3 m-thick section immediately overlies the MFIF, comprising a distinct package of Fe-rich beds that transition up the section (Figs 4A & 5). The lower 1-2 m consist of fine-grained sandstone beds that are well to moderately sorted, containing a 20-40 cm thick portion dominated by plane parallel-laminated sandstone/sandy tuff, massive to plane parallel-laminated sandstone/sandy tuff, and massive sandstone/sandy tuff lithofacies (Fig. 5; Supplementary Fig. 1). The fabric of these Fe-rich sandstone facies consists of sub-angular to sub-rounded and 100–600 μm fine to medium-grained volcaniclastic K-feldspar grains, making up to 75% of the total rock, with variable amounts of quartz and clay mineral grains.

The latter are overlain by a ~1-1.5 m sequence of poorly-sorted tabular clast-supported pebble-to-cobble conglomerate beds with an erosional base, grading upward into coarse to medium-grained sandstone/sandy tuff beds, with alternating conglomerate cycles (Fig. 5), averaging 20-40 cm in thickness. The cobble/pebble conglomerate clasts include intraformational volcanic rocks (dacite, andesite), allochthonous volcaniclastic sandstone, and volcaniclastic microclasts (e.g. K-feldspar), cemented by hematite (Fig. 5; Chi Fru et al., 2013; Kilias et al., 2013a). Towards the westernmost edge of the "Little Vani" section, there is a facies change from the graded pebbly conglomerate/sandy tuff rhythms to a predominantly Fe-rich conglomerate bed (Fig. 6A), termed the conglomerate-hosted IF (CIF) in Chi Fru et al. (2015), with a maximum thickness of ~0.5 m and a cobble size range of ~10 cm. The Fe-rich conglomerate bed transitions upward into medium-grained pebbly reddish

ferruginous sandstones with thin volcanic rock and sandstone pebble lenses. This, in turn, grades upwards into a very-fine-grained greenish glauconite-bearing plane parallel-laminated sandstone to siltstone bed; characterized by soft-sediment deformation structures, such as flame structures, convolute bedding and lamination structures, loop bedding, load casts, and pseudonodules (Supplementary Figs 1-2).

The "Little Vani" section is eventually capped along an erosional surface by an overlying 1-2 m thick section dominated by medium to fine-grained and moderately to poorly-sorted reddish Fe-rich tabular sandstone beds, 10–40 cm thick, topped by patchy sub-cm to cm-thick Mn-rich sandstones (Fig. 5; Supplementary Figs 1-2). Dominant lithofacies of the Fe-rich sandstone cap include planar and hummocky cross-bedding, exhibiting bioturbation in places. The Fe-rich lithofacies cap is laterally discontinuous, thinning out basinwards towards the N-NE, and can be observed smoothly grading into a 1-2 m thick section composed of cm to sub-cm-thick Mn–rich volcaniclastic sandstone lithofacies, described below in Section B. No Fe-rich hydrothermal feeder veins are obvious in the MFIF. However, feeder veins and Mn horizons can be observed to truncate laminations in the MFIF, and up through the whole "Little Vani" section (e.g., Figs 4C & 5).

The MFIF rests directly on the submarine dacites-andesites that were deposited in a relatively shallow submarine environment (Stewart and McPhie, 2006). The fine-grained, finely laminated nature of the MFIF, and, the lack of evidence of current or wave structures (e.g., symmetric ripples or hummocky cross-stratification), coupled to the absence of volcanogenic detrital particles and intraclast breccia structures, indicate a low energy sedimentation environment, marked by negligible volcanic interference (e.g., Tice and Lowe, 2006; Konhauser et al., 2017). This interpretation is supported by the observed enrichment of Fe in the MFIF; a

characteristic of relatively deeper water lithofacies (Konhauser et al., 2017). This view is compatible with the proposition that hematite enrichment in the MFIF was under the control of photoferrotrophic biofilms (Chi Fru et al., 2013) known to thrive at lower light intensities (Kappler et al., 2005; Li et al., 2013; Konhauser et al., 2017). The quiet environmental conditions would have ensured the formation of such stable photoferrotrophic biofilms over extended periods of time that would have facilitated the oxidation of hydrothermally released Fe(II) and the depositon of Fe(III) minerals.

In the overlying sandstone-conglomerate facies, the presence of sedimentary structures indicative of wave action and currents (e.g. cross-stratification), that signify rapid deposition during a high energy event, are consistent with a switch to a shallow-submarine high energy environment (Stewart and McPhie, 2006; Chi Fru et al., 2015). This shift in depositional environments may have been controlled by a combination of submarine volcano-constructional processes, synvolcanic rifting and volcano-tectonic uplift known to have formed the CVSB (Papanikolaou et al., 1990; Stewart and McPhie, 2006).

3.2 Section B (36°44'35.11''N, 24°21'11.25''E)

This ~8-10 m thick fault-bounded stratigraphic section, here referred to as "Magnus Hill", is the type section that contains the NFIF (Figs 2 & 7; Supplementary Figs 3-4). Two lithostratigraphic units—a lower unit A and an upper unit B—are identified in this study. Unit A is made up of a lower sandstone facies that is ~4-5 m thick, dominated by a Mn-oxide cement, overlain by reddish brown Fe-rich massive sandstone beds (Fig. 8 & Supplementary Figs 3-4). The lower sandstone facies represents the host of the main economic grade Mn oxide ores in the CVSB. This constitutes part of a separate study devoted to the Mn ores and will not be dealt with

Ernest Chi Fru 22/2/2018 09:18
Deleted: The overlying lithofacies sequence record a switch to faster accumulation of volcaniclastic turbidites on the quiet MFIF deposit, with the fine, medium to coarse-grained sandstone lithofacies typifying deposition during low and high density turbiditic flows in the middle to inner parts of a turbidite fan-like environment (Lowe, 1982; Mutti 1992; Talling et al., 2012; Orme and Laskowski, 2016; Shanmugam, 2016; Wang et al., 2017). Massive conglomerates containing both allochthonous sandstone clasts and intraformational andesite-dacite are interpreted as channelized submarine debris flows or slump deposits sourced from adjacent topographic highs (Lowe, 1982; Stewart and McPhie, 2006; Orme and Laskowski, 2016). Also, deposition from a waning low density turbidity current is indicated by the upward fining bed of pebbly Fe-rich sandstone, greenish glauconite bearing sandstone and laminated siltstone. Up section, the abundance of parallel and cross stratified Fe-rich and Mn-rich sandstone facies along an erosional surface, reflect a change in deposition to a high energy, shallow submarine shoreface/foreshore setting, above a wave base. ... [1]

further here. Unit B, ~5 m thick, unconformambly overlies unit A and comprises two distinct packages of beds that transition up section from brownish pebble conglomerate layers (0.5-1.0 m thick), in contact with the very fine-grained NFIF deposit (Supplementary Fig. 8 & 9). The NFIF is capped by patchy cm-thick crustiform Mn oxides. Bifurcating feeder veins composed of barite, quartz and Mn-/Fe-oxide minerals cut through the underlying sandstone beds (Supplementary Fig. 4).

The NFIF is composed of strongly banded Fe-rich rocks (Fig. 7) exposed on the topmost part of "Magnus Hill". About 2-3 m thick, the NFIF consists of mm to sub-mm thick, dark grey and brown Fe-rich bands, interbanded with reddish brown Si-rich layers (Figs 7 & 9-11; Supplementary Figs 10-11). Sedimentary structures in the NFIF are predominantly characterized by rhythmic mm to sub-mm thick laminations (e.g., Fig. 7). The iron oxide-rich bands made up mainly of hematite (Table 1 & Fig. 10C) are typically composed of very fine-grained angular to sub-angular volcanic dust material (i.e., fine volcanic ash with particle size under 0.063 mm, K-feldspar, tridymite and cristobalite (Table 1) in an amorphous Si and crystalline hematite matrix (Fig. 12)). The predominantly amorphous Si-rich bands are typically planar, finely laminated and composed of microcrystalline to cryptocrystalline ferruginous chert.

The NFIF is directly overlain by a ~1 m thick laminated to massive well-indurated, nodular-pisolitic ironstone bed (Fig. 8A, C & D) that locally preserves a sub-horizontal fabric reflecting the bedding in the original sediment or contain various ferruginous clasts such as fragments, nodules, pisoliths, and ooliths set in a hematite-rich siliceous matrix (Fig. 8C). Scattered cm scale pisoliths display a crude concentric internal layering, characterized by open and vermiform voids filled by cauliflower-like Mn oxides overprint (Fig. 8D). The ferruginous NFIF lithofacies are interpreted

Ernest Chi Fru 22/2/2018 09:28

Deleted: Sandstone beds are moderately to well-sorted and 5-15 cm thick, and Mn-mineralized lithofacies include plane parallel-laminated sandstone, plane parallel laminated to rippled sandstone, planar cross-bedded sandstone, and massive sandstone. Secondary lithofacies include thinly bedded (1-5 cm thick) greenish glauconite-bearing heterolithic sandstone and thin (< 5 cm thick) white to pale-brown sandy tuff beds interbedded with the other Lithofacies. The sandstone facies host the main economic grade Mn oxide ores in the CVSB, which typically construct texturally diverse cements associated with a variety of volcaniclastic detritus (i.e., K-feldspar, lithic fragments, altered volcanic glass, quartz, sericitized plagioclase, chloritized biotite) and authigenic barite and or glauconite. This constitutes part of a separate study devoted to the Mn ores and will not be dealt with further here, as the focus of the current study is on the IFs. Kilias (2011), however, suggested that many of the sedimentary structures identified within the Mn–mineralized sandstone lithofacies are associated with microbial mat growth.

476 to represent the deepest water deposits in the "Magnus Hill" section based on its very
477 fine-grained sedimentary composition, fine laminations and a paucity of intraclast
478 breccias. These, combined with the lack of evidence for wave and current-formed
479 sedimentary structures (e.g., hummocky cross-stratification, trough, ripple cross-
480 stratification, and erosional contacts), indicate quiet water low energy sedimentation,
481 likely below wave base (Simonson and Hassler, 1996; Trendall, 2002; Krapež et al.,
482 2003; Konhauser et al., 2017).

483 We interpret that each graded Fe oxide-rich band of the NFIF (Supplementary
484 Fig. 9), represents an individual fallout deposit from a proximal pyroclastic eruption.
485 This interpretation is supported by normal grading in fine volcanic ash content that
486 reflects their likely origin as pyroclastic fallout deposits in an otherwise quiet water
487 setting. For example, tridymite is a stable SiO_2 polymorph formed at low pressures of
488 up to 0.4 GPa and at temperatures of ~870-1470 ^{o}C (Swamy et al., 1994; Morris et al.,
489 2016). The coincidence of tridymite formation with silicic volcanism is in agreement
490 with the widespread distribution of andesite, dacite and rhyolite lava domes in the
491 CVSB. For example, vapour phase production of tridymite together with sanidine
492 identified in this study (Fig. 10) and Fe oxides is principally associated with rhyolite
493 ash flow (Breitkreuz, 2013; Galan et al., 2013). Similarly, Cristobalite is a SiO_2
494 polymorph associated with high temperature rhyolitic eruptions (Horwell et al., 2010).
495 Finally, in situ carbonaceous laminations are absent, suggesting that benthic microbial
496 mat growth had no influence on deposition of the NFIF. Ironstones overlying the
497 NFIF are difficult to interpret with the existing data, but may represent supergene
498 ferruginous duricrust formation resulting from subaerial weathering (Anand et al.,
499 2002).
500

Ernest Chi Fru 22/2/2018 09:31
Deleted: (e.g., Trower and Lowe, 2016, and references therein)

Ernest Chi Fru 22/2/2018 09:33
Deleted: This interpretation is consistent with (1) up section lithofacies change from predominantly sandstone facies of the lower unit to conglomerate facies (Fig. 8B), probably related to a series of channel deposits in an inner-turbidite fan-like setting (Orme and Laskowski, 2016). This sedimentary sequence shows overall deepening from a tidal to shoreface zone depositional environment to an offshore zone during periods of high sea level stand (Trower and Lowe, 2016); (2) conclusions of previous workers suggest that lithofacies with Fe-rich composition similar to the NFIF, were deposited from seawater in a basinal settings (Lowe and Byerly, 1999; Tice and Lowe, 2006). The hypothesized deepening of the "Magnus Hill" section is generally consistent with the interpretation that active rifting was occurring during the filling of the CVSB (Papanikolaou et al., 1990; Stewart and McPhie, 2006; Liakopoulos et al., 2001; Papavassileiou et al., 2017), resulting in the transition from a relatively shallow and deeper water setting represented by the sandstone and conglomeratic deposits, to a relatively deeper quiet water environment, characterized by the finely laminated NFIF facies (Trower and Lowe, 2016).

Ernest Chi Fru 22/2/2018 09:33
Deleted: Sedimentary structures and microbial mat fabrics (Kilias et al., 2011) in lithostratigraphic unit A are interpreted to record a variation between storm-dominated shallow-marine (lower shoreface), stable shallow-marine environment with low sedimentation rate in an upper to middle shoreface, and tide-influenced environments (e.g. Noffke et al., 2003; Ramos et al. 2006; Kilias, 2011; Ossa et al., 2016).

Ernest Chi Fru 22/2/2018 09:36
Deleted: s 8 &

Ernest Chi Fru 23/2/2018 20:46
Deleted: (Stiegler et al., 2011; Trower and Lowe, 2016)

Ernest Chi Fru 23/2/2018 21:36
Deleted: (Lowe, 1999)

Ernest Chi Fru 23/2/2018 21:36
Deleted: Koike et al., 2013;

Ernest Chi Fru 22/2/2018 09:39
Deleted: (Trower and Lowe, 2016)

Ernest Chi Fru 22/2/2018 09:41
Deleted: primary granular iron formations (GIF); i.e., a facies transition from BIF-style to GIF-style IF (e.g., Bekker et al., 2010), or

3.3 Geochemistry

3.3.1 Geochemistry of the individual Fe-rich and Si-rich bands

The SEM-EDS-electron micrographs of the NFIF thin sections reveal distinct Fe bands and Si-rich layers alternating periodically with each other in a fine sediment matrix as shown by the grain size (Figs 9 & 11 & Supplementary Figs 9-11). Laser ablation ICP-MS line analysis indicates Si and Fe count intensities in the Milos BIF-type rocks are comparable to the 2.5 Ga Precambrian BIF reference from the Kuruman IF formation, Transvaal Supergroup, South Africa (Fig. 11). The laser ablation ICP-MS data further show an inverse correlation between Fe and Si, the two major elemental components of BIFs, irrespective of the thousands of millions of years gap separating the Precambrian deposit from the recently formed Milos IF formation.

Ernest C 27/2/2018 18:49
Deleted: that dramatic fluctuations in Fe concentrations control the Si to Fe ratio in both types of rocks, despite the thousands of millions of years gap between them.

3.3.2 Mineralogy of the individual Fe-rich and Si-rich bands

No other Fe(III)(oxyhydr)oxide minerals have been identified in the Cape Vani Fe-rich facies different from hematite. Electron imaging of the NFIF Fe-rich bands suggests Si, Al and K-rich phases are mostly associated with the volcaniclastic material predominated by K-feldspar clasts (Fig. 9; Supplementary Figs 10 & 11). A unique feature of the NFIF is that the hematite in the Fe-rich bands occurs in tight association with a carbonaceous material (Fig. 10C), but not for the hematite in the Fe-rich sandstones and in the MFIF. This is also the case for the CIF overlying the MFIF. Hematite showing a fluffy texture and at times presenting as framboidal particles, is sprinkled in the Si-rich cement containing traces of Al and K in the MFIF rocks (Fig. 3). Lack of association of the framboidal-iron-rich particles with S, following SEM-EDS analysis, rules out a pyrite affiliation and is consistent with the

non-sulfidic depositional model suggested by the sequential iron extraction redox proxy (Fig. 13D). TEM analysis suggests platy nano-Fe oxide-rich particles predominate in the NFIF and MFIF, confirmed by overlaid X-ray Energy Dispersive spectra taken from selected areas (Fig. 12) and consistent with the XRD data showing hematite in both samples. The platy hematite needles in the Milos BIF-type rocks are morphologically, and by size, comparable to hematite needles reported in the ~2.5 Ga Kuruman BIFs (Sun et al., 2015).

Unlike the Fe-rich bands, volcaniclasts in the Si-rich bands are much smaller in size, occurring mainly as fine-grained (Supplementary Fig. 8-11), signifying predominant precipitation during periods of weakened hydrothermal activity. The SiO_2 matrix in both the MFIF and NFIF are fine-grained, occurring mainly as amorphous opal in the NFIF (Figs 10B & 12A-B), whereas in the MFIF it is mainly present as crystalline quartz (Fig. 12C-D). Relative concentrations of Al, K and Ti in the samples are generally low, with bulk-measured concentrations in both the Si-/Fe-rich bands, together with the SiO_2 and Fe_2O_3 content, strongly covarying with continental crust concentrations (Fig. 13A). Mn impregnation of the MFIF, preserved in the form of replacement layers mostly identified as cryptomelane ($[K(Mn^{4+},Mn^{2+})_8O_{16}$) (Table 1), is below detection in the NFIF. Rare hausmannite ($(Mn^{2+}Mn^{3+}{}_2O_4$) was detected in a few cases in the MFIF (Fig. 10D).

3.3.3 Hydrothermal versus continental weathering

Trends of major elements from which CIA indices were calculated (Fig. 13B), covary with those of the continental crust (Fig. 13A). Continental crust averages, refer to the zone from the upper continental crust to the boundary with the mantle (Rudnick & Gao, 2003). The calculated CIA indices average 52 with one outlier at 22 (Fig. 13B).

No distinct relationship could be established between the CIA indices and the respective IFs or between the distinct alternating Si- and Fe-rich bands (Fig. 13). Highly weathered clay minerals resulting from the chemical decomposition of volcanic rocks, e.g., kaolinite representing maximum CIA values of 100 or 75-90 for illite, are absent in the analyzed materials. The absence of carbonates in the rocks strengthened the CIA indices, since CIA indices are expected to be lower when Ca carbonates are present (Bahlburg and Dobrzinski, 2011). TiO_2 content, a detrital proxy, is mostly constant and covaries with the CIA values (Fig. 13B), suggesting little variability and limited continental weathering input. A fairly strong negative linear correlation was found between SiO_2 and Fe_2O_3 values normalized to TiO_2 (inset, Fig. 13B).

3.3.4 Redox reconstruction

Redox reconstruction by sequential iron extraction (Poulton and Canfield, 2005, 2011; Guilbaud et al., 2015; Sperling et al., 2015) is consistent with deposition of both the MFIF and NFIF facies beneath an anoxic, ferruginous bottom water body (Fig. 13C-D). The shale-normalized REE values ($REE_{(SN)}$) for both the MFIF and NFIF are consistent with previous reports (Chi Fru et al., 2013, 2015), showing patterns typical of marine sedimentary environments affected by hydrothermal activity throughout Earth's history (e.g., Planavsky et al., 2010). There is a notable absence of significant negative $Ce_{(SN)}$ anomalies for both the MFIF and NFIF (Fig. 14A-B). These observations are statistically corroborated by true Ce anomalies. Further, the Eu/Eu* anomaly averages for the MFIF and NFIF and the distinct Fe-/Si-rich bands, suggest a ~2× higher Eu/Eu* signal for the Si-rich bands relative to the Fe-rich bands and between the MFIF and NFIF deposits (Fig. 14C). Average Pr and

Ernest C 27/2/2018 21:13
Deleted: calculated as Ce/Ce* ($Ce_{(SN)}/0.5Pr_{(SN)} + 0.5La_{(SN)}$) and Pr/Pr* ($Pr_{(SN)}/0.5Ce_{(SN)} + 0.5Nd_{(SN)}$) and considered significant when Ce/Ce* 0and Pr/Pr* is less than and greater than 1, respectively (Bau et al., 1996; Planavsky et al., 2010) (Fig. 14B).

Yb shale-normalized ratios (Pr/Yb*), a light vs. heavy REE enrichment proxy (Planavsky et al., 2010), indicate similar depleted levels of light and heavy REE in both the NFIF and MFIF, as well as in the Fe- and Si-rich bands (Fig. 14C). This independent verification of the anoxic depositional conditions using the sequential Fe proxy, suggests the NASC normalization protocol effectively captures the redox depositional conditions of the Milos IF.

3.4 Lipid biomarker distribution and chemotaxonomy

Bulk $\delta^{13}C_{org}$ averaged −25.4‰ (SD:±0.22); −25.2‰ (±0.26) for NFIF Fe-/Si-rich bands and −25.6‰ (SD:±0.12) for bulk MFIF, respectively (Table 2). A fractionation effect between the alternating Fe-/Si-rich layers ($\Delta^{13}C_{Fe\text{-}rich\ NFIF\text{-}Si\text{-}rich\ NFIF}$) is estimated to be ~0.23‰ (SD±0.036), while $\Delta^{13}C_{Fe\text{-}rich\ NFIF\text{-}MFIF}$ and $\Delta^{13}C_{Si\text{-}rich\ NFIF\text{-}bulk\ MFIF}$, is 0.13‰ (SD:±0.11) and 0.36‰ (SD:±0.14), respectively. These differences are small and within the margin of error of analysis, suggesting no strong distinction in $\delta^{13}C_{org}$ preserved in the different IFs and their various facies. They are interpreted to mean similar carbon fixation processes operated during intervals of predominant Si and Fe(III)(oxyhydr)oxides deposition in both IFs. Attempts to discriminate between these environments by lipid biomarker analysis revealed mainly C_{16}-C_{19} fatty acid methyl esters (FAME) in the Fe-rich NFIF bands and in bulk MFIF, while the Si-rich NFIF bands contain mainly C_{12}-C_{21} FAMEs, suggesting either selective preservation (lipid recovery was lower in the Fe-rich MFIF bands) or shifts to different potential biological populations during the deposition of the different layers. Preserved lipids discriminate against typical microbial lipid biomarkers like hopanoids, while C3 plant FAME are detected in all studied materials (Fig. 15). However, the anaerobic bacteria indicator, $10MeC_{16:0}$ FAME, was identified in a few bands.

660

661 **4 Discussion**

662 **4.1 Sedimentological processes**

663 The three sub-basin division of the CVSB is consistent with previous proposals
664 suggesting that sedimentation within the CVSB was characterized by active
665 synvolcanic rifting which must have been important in shaping basin topography and
666 the creation of sub-basin architecture (Papanikolaou et al., 1990; Stewart and McPhie,
667 2006; Liakopoulos et al., 2001; Papavassiliou et al., 2017). Moreover, this tectonic
668 regime would suggest that the location(s) of volcanism were continually changing
669 relative to the two stratigraphic sections, which themselves were also being affected,
670 i.e. changes in depositional water depth and sedimentation style or and/or that local
671 submarine or subaerial topographic highs impeded the lateral continuity of
672 sedimentary units (Stewart and McPhie, 2006). Chi Fru et al. (2015) have suggested
673 there is an upward deepening of the overall depositional setting recorded in the "Little
674 Vani" section, consistent with rifting during CVSB infilling time.

675 The CVSB floored by dacitic/andesitic lava domes and overlain by
676 vocaniclastic infill, dates back to Upper Pliocene-Lower Pleistocene. A complex
677 mosaic of lithologically diverse sedimentary units (blocks), confined by neotectonic
678 marginal faults, characterizes the CVSB (Fig. 2). The most pronounced of these faults
679 being the NW-trending Vromolimni-Kondaros fault (Papanikolaou et al., 1990) that
680 has been proposed as the trigger of the hydrothermal activity that deposited Mn ore in
681 the CVSB (Papanikolaou et al., 1990; Liakopoulos et al., 2001; Alfieris et al., 2013;
682 Papavassiliou et al., 2017). The stratigraphically tight coupling between Mn and Fe
683 deposition, linked by Fe oxide minerals in feeder-veins, and positive Eu anomalies
684 (Fig. 14) indicating vent-sourced Fe (Maynard, 2010), associate Fe mineralization to

685 fault-triggered hydrothermalism in the CVSB. This is consistent with models of
686 geothermal fluid circulation along fault lines as conduits for the Mn-rich fluids that
687 formed the Milos Mn ore deposit (Hein et al., 2000; Liakopoulos et al., 2001; Glasby
688 et al., 2005; Kilias, 2011; Papavassiliou et al., 2017). More importantly, the overall
689 complex neotectonic structure of the CVSB (Papanikolaou et al., 1990) would explain
690 the creation of restricted basins, with sedimentological, lithological and geothermal
691 conditions that enabled the development of unique biogeochemical circumstances in
692 which the NFIF and MFIF formed.

693 The presence of the three depositional basins is supported by the fact that the
694 sequence lithologies in each fault-bound unit are characterized exclusively by
695 occurrences of specific and variably thick stratigraphic packages that tend to be
696 absent in others. For example, the MFIF occurs restricted to basin 1 and the NFIF to
697 Basin 3. Basin 2 is further distinguished by 35-50 m thick interbedded ore-grade Mn-
698 mineralized and glauconitic sandstones/sandy tuffs, much less developed in Basins 1
699 and 3 (Fig. 2). The presence or absence of a stratigraphic sequence, together with its
700 thickness variation, are interpreted as a result of local syntectonic sediment formation
701 conditions in each basin as a result of block tectonic movements along fault lines
702 (Papanikolaou et al., 1990). It may also be attributed to unique basin scale water
703 column redox conditions (e.g. Bekker et al., 2010, and references therein), post-
704 depositional erosion and changing sea level stand (Cattaneo & Steel, 2000).

705 The lack of hydrothermal feeder veins or seafloor exhalative structures (i.e.,
706 chimneys) in the MFIF and NFIF lithologies, suggests that hydrothermal Fe(II) was
707 delivered by diffuse flow and that the Milos-IF formed on the seafloor.
708 Further, mineralisation of the MFIF is suggested to have occurred during two major
709 hydrothermal venting stages. The first produced the MFIF and the second

contaminated it with cryptomelane. Cryptomelane in the MFIF is therefore not a replacement product of primary Mn oxides formed during the deposition of the MFIF, because the anoxia prevailing in Basin 1 at the time (Figs 2 & 13C) would have precluded the precipitation of Mn oxide minerals, hinting that a second phase hydrothermal fluid emission rich in dissolved Mn, directly precipitated cryptomelane from solution as a secondary mineral relative to the primary Fe(III)(oxyhydr)oxides in the MFIF. This occurred during an episode when the MFIF deposit must have been exposed to oxygenated fluids, most likely through mixing with seawater at depth, indicated by the abundance of cryptomelane at the base of the MFIF. Our model for cryptomelane precipitation in the MFIF is therefore different from the one suggesting diagenetic transformation of primary Mn ores at Milos (Hein et al., 2001; Liakopoulous et al., 2001; Papavassiliou et al. 2017).

Geomorphological/chemical reconfiguration orchestrated the deposition of the NFIF in a deeper, small-restricted basin (Fig. 2). The deepening of Basin 3 is reflected in the underlying graded conglomerate bed that exhibits an upward fining trend, followed by transition into the fine-grain NFIF. The conglomerate bed may represent rapid deposition during a high-energy event, i.e. storm or mass flow, whereas the upward fining in the bed is better explained by the depositional mechanism losing energy through time. These high-energy conditions apparently must have ceased during the deposition of the overlying NFIF, where we interpret that increased abundance of finely laminated IF and decreased evidence of storm and/or mass flow reworking reflects deepening conditions. The hypothesized deepening of Basin 3 is consistent with the interpretation that active rifting was an important mechanism in the formation of the CVSB (Papanikolaou et al., 1990).

Ernest Chi Fru 22/2/2018 09:53
Deleted: The deepening of Basin 3 is strongly demonstrated by an underlying fine upward grading of a transgressive-type Fe-rich lag deposit, that transitions into the NFIF. This uplifting into shallower water event that prompted second generation deposition of Mn oxides in Basin 2 and the substitution of Fe(III)(oxyhydr)oxides by Mn in sub-Basin 1, potentially triggered this environmental change in Basin 3. The MFIF and NFIF sequences are therefore temporally and spatially distinct (Fig. 2).

4.2 Formation Mechanism of The Milos BIFs

4.2.1 Paragenetic sequence

It is stressed that the previously generalized model proposed for biological deposition of the Milos IF, refers exclusively to parts of what is now designated as MFIF (Chi Fru et al., 2013). The NFIF is strongly banded, but does not display the typical microfossils seen in the MFIF, where diffused microbanding apparently relates to the distribution of microbial mats in thin sections (Chi Fru et al., 2013, 2015). The distinction of microcrystalline quartz and amorphous silica phases in the MFIF and NFIF, respectively, together with nano-crystalline hematite particles, suggests a primary amorphous silica origin in both deposits, diagenetically transformed to quartz in the MFIF. The difference in silica crystallinity between the IFs is concurrent with the older age predicted for the MFIF relative to the NFIF, from reconstructed sequence stratigraphy (Fig. 2). Hematite in BIFs is generally interpreted, based on thermodynamic stability, to be a transformation of various primary Fe(III) minerals, with ferrihydrite often proposed as the principal precipitate from the water column (Glasby and Schulz, 1999; Bekker et al., 2010; Johnson et al., 2008; Percoits et al., 2009). It is thought that acidic pH yields mainly goethite while hematite is produced at circumneutral pH (Schwertmann and Murad, 2007). The notable absence of diagenetic magnetite and Fe carbonates (siderite and ankerite), point to negligible coupling of primary Fe(III) oxyhydroxides reduction to organic matter oxidation by the dissimilatory iron-reducing bacteria during burial diagenesis (Johnson et al., 2008). Minor occurrence of iron-silicate phases (Chi Fru et al., 2015) indicates an origin of the hematite precursor in seawater independent of the iron silicate proposed in some cases (Fischer and Knoll, 2009; Rasmussen et al., 2013, 2014). The up to 50 wt% Fe content recorded in the Fe-rich bands, indicate that large amounts of

772 dissolved Fe(II) was intermittently sourced and deposited as primary Fe(III) minerals,
773 through various oxidative processes in the depositional basin.

774 Importantly, the CIA analysis does not support mass weathering and
775 mineralization of terrestrial Fe and Si, in agreement with the absence of rivers
776 draining into the CVSB (Chi Fru et al., 2013). The specific identification of plant
777 biolipids would at face value imply post-depositional contamination. However,
778 samples were sawn to remove exposed layers and only the laminated bands for the
779 NFIF were analyzed. Modern sediments from Spathi bay, located Southeast of Milos
780 Island where hydrothermal activity is presently ensuing at 12.5 m below sea level,
781 revealed similar plant lipids as recorded in the Quaternary IF (Fig. 15G). Post-
782 depositional contamination with terrestrial plant lipids is therefore ruled out for the
783 idea that recalcitrant plant biomass probably entered the sediments via seawater
784 entrainment at the time of deposition (see Naden et al., 2005). This finding
785 necessitates the careful interpretation of bulk $\delta^{13}C_{org}$ values obtained from both the
786 modern and ancient Milos sediments, involving in situ and ex situ biological
787 contributions to $^{13}C_{org}$ fractionation by various known carbon fixation pathways
788 (Preuß et al., 1989; Berg et al., 2010).

789

790 **4.2.2 Tectono-sedimentary processes and band formation**

791 Fluctuation in hydrothermal activity is proposed to account for the banding in the
792 NFIF (Fig. 16), under redox depositional conditions inferred to be mainly reducing
793 for both investigated IFs, consistent with previous reports (Chi Fru et al., 2013, 2015).
794 Positive Eu anomalies indicate a hydrothermal origin for all but one of the sample
795 suite (Fig. 14A). However, statistically calculated Eu/Eu* anomalies ($Eu_{(SN)}/$
796 $(0.66Sm_{(SN)} + 0.33Tb_{(SN)})$) to correct for differences in Gd anomalies commonly

Ernest C 26/2/2018 22:26

Deleted: Such indication of mixing of the hydrothermal fluids with seawater may be interpreted to negate a reducing depositional environment as suggested by the Ce anomalies. However, Pichler & Veizer (1999) demonstrated that in the unconfined seafloor shallow hydrothermal vent fields at Tatum Bay, Papua New Guinea, experiencing little or no water column stratification, as low as 11% seawater is involved in the precipitation of Fe(III)(oxyhydr)oxides from hydrothermal fluids and at maximum 57%. It is therefore suggested that seawater mixing during deposition was at the lower limits. This is demonstrated by the REE analysis and the presence of anaerobic bacteria biomarkers in the NFIF formation, coupled to sediment lithology and stratigraphy, as explained below.

encountered in seawater (Planavsky et al., 2010) are in the range of 0.1-0.58, averaging 0.42. The lack of statistically significant true negative Ce anomalies (Fig. 14B) supported by sequential Fe redox reconstruction (Fig. 3C-D; Planavsky et al., 2010; Poulton and Canfield, 2005, 2011; Guilbaud et al., 2015; Sperling et al. 2015), indicate a reducing depositional environment for both The MFIF and the NFIF.

CIA analyses traditionally provide relative information on contributions from chemical weathering to sediment deposition, linked to operative hydrological and climatological patterns on land. This information is often gleaned from ancient and modern soils and from reworked siliclastic deposits in marine basins (Maynard, 1993; Bahlburg & Dobrzinski, 2011). The calculated CIA values, however, are closer to the range obtained for unweathered and or only minimally weathered volcanic rocks (e.g., Nesbitt & Young, 1982; Bahlburg & Dobrzinski, 2011), thus pointing to a predominantly volcanic and/or hydrothermal provenance for the clastic sedimentary materials in the IFs.

It has been suggested that the release of reduced submarine hydrothermal fluids contributed towards maintaining water column anoxia during the deposition of Precambrian BIFs (Bekker et al., 2010). The calculated Eu anomalies (Fig. 14) and petrographic data showing volcaniclastic detritus (i.e., K-feldspar, sanidine, tridymite, cristobalite) as key rock components are in agreement with a submarine hydrothermal source for the investigated IFs. The coarse volcaniclastic detritus embedded in the Fe-rich bands compared to the finer particles in the Si-rich layers, highlights rapid oxidation of Fe(II) that coincided with periodic cycles of hydrothermal/volcanic discharge of new materials into the water column. However, the fine-grained nature of both the MFIF and NFIF deposits suggests that deposition likely occurred away from where such activity was occurring or that volcanic/hydrothermal discharge of Fe

Ernest C 23/2/2018 13:26
Deleted: The values are closer to the anoxic water column values calculated for Archean IFs, compared to Paleoproterozoic IFs (Planavsky et al., 2010), which may be due to their deposition in an active volcanic center like most of the Archean Agloma BIFs (Bekker et al., 2010; Chi Fru et al., 2015).

Ernest C 23/2/2018 15:24
Deleted: These reducing conditions are confirmed and shown to have been mainly ferruginous by sequential iron reconstruction of depositional setting redox . The sequential iron proxy records the immediate redox state of the water mass beneath which the sediment accumulated ().

Ernest C 27/2/2018 19:04
Deleted: indices traditionally provide

Ernest C 27/2/2018 19:05
Deleted: indices

and Si was non-eruptive and disruptive. The Fe-rich bands repetitively revealed hematite grains cementing the denser volcaniclastic fragments that gradually diminish upwards into a zone of fine-grained hematite before transitioning into Si-rich bands consisting mainly of finer volcaniclastic detritus. These observations provide three valuable interpretational considerations for proposing a model for the formation of the alternating Si and Fe-rich bands.

1. The Si and Fe oxides-rich bands are primary precipitates formed in the water column, by a process in which the precipitation of amorphous Si occurred during quiescent non-volcanic intervals, with the oxidation and precipitation of reduced Fe intermittently introduced into the water column by volcanic/hydrothermal activity to form the Fe oxides.
2. The repetitive zonation of distinct particle sizes, suggests density gradient sedimentation that requires a water column-like environment, rather than diagenetic alteration of pre-formed sediments by hydrothermal fluids.
3. The reducing depositional conditions do not support sediment diagenesis as an alternative model for explaining the origin of the Milos IF. This is because the oxidation of ferrous Fe supplied in reduced hydrothermal fluids, must interact with a sizeable pool of oxygen, enabling microaerophilic bacteria oxidation of ferrous iron to Fe(III)(oxyhydr)oxides (Johnson et al., 2008). Otherwise, light-controlled photoferrotrophy, an extremely rare sediment characteristic, precipitates Fe oxides in the absence of oxygen in sunlight environments Weber et al., 2006).

4.2.3 Biological involvement

Ernest C 26/2/2018 21:51

Deleted: <#>The style of deposition of the MFIF and NFIF is distinct from the post-depositional infilling of a porous sandstone sediment matrix during the formation of the Mn ores. Instead the deposition of the MFIF and NFIF in restricted portions in the basins not associated with previously accumulated sandstones, and the difficulty and lack of evidence to provide a viable biogeochemical mechanism for the formation of the even bands of alternating Si and Fe-rich layers of several meters high and wide, does not support post-depositional pore filling of a porous sandstone matrix by Fe, as a potential pathway to the formation of the Milos IF.

Hematite precipitation in the MFIF on microbial filaments (Chi Fru et al., 2013) was previously used to propose a generalized basin-scale mechanism for the deposition of Fe-rich rocks in Cape Vani. However, such filaments are absent in the NFIF, while pure hematite grains are tightly bound to relics of an organic matter signal carrying a maximum $\delta^{13}C_{org}$ signature of -25‰ (Table 2). Similar processes are recorded in modern marine sediments where interactions between Fe and free organic matter has been reported to enable the preservation up to 21.5wt% of total organic carbon over geological time scales (Lalonde et al., 2012). Moreover, Fe generally traps and preserves organic matter at redox interfaces (Riedel et al., 2013). The data appear to suggest that the mechanism of Fe(III) (oxyhydr)oxide precipitation and preservation varied between the two IFs. The photoferrotrophic-like filamentous fossils reported in the MFIF (Chi Fru et al., 2013), are absent in the NFIF. This does not, however, rule out the potential role of microbial involvement in Fe(II) oxidation, as diverse microbial taxa carry out this process, several of which are non-filamentous (Chi Fru et al., 2012). However, our data is insufficient to enable clear quantification of the levels of abiotic vs. biotic contribution to Fe(II) oxidation in the NFIF. Nevertheless, the inferred predominantly anoxic depositional conditions as explained above, together with the identification of anaerobic bacteria biomarkers in the laminated bands, intuitively favor significant contribution of anaerobic biological Fe(II) oxidation in the precipitation of primary Fe(III)(oxyhydr)oxides in the NFIF. See Weber et al., 2006, for a review of potential biological pathways to anaerobic Fe(II) oxidation.

Briefly, anaerobic microbial Fe(II) oxidation can proceed via nitrate reduction and by photoferrotrophy to deposit Fe(III)(oxyhydr)oxides. These mechanisms have been linked to microbial contribution to BIF formation (Weber et al., 2006; Kappler et al., 2005) and also for the MFIF (Chi Fru et al., 2013). However, it is also possible

Ernest C 27/2/2018 19:08
Deleted: lack of similar

Ernest C 27/2/2018 19:08
Deleted: ,

Ernest C 27/2/2018 19:09
Deleted: since

925 that microaerophilic neutrophilic Fe(II)-oxidizing bacteria likely played an important
926 role, assuming a depositional setting analogous to the Santorini caldera and Kolumbo
927 shallow submarine volcanoes, where such low-O_2-dependent microbial Fe(II)
928 oxidation has been identified to actively precipitate Fe(III) (oxyhydr)oxides (Kilias et
929 al., 2013b; Camilli et al., 2015). It appears that in the MFIF, precipitating
930 Fe(III)(oxyhydr)oxide minerals were bound and preserved free of organic carbon or
931 that such organic carbon was diagenetically degraded. As was previously shown,
932 Fe(III)(oxyhydr)oxides completely replaced the organic content of the filamentous
933 microfossils in the MFIF (Chi Fru et al., 2013).

934 The $10MeC_{16:0}$ FAME identified in the rocks has been reported in anaerobic
935 organisms coupling nitrite reduction to methane oxidation (Kool et al., 2012), in
936 sulfate and iron-reducing bacterial species such as Desulfobacter, Desulfobacula
937 (Bühring et al., 2005; Dowling et al., 1986; Taylor and Parkes, 1983), Geobacter,
938 Marinobacter and the marine denitrifier, Pseudomonas nautical (Kool et al., 2006;
939 Bühring et al., 2005; Dowling et al., 1986). It had previously been proposed that post-
940 depositional denitrification was a potential pathway for early organic matter removal,
941 justified by the low rock organic carbon and nitrogen content in the Milos BIF-type
942 rocks (Chi Fru et al., 2013, 2015; Table 2). Equally, the detected $10MeC_{16:0}$ FAME
943 has also been found in anaerobic oxidation of methane (AOM) communities (Alain et
944 al., 2006; Blumenberg et al., 2004), originating from sulfate reducing bacteria.
945 However, bulk sediment $\delta^{13}C_{org}$ of −20‰ does not reflect AOM activity that is
946 expected to produce bulk $\delta^{13}C_{org}$ values that are ≤−30‰. Low $10MeC_{16:0}$ FAME
947 concentrations frustrated attempts at acquiring its compound specific isotopic
948 signature to enable further biomolecular level reconstruction of active microbial
949 metabolisms to explain Fe deposition mechanisms.

It is nevertheless puzzling why potential microbial biomarkers typical of marine or hydrothermal vent environments are hardly preserved in the rocks, given that microfossil evidence indicates a vast community of diverse prokaryotic assemblages in the adjacent MFIF (Chi Fru et al., 2013, 2015). Moreover, sediments of the modern Milos hydrothermal system and elsewhere on the HVA, are ubiquitously colonized by microbial life, characterized by the marked large-scale absence or low abundance of higher life forms, including plants (Kilias et al., 2013b; Camilli et al., 2015; Oulas et al., 2015). One possibility could be the discriminatory preservation of lipids related to their selectivity and reactivity towards Fe(III)(oxyhydr)oxides and clays or different pathways to diagenetic degradation (e.g., Canuel & Martens, 1996; Lü et al., 2010; Riedel et al., 2013). As noted, the carbonaceous materials in the BIF-type NFIF rocks occur in tight association with hematite.

Importantly, prokaryotic biomarkers are suggested to poorly preserve in these young BIF analogues. This raises the possibility that this may provide an important explanation for why lipid biomarkers are yet to be extracted from Precambrian BIFs. Moreover, the data are compatible with the low C_{org} recorded in BIFs of all ages, suggesting that the low C_{org} abundance may not be due to metamorphism as often proposed (Bekker et al., 2010) or to C_{org} oxidation by dissimilatory iron reducing bacteria to form ^{13}C-depleted siderite and ankerite during diagenesis (Johnson et al., 2008; Bekker et al., 2010). The Milos BIF-type rocks are unmetamorphosed and lack iron carbonate, yet have vanishingly low C_{org} levels similar to the ancient metamorphosed BIFs. However, an alternative possibility is that the iron oxides may have been reduced through biological oxidation of organic carbon, but carbonate saturation was not reached (Smith et al., 2013).

975

976 **4.2.4 Mn layers and the deposition of the Si-Fe-rich facies**

977 Cryptomelane [K(Mn4+,Mn2+)8O16], which commonly occurs in oxidized Mn
978 deposits resulting from mineral replacement and as open space fillings (Papavassiliou
979 et al., 2016), is also common in the MFIF. This supports the idea of post-depositional
980 impregnation of the base of the MFIF by Mn-rich fluids. Microscopic analysis
981 supports the epigenetic origin of the Mn in the MFIF by revealing Mn oxides growing
982 along fractures, impregnating and replacing Fe minerals (Fig. 4B-F). The
983 macroscopically evident thinning out to disappearance of such Mn-rich horizons up
984 the MFIF, coupled by their development along microfractures emphasizes this
985 epigenetic origin. Mn is not a common feature of the NFIF, even though it sits on top
986 of a thin sandstone layer that is highly mineralized with Mn, locally forming the cap
987 of the main Mn ore at Cape Vani. The generally accepted view is that Mn-rich
988 hydrothermal fluids rose and mineralized the Cape Vani sandstones (Hein et al., 2000;
989 Liakopoulos et al., 2001; Glasby et al., 2005). Based on the stratigraphic location of
990 the MFIF, which pre-dates the Mn-rich sandstones, it is proposed that impregnation of
991 the MFIF by Mn was coeval with large-scale Mn ore mineralization of the Cape Vani
992 sandstones, implying the entire basin was likely oxygenated at the time. The lack of
993 Ce anomalies, confirmed by the sequential Fe extraction proxy data, suggests that
994 both the MFIF and the NFIF formed in anoxic settings. Similar data for the Mn oxides
995 have suggested formation in oxic settings (Glasby et al., 2005; Chi Fru et al., 2015).
996 This implies that Mn epigenetically replaced the MFIF, either because the basin was
997 tectonically uplifted into a high–energy oxygenated shallow water setting or that sea
998 level dropped, leading to partial metasomatism of the base of MFIF, when oxygenated
999 seawater mixed with reduced hydrothermal fluids and precipitated Mn. The lack of

Ernest C 27/2/2018 19:11

Deleted: Cryptomelane [$K(Mn^{4+},Mn^{2+})_8O_{16}$], commonly occurring in oxidized manganese deposits resulting from mineral replacements and as open space fillings (Papavassiliou et al., 2016), common in MFIF, supports the idea of post-depositional impregnation of the base of the MFIF by Mn-rich fluids as discussed above.

Ernest C 27/2/2018 19:13

Deleted: However, more sensitive proxies are needed to resolve and confirm the stratigraphic and REEs-dependent interpretation of potential redox conditions.

significant Ce anomalies in the dataset, combined with the inferred deepening of basin 3 and the anoxic depositional conditions suggested by the sequential iron redox proxy, further indicate that for the final deposition of the NFIF, an eventual deepening event must have been triggered, resulting in deoxygenation of parts of the CVSB.

All of this is feasible with the three-basin-fault-bounded hypothesis as a requirement for movement along fault lines in response to temporal tectonic activation. The upward sequence transition from the Mn-rich sandstone facies, through the pebbly conglomerate and the final termination in the overlying mud-grained NFIF (Fig. 8B), reflect sedimentary features formed during multiple changes in seawater levels (Cattaneo & Steel, 2000).

Uplifting is suggested by potential weathering of the NFIF to form the ferruginous duricrust cap. Comparable ferruginous layers on Precambrian BIFs are linked to pervasive subaerial chemical weathering, via the dissolution of the silica-rich layers and precipitation of relatively stable Fe oxides in the spaces between more resistant hematite crystals (e.g., Dorr, 1964; Shuster et al., 2012; Levett et al., 2016). This collective evidence supports the existence of a geodynamic tectonic system capable of producing shallow oxic to deeper anoxic basin conditions at different times that would explain the existence of Mn and Fe oxide layers within the same sedimentary sequence. For example, it is common knowledge that both Fe and Mn oxides will precipitate in the presence of oxygen (Roy, 1997, 2006), with kinetic rates usually being faster for the oxidation of reduced Fe than reduced Mn. In the Fe(II)-rich conditions that prevail in anoxic settings, abiotic reactions between Fe(II) and Mn oxides, produce Fe(III) leading to the dissolution of the Mn oxides to form reduced Mn, implying Mn oxides should not accumulate (Dieke, 1985). Moreover, under these conditions, biological precipitation of Fe(III) can occur rapidly, leaving dissolved Mn

Ernest Chi Fru 11/3/2018 22:22
Deleted: strongly implies that the underlying Mn-rich facies and NFIF layers formed in shallower and deeper waters, respectively, or that they are separated by an erosional unconformity.underlying Mn-rich layer into the conglomeratic deposit

Ernest Chi Fru 11/3/2018 22:38
Deleted: This study proposes that the NFIF that overlies the transgressive-type conglomeratic lag along an erosional contact surface was likely deposited during maximum flooding, when the basin became stagnant and stratified, and subsequently was uplifted to emergence

Ernest C 23/2/2018 13:31
Deleted: Similar transgression-type lithologies are indicated to have regulated primary sedimentation styles during the deposition of nearshore Paleoproterozoic BIFs (Pufahl and Fralick, 2004; Pufahl et al., 2014).

Ernest Chi Fru 23/2/2018 12:29
Deleted: Moreover, deposition of BIFs in sandstone/grainstone-dominated environments has also been suggested for Precambrian IFs (Simonson, 1985; Simonson and Goode, 1989; Pufahl and Fralick, 2004).

Ernest C 26/2/2018 22:08
Deleted: the

in solution to be deposited when oxygen becomes available. Given that the hydrothermal fluids of the Hellenic Volcanic Arc are commonly enriched in both reduced Fe and Mn, the deposition of the MFIF and NFIF therefore implies there was an existing mechanism that enabled the kinetic discrimination and deposition of the oxides of Fe and Mn into separate settings, most likely dependent on prevailing redox conditions. The accumulation of the ferruginous duricrust layer, overprinted by redox sensitive Mn-nodules, above the NFIF indicates a new shallowing event might have terminated the formation of the NFIF.

4.2.5 Modern analogues on the HVA

Mechanistic explanation for the development of potential stratified waters and reducing conditions during the deposition of the Milos BIF is problematic. However, evidence is available from present shallow submarine hydrothermal analogues in the central part of the HVA, to which the CVSB belongs. These include:

(1) The crater floor of the Kolumbo shallow-submarine volcano (~600×1200 m), which rises from 504 to 18 m below sea level near Santorini, (Sigurdsson et al., 2006; Kilias et al., 2013b).

(2) The N part of Santorini's submerged caldera walls, which rises from 390 m below sea level to over 300 m above sea level (Druitt et al., 1999; Friedrich et al., 2006; Nomikou et al., 2013; Camilli et al., 2015).

(3) The coastal embayments at the Kameni emergent volcanic islands in the centre of the Santorini caldera (Hanert, 2002; Nomikou et al., 2014; Robbins et al., 2016).

The benthic waters within Kolumbo's crater potentially sustain O_2 depleted conditions via stable CO_2-induced water column densification, and accumulation of

acidic water (pH~5), extending ~10 m above the CO_2 venting crater floor (Kilias et al., 2013b). This phenomenon is believed to lead not only to obstruction of vertical mixing of bottom acidic water, but also to O_2 deprivation by precluding efficient transfer of oxygenated surface seawater into the deeper crater layer. In addition, diffuse CO_2 degassing is believed to be linked to the formation of Fe microbial mats and amorphous Fe(III) oxyhydroxides on the entire Kolumbo crater floor (Kilias et al., 2013b). Prerequisites for the O_2-depleted conditions to happen are the closed geometry of the Kolumbo crater and the virtually pure CO_2 composition of the released hydrothermal vent fluids that produce O_2 stratification along a stable CO_2-pH gradient.

A similar scenario is reported for the Santorini caldera, where large (~5 m diameter) CO_2-rich, acidic (pH, ~5.93) hydrothermal seafloor pools and flow channels, develop within m-thick microbial Fe-mats on the seafloor slope at 250-230 m below sea level. Persistent hypoxia exists in these pools, representing concentrated seafloor CO_2 accumulation centers generated by hydrothermal venting (Camilli et al., 2015). Here, the dissolved O_2 content (~80 μM or less) in the pools is ~40 % depleted relative to the surrounding ambient seawater (Camilli et al., 2015). These hypoxic conditions are comparable to or even lower than those measured in the CO_2-rich oxygen minimum zones of coastal oceans, relative to seawater existing in equilibrium with atmospheric pO_2 and pCO_2 pressures (Paulmier et al., 2008, 2011; Franco et al., 2014). These conditions enable strong redox stratification of the pool waters, in which unique Si- and Fe-rich microbial mats are associated with amorphous opal and Fe(III)(oxyhydro)xides (Camilli et al., 2015). Importantly, the Fe microbial mats in these CO_2-rich hypoxic pools are affiliated with specific microaerophilic Fe(II)-oxidizing bacteria that accumulate Fe(III) oxyhydroxides (Camilli et al., 2015; Oulas

et al., 2015). These Fe bacteria are implicated in the deposition of the Precambrian BIFs (Konhasuer et al., 2002; Planavsky et al., 2009; Bekker et al., 2010).

Hypoxia is also associated with the water column of the Fe(III)-rich coastal embayments and their hydrothermal vents (≤1.0 m water depth), Kameni islands (Hanert, 2002; Robbins et al., 2016 and references therein). Venting fluids are warm (20-40 ^{o}C), acidic to circumneutral (pH 5.5-6.9), enriched in CO_2, Fe and Si (Georgalas & Liatsikas, 1936, Boström et al., 1990; Handley et al., 2010; Robbins et al., 2016). Water column stratification is expressed as decreasing O_2 with depth that is positively related to Fe(III)(oxyhydr)oxide density and microaerophilic Fe(II)-oxidizing bacterial prevalence (Hanert, 2002). Robbins et al. (2016) found that Fe(III)-rich suspended particulate material in these "Fe bays" may be associated with anoxia, extending up to the air-seawater interface, near the hydrothermal vents (Hanert, 2002). They consist of ferrihydrite, goethite and microaerophilic Fe(II) oxidizers.

However, the biogeochemical occurrence of these phenomena within the localized confines of the Santorini caldera and Kolumbo crater, may however be difficult to achieve in ordinary shallow submarine hydrothermal settings, such as those occurring on the coast of present day Milos. The same may be true for Tatum Bay, where non-volcanic and unconfined diffuse hydrothermalism is widespread (Dando et al., 1996; Pichler & Dix, 1996; Pichler & Veizer, 1999; Stüben et al., 1999; Rancourt et al., 2001; Varnavas et al., 2005).

In the Kolumbo and Santorini hydrothermal fields, benthic pH averages 5.5 and the deposition of carbonates is markedly absent (Kilias et al., 2013b, Camilli et al., 2015; Robins et al., 2016). This conforms to observations in the MFIF and NFIF units where carbonate mineralization is not detected, thereby suggesting a similar low pH

depositional environment for both the MFIF and NFIF. Ubiquitous Fe(III)(oxyhydr)oxide precipitation and enriched Si content are prevalent in the CO_2-rich-hypoxic shallow submarine Santorini caldera slope pools and the Kameni Fe-embayments where sulfide precipitation is inhibited (Camilli et al., 2015), or extremely rare (Robbins et al., 2016). Such sulfide-poor conditions are critical for the formation of BIFs (Bekker et al., 2010).

A high Si-Fe(III)(oxyhydr)oxide content, absence of carbonate and sulfide mineralization, coupled to a generally low S content have also been demonstrated for the CVSB Fe formations (Chi Fru et al., 2013, 2015). This depositional situation is different, for example, from the unconfined shallow submarine hydrothermal systems in Tatum Bay and Bahia Concepcion Bahia Carlifornia Sur, Mexico, where authigenic carbonate deposition is widespread (Canet et al., 2005; Pichler & Veizer, 1996, 2005). Moreover, there is strong geological evidence that within volcanic crater environments associated with high CO_2 emission, long-term water column redox stratification is possible under these special conditions. Further evidence is found in volcanic crater lakes (for example the shallow 205 m deep lake Nyos in Cameroon—renowned as one of Earth's three CO_2 saturated volcanic lakes (Ozawa et al., 2016; Kling et al., 2005). Here CO_2-induced water column stratification is associated with bottom reducing conditions characterized by a low sulfate and high Fe bottom water content relative to surface concentrations (Tiodjio et al., 2014).

5 Concluding remarks

This study shows the following new insights in light of what was previously known:

Ernest Chi Fru 22/2/2018 10:08

Deleted: Moreover, the anoxic amorphous Si-Fe(III)(oxyhydr)oxide-rich-sulfide-poor shallow submarine environments at Kameni islands, have been independently proposed as a modern analogue environment for Precambrian BIF precipitation (Hanert, 2002; Robins et al., 2016).

1. At least two distinct IFs (MFIF and NFIF) formed from hydrothermal mud, within two localized sub-basins in the ~1 km-long CVSB, ~2.66-1.0 Myr ago, controlled by local tectonism.
2. Local conditions of elevated and cyclic supply of ferrous Fe and dissolved Si, accompanied by strict bottom water anoxic conditions in a localized reservoir cut off from the open ocean, can in principle allow the deposition of BIF-type rocks in a modern marine setting. The rarity of these types of deposits however suggests that such conditions are extremely difficult to attain under the modern oxygen-rich atmosphere.
3. A working model that band formation may involve potential Fe(III)(oxyhydr)oxide filling of sediment pores and fractures during diagenesis, is not supported by the data. In addition to the lack of observation of such phenomena, as demonstrated for replacive Mn mineralization, calculated Ce and Eu anomalies, together with preliminary sequential iron extraction analysis (Poulton and Canfield, 2011; data not shown), are suggestive of anoxic depositional conditions likely induced by the release of reduced hydrothermal/volcanic fluids into a cutoff sedimentary basin.
4. The precipitation of Fe(III) and Mn oxides require oxygen. In the absence of oxygen, Mn is not oxidized, while light and photoferrotrophy will oxidize reduced Fe to Fe(III)(oxyhydr)oxides. Both light and photoferrotrophy are however extremely rare characteristics of anoxic sediments, but a common feature of anoxic Fe^{2+}-rich waters, where photoferrotrophy is widespread (Weber et al., 2006). Collectively, these observations provide an important feasible mechanism for the knife sharp separation of the Mn oxide-rich ores in the CVSB that are also Fe(III)(oxyhydr)oxide-rich, from the highly

localized MFIF and NFIF deposits that are Fe(III)(oxyhydr)oxide-rich but Mn oxide-poor.

5. The mechanism of formation of the MFIF and NFIF therefore most likely involved exhalative release of reduced hydrothermal/volcanic fluids into a restricted and deoxygenated seafloor water column where the oxidation of reduced Fe to Fe(III)(oxyhydr)oxides occurred, most likely by the activity of photoferrotrophs (Chi Fru et al., 2013). Microaerophilic oxidation of Fe(II) was likely critical, but that remains to be shown.
6. Episodic intensification of hydrothermal activity is identified as a main mechanism for the formation of the millimetric BIF bands, adding to the biological mechanism that was inferred from fossil records in the MFIF (Chi Fru et al., 2013, 2015).
7. Abiotic Si precipitation was apparently much slower relative to Fe(III) precipitation, resulting in Fe-rich bands in the NFIF forming in association with large fragments of volcaniclast and the Si-rich bands with finer Si grains.
8. A combination of the above processes produced pulses of Si and Fe in the millimetric Si and Fe-rich bands in the NFIF.
9. The Milos rocks fulfill sedimentological, chemical and mineralogical characteristics that established them as potentially the youngest known BIFs; following the simplistic definition that BIFs are sedimentary rocks composed of alternating layers of Fe and Si containing at least 15% Fe.
10. Whether the rocks described here are analogues of Precambrian BIFs or not, and whether the proposed formation mechanisms match those that formed the ancient rocks, is opened to debate. However, there are many similarities to proposed Precambrian BIF depositional models (e.g. Klien, 2005; Beukes and

Gutzmer, 2008; Smith et al., 2013; Bekker et al., 2010; Klein and Beukes, 1992). Importantly, the present study provides mechanisms by which rocks with alternating Fe and Si-rich bands can be formed in the modern ocean.

Data availability. Data can be accessed by request from any of the authors

Author contributions. ECF, SK and MI designed the study. ECF, SK, KG and MI performed fieldwork. ECF, JER, KG, IM and QH performed research. ECF, SK, KG, MI, QH and JER interpreted data. ECF and SK wrote paper.

Competing interests. The authors declare that they have no conflict of interest.

Acknowledgments. Ariadne Argyraki, Nicole Posth, Nolwenn Callac and Eva Zygouri are acknowledged field assistance during sampling and for stimulating intellectual discussions. Special thanks to Christoffer Hemmingsson for contributing to the SEM and XRD analyses. This work is funded by the European Research Council grant No. 336092 to ECF and the Swedish Research Council grant No. 2012-4364 to MI.

References

Alain, K., Holler, T., Musat, F., Elvert, M., Treude, T., and Kruger M.; Microbiological investigation of methane- and hydrocarbon-discharging mud volcanoes in the Carpathian Mountains, Romania. Environ. Microbiol., 8, 574–590, 2006.

1240 Alfieris, D. and Voudouris, P.: Ore mineralogy of transitional submarine magnatic-
1241 hydrothermal deposits in W. Milos Island, Greece. Bul. Acad. Sci., 43, 1–6, 2005.
1242 Alfieris, D.; Geological, geochemical and mineralogical studies of shallow submarine
1243 epithermal mineralization in an emergent volcanic edifice, at Milos Island (western
1244 side), Greece. PhD thesis, Department Geowissenschaften der Universität
1245 Hamburg, 2006.
1246 Alfieris, D., Voudouris, P., and Spry, P.: Shallow submarine epithermal Pb–Zn–Cu–
1247 Au–Ag–Te mineralization on western Milos Island, Aegean Volcanic Arc, Greece:
1248 Mineralogical, geological and geochemical constraints. Ore Geol. Rev., 53, 159–
1249 180, 2013.
1250 Anand, R. R., Paine, M., and Smith, R.E.: Genesis, Classification and Atlas of
1251 Ferruginous Materials, Yilgarn Craton. CRC LEME Open File Report vol. 13,
1252 CSIRO Exploration and Mining, Perth, 2002.
1253 Bahlburg, H. and Dobrzinski, N.: A review of the Chemical Index of Alteration (CIA)
1254 and its application to the study of Neoproterozoic glacial deposits and climate
1255 transition. Geol. Soc. London Mem., 36, 81–92, 2011.
1256 Bau, M. and Dulski, P.: Distribution of yttrium and rare- earth elements in the Penge
1257 and Kuruman Iron-Formations, oxidative scavenging of cerium on hydrous Fe
1258 oxide, Transvaal Supergroup, South Africa. Precambrian Res., 79, 37–55, 1996.
1259 Berg, I.A., Kockelkorn, D., Ramos-Vera, W.H., Say, R.F., Zarzycki, J., Hügler, M.,
1260 Alber, B.E., and Fuchs, G.: Autotrophic carbon fixation in archaea. Nat. Rev.
1261 Microbiol., 8, 447–460, 2010.
1262 Bekker, A., Slack J.F., Planavsky, N., Krapež B., Hofmann, A., Konhauser, K.O., and
1263 Rouxel, O.J.: Iron formation: The sedimentary product of a complex interplay

among mantle, tectonic, oceanic, and biospheric processes. Econ. Geol., 105, 467–508, 2010.

Beukes, N.J., and Gutzmer, J.: Origin and Paleoenvironmental significance of major Iron Formations at the Archean-Paleoproterozoic boundary. Econ. Geol. 15, 5–47, 2008.

Beukes, N.J., Swindell, E.P.W., Wabo, H.: Manganese deposits of Africa, Episodes v. 39, 285–317, 2016.

Blumenberg, M., Seifert, R., Reitner, J., Pape, T., and Michaelis, W.: Membrane lipid patterns typify distinct anaerobic methanotrophic consortia. Proc. Natl. Acad. Sci. U.S.A., 101, 11111–11116, 2004.

Boström, K., Honnorez, J., Joensuu, O., and Rydell, H.: Chemistry of hydrothermal solutions in drill hole GPK-1, Palaea Kameni, Santorini, Greece. Proceedings of the third international congress, Santorini, Greece. 3, 257–260, 1990.

Bronn, H.G.: Ubersicht der Fossilen Uberreste in den tertiären subappeninischen Gebirgen. Italiens Tertiär-Gebilde und deren organische Einschlüsse. Heidelberg pp. XII + 176 + 1 pl, 1831.

Bouma, A.H.: Sedimentology of Some Flysch Deposits. Amsterdam, Elsevier, pp. 168, 1962.

Breitkreuz, C.: Spherulites and lithophysae—200 years of investigation on hightemperature crystallization domains in silica-rich volcanic rocks. Bull. Volcanol., 75, 1–16, 2013.

Bühring, S.I., Elvert, M., and Witte, U.: The microbial community structure of different permeable sandy sediments characterized by the investigation of bacterial fatty acids and fluorescence in situ hybridization. Environ. Microbiol., 7, 281–293, 2005.

Ernest Chi Fru 26/2/2018 10:55
Deleted: Beukes, N. J. and Klein, C.: Geochemistry and sedimentology of a facies transition—from microbanded to granular iron-formation—in the early Proterozoic Transvaal Supergroup, South Africa. Pre. Res., 47, 99–139, 1990.

1295 Camilli, R., Noumikou P., Escartin, J., Ridao, P., Mallios, A., Kilias, S.P., Argyraki,
1296 A., and the Caldera Science Team: The Kallisti Limnes, carbon dioxide
1297 accumulating subsea pools. Sci. Rep., 5, 12152, doi:10.1038/srep12152.
1298 Canuel, E.A. and Marten, C.S.: Reactivity of recently deposited organic matter:
1299 Degradation of lipid compounds near the sediment-water interface. Geochim.
1300 Cosmo. Acta, 60, 1793–1806, 1996.
1301 Canet, C., Prol-Ledesma, R.M., Torres-Alvarado, I., Gilg, H.A., Villanueva, R.E., and
1302 Cruz, R.L.S.: Silica-carbonate stromatolites related to coastal hydrothennal venting
1303 in Bahia Concepcion, Baja California Sur, Mexico. Sed. Geol., 174, 97–113, 2005.
1304 Cattaneo, A. and Steel, R.J.: Transgressive deposits: a review of their variability.
1305 Earth Sci. Rev., 62, 187–228, 2003.
1306 Chi Fru, E., Ivarsson, M., Kilias, S.P., Bengtson, S., Belivanova, V., Marone, F.,
1307 Fortin, D., Broman, C., and Stampanoni, M.: Fossilized iron bacteria reveal a
1308 pathway to the origin banded iron formations. Nat. Comm., 4, 2050 DOI:
1309 10.1038/ncomms3050, 2013.
1310 Chi Fru, E., Ivarsson, M., Kilias, S.P., Frings, P.J., Hemmingsson, C., Broman, C.,
1311 Bengtson, S. and Chatzitheodoridis, E.: Biogenicity of an Early Quaternary iron
1312 formation, Milos Island, Greece. Geobiology, 13, 225–44, 2015.
1313 Dando, P.R., Hughes, J.A., Leahy, Y., Niven, S.J., Taylor, L.J. and Smith, C.: Gas
1314 venting rates from submarine hydrothermal areas around the island of Milos,
1315 Hellenic Volcanic Arc. Cont. Shelf Res., 15, 913–925, 1995.
1316 Dieke, P. Concentration of Mn and separation from Fe in sediments—I.
1317 Kinetics and stoichiometry of the reaction between birnessite and
1318 dissolved Fe(II) at 10°C. Geochim. Cosmo. Acta, 49, 1023–1033, 1985.

1319 Dorr, J.V.N.: Supergene iron ores of Minas Gerais, Brazil. Econ. Geol., 59, 1203,
1320 1964.
1321 Dowling, N.J. E., Widdel, F., and White, D.C.: Phospholipid ester-linked fatty-acid
1322 biomarkers of acetate-oxidizing sulfate-reducers and other sulfide-forming
1323 bacteria. J. Gen. Microbiol., 132, 1815–1825, 1986.
1324 Druitt, T. H. L., Edwards, R. M., Mellors, D. M., Pyle, R. S. J., Sparks, M., Lanphere,
1325 M. D., and Barreirio, B.; Santorini Volcano. Geol. Soc. Mem. London, 19, 165,
1326 1999.
1327 Fischer, W.W. and Knoll, A.H.: An iron shuttle for deepwater silica in Late Archean
1328 and early Paleoproterozoic iron formation. Geol. Soc. Am. Bull., 121, 222–235,
1329 2009.
1330 Franco, A.C., Hernández-Ayón, J.M, Beie,r E., Garçon, V., Maske, H., Paulmier, A.,
1331 Färber-Lorda, J., Castro, R., and Sosa-Ávalos, R.: Air-sea CO_2 fluxes above the
1332 stratified oxygen minimum zone in the coastal region off Mexico. J. Geophy. Res.,
1333 119, 2923–2937, 2014.
1334 Friedrich, W.L., Kromer, B., Friedrich, M., Heinemeier, J., Pfeiffer, T., and Talamo,
1335 S.: Santorini eruption radiocarbon dated to 1627-1600 BC. Science, 312, 548–548,
1336 2006.
1337 Fytikas, M., Innocenti, F., Kolios, N., Manetti, P., Mazzuoli, R., Poli, G., Rita, F., and
1338 Villari, L.: Volcanology and petrology of volcanic products from the island of
1339 Milos and Neighbouring islets. J. Vol. Geotherm. Res., 28, 297–317, 1986.
1340 Galan, L.D.P., Doval, M., La Iglesia, A., Soriano, J., and Chavez, L.: Occurrence of
1341 silica polymorphs nanocrystals in tuffaceous rocks, Province of the Mesa Central,
1342 Mexico, and their formation from subcritical Si-rich fluids. Am. Mineral., 98, 977–
1343 985, 2013.

1344 Georgalas, G., and Liatsikas, N.: Die Historische entwickelung des Dafni-Ausbruches
1345 1925-1926. In Santorin, Der Werdegand eines Inselvulkans und sein Ausbruch
1346 1925-1928, V. 2 (ed. Reck, H.). Verlag von Dietrich Reimer, Berlin, 1–96 pp,
1347 1936.
1348 Glasby, G.P. and Schulz, H.D.: Eh, pH diagrams for Mn, Fe, Co, Ni, Cu and As under
1349 seawater conditions: application of two new types of the Eh, pH diagrams to the
1350 study of specific problems in marine geochemistry. Aquatic Geochem., 5, 227–
1351 248, 1999.
1352 Glasby, G.P., Papavassiliou, C.T., Mitsis, J., and Valsami-Jones, E.: The Vani
1353 manganese deposit, Milos island, Greece: A fossil stratabound
1354 Mn−Ba−Pb−Zn−As−Sb−W-rich hydrothermal deposit. Develop. Volcanol., 7,
1355 255–291, 2005.
1356 Gromet, L.P., Dymek, R.F., Haskin, L.A., and Korotev, R.L.: The North American
1357 shale composit: Its compilation and major trace element characteristics. Geochim.
1358 Cosmo. Acta, 48, 2469–2482, 1984.
1359 Gross, G.A.: A classification of iron-formation based on depositional Environments.
1360 Can. Min., 18, 215–222, 1980.
1361 Guilbaud, R., Poulton, S.W., Butterfield, N.J., Zhu, M., and Shields-Zou, G.A.: A
1362 global transition to ferruginous conditions during the early Neoproterozoic. Nat.
1363 Geosci. 8:466–470, 2015.
1364 Handley, K. M., Boothman, C., Mills, R. A., Pancost, R. D., and Lloyd, J. R.:
1365 Functional diversity of bacteria in a ferruginous hydrothermal sediment. ISME J.,
1366 4, 1193-1205, 2010.

Ernest Chi Fru 23/2/2018 20:15
Deleted: Han, C., Xiao, W., Su, B., Chen, Z., Zhang, X., Ao, S., Zhang, J., Zhang ,Z., Wan, B., Song, D., and Wang, Z.: Neoarchean Algoma-type banded iron formations from Eastern Hebei, North China Craton: SHRIMP U-Pb age, origin and tectonic setting. Precam. Res., 251, 212–231, 2014.

Hanert, H. H.: Bacterial and chemical iron oxide deposition in a shallow bay on Palaea Kameni, Santorini, Greece: microscopy, electron probe microanalysis, and photometry of in situ experiments. Geomicrobiol. J., 19, 317–342, 2002.

Hein, J. R., Stamatakis, M. G., and Dowling, J. S.: Trace metal-rich Quaternary hydrothermal manganese oxide and barite deposit, Milos Island, Greece. Applied Earth Science: Trans. Inst. Min. Metal. Section B., 109, 67–76, 2000.

Horwell, C.J., le Blond, S., Michnowicz, S. A. K. and Cressey, G.: Cristobalite in a rhyolitic lava dome: evolution of ash hazard. Bull. Volcanol. 72, 249-253, 2010.

Ichihara, K. and Fukubayashi, Y.: Preparation of fatty acid methyl esters for gas-liquid chromatography. J. Lipid Res., 51, 635–40, 2010.

James, H. L.: Sedimentary facies of iron-formation. Econ. Geol., 49, 235−293, 1954.

Johnson, C. M., Beard, B. L., and Roden, E. E.: The iron isotope fingerprints of redox and biogeochemical cycling in modern and ancient Earth. Ann. Rev. Earth Plan. Sci., 36, 457–493, 2008.

Kappler, A., Pasquero, C., and Newman, D.K.: Deposition of banded iron formations by anoxygenic phototrophic Fe(II)-oxidizing bacteria. Geology, 33, 865–868, 2005.

Kilias, S. P., Detsi, K., Godelitsas, A., Typas, M., Naden, J., and Marantos, Y.: Evidence of Mn-oxide biomineralization, Vani Mn deposit, Milos, Greece. In: Proceedings of the ninth biennial Meeting of the Society for Geology Applied to Mineral Deposits, Dublin, Ireland. Irish Assoc. Econ. Geol. 1069–1072 pp, 2007.

Kilias, S. P.: Microbial mat-related structures in the Quaternary Cape Vani manganese-oxide (-barite) deposit, NW Milos island, Greece. Soc. Sed. Geol. Sp. Pub., 101, 97–110, 2011.

Ernest Chi Fru 23/2/2018 20:16
Deleted: Hein, J. R. and Conrad, T. A.: Copper-nickel-rich, amalgamated ferromanganese crust-nodule deposits froms Shatsky Rise, NW Pacific. Geochem. Geophy. Geosyst., 13, Q10022, doi:10.1029/2012GC004286, 2012.

Ernest Chi Fru 23/2/2018 20:17
Deleted: Hickman, A.H.: Regional review of the 34236–3350 Ma Strelley Pool Formation, Pilbara Craton, Western Australia. Geol Survey West Australia, 215, 1-23, 2008.

Ernest Chi Fru 23/2/2018 20:18
Deleted: James, H. L.: Distribution of banded iron-formation in space and time. Dev. Pre. Geol., 6, 471–490, 1983.

Kilias, S. P., Chatzitheodoridis, E., and Lyon, I.: Molecular, chemical and morphological evidence for hematite biogenicity at the Quaternary Cape Vani Mn-(Ba-Fe) deposit, Milos, Greece. Bull. Geol. Soc., 47, 834-842, 2013a.

Kilias, P. S., Nomikou, P., Papanikolaou, D., Polymenakou, P. N., Godelitsas, A., Argyraki, A., Carey, S., Gamaletsos, P., Mertzimekis, T. J., Stathopoulou, E., Goettlicher, J., Steininger, R., Betzelou, K., Livanos, I., Christakis, C., Bell, K. C.: and Scoullos, M. New insights into hydrothermal vent processes in the unique shallow-submarine arc-volcano, Kolumbo (Santorini), Greece. Sci. Rep., 3, doi:10.1038/srep02421, 2013b.

Klein, C.: Some Precambrian banded iron-formations (BIFs) from around the world: Their age, geologic setting, mineralogy, metamorphism, geochemistry, and origins. Am. Min., 90, 1473–1499, 2005.

Kling, G. W., Evans, W. C., Tanyileke, G., Kusakabe, M., Ohba, T., Yoshida, Y., and Hell, J. V.: Degassing Lakes Nyos and Monoun: Defusing certain disaster. Proc. Natl. Acad. Sci. U.S.A., 102, 14185–14190, 2005.

Klein, C., and Beukes, N.J.: Time distribution, stratigraphy and sedimentologic setting, and geochemistry of Precambrian Iron Formation. In Schopf, J. W., and Klein, C.: The Proterozoic Biosphere: A multidisciplinary study, 139 – 146. Cambridge University Press, New York, 1992.

Konhauser, K. O., Planavsky, N. J., Hardisty, D. S., Robbins, L. J., Warchola, T. J., Haugaard, R., Lalonde, S. V., Partin, C. A., Oonk, P .B. H., Tsikos, H., and Lyons, T.W.: Iron formations: A global record of Neoarchaean to Palaeoproterozoic environmental history. Earth Sci. Rev., 172, 140-177, 2017.

Krapež, B., Barley, M. E., Pickard, A .L.: Hydrothermal and resedimented origins of the precursor sediments to banded iron formations: Sedimentological evidence

Ernest Chi Fru 23/2/2018 20:22

Deleted: Konhauser, K. O., Hamade, T., Riaswell., R., Morris, R. C., Ferris, F. G., Southam, G. and Canfied, D. E.: Could bacteria have formed the Precambrian banded iron formations? Geology, 12, 1097–1082, 2002.

from the early Palaeoproterozoic Brockman Supersequence of Western Australia. Sedimentology, 50, 979-1011, 2003.

Lalonde, K., Mucci, A., Quellet, A. and Gélinas, Y.: Preservation of organic matter in sediments promoted by iron. Nature, 483, 198–200, 2012.

Levett, A., Gagen, E., Shuster, J., Rintoul, L., Tobin, M., Vongsvivut, J., Bambery, K., Vasconcelos, P., and Southam, G.: Evidence of biogeochemical processes in iron duricrust formation. J. South. Am. Earth Sci., 71, 131–142, 2016.

Li, W., Czaja, A. D., Van Kranendonk, M. J., Beard, B. L., Roden, E. E., Johnson, C. M.: An anoxic, Fe(II)-rich, U-poor ocean 3.46 billion years ago. Geochim. Cosmo. Acta, 120, 65-79, 2013.

Liakopoulos, A., Glasby, G. P., Papavassiliou, C. T. and Boulegue, J.: Nature and origin of the Vani manganese deposit, Milos, Greece: an overview. Ore Geol. Rev., 18, 181–209, 2001.

Lü, D., Song, Q., and Wang, X.: Decomposition of algal lipids in clay-enriched marine sediment under oxic and anoxic conditions. Chin. J. Oceanogr. Limnol., 28, 131–143, 2010.

Marschik, R., Bauer, T., Hensler, A.-S., Skarpelis, N., and Hölzl, S. Isotope Geochemistry of the Pb-Zn-Ba(-Ag-Au) Mineralization at Triades-Galana, Milos Island, Greece. Res. Geol., 60, 335–347, 2010.

Maynard, J. B.: Chemistry of modern soils as a guide to interpreting Precambrian Paleosols. J. Geol., 100, 279–289, 1993.

Maynard, J. B.: The chemistry of manganese ores through time: a signal of increasing diversity of earth-surface environments. Econ. Geol., 105, 535–552, 2010.

McLennan, S.B.: Rare earth elements in sedimentary rocks. Influence of provenance and sedimentary processes. In: B.R. Lipin and G.A. McKay (Editors),

Ernest C 23/2/2018 13:35
Deleted: Lowe, D.R.: Sediment gravity flows: II. Depositional models with special reference to the deposits of high-density turbidity currents. J. Sed. Petrol., 52, 279–297, 1982. ... [2]

Geochemistry and Mineralogyof the Rare Earth Elements. Mineralogical Society of America, Washington, pp. 169-200, 1989.

Miall, A. D. Lithofacies types and vertical profile models in braided river deposits. Can. Soc. Pet. Geol. Mem., 5, 597–604, 1978.

Miall, A. D.: Architectural element analysis: a new method of facies analysis applied to fluvial deposits. Earth Sci. Rev., 22, 261e308, 1985.

Morris, R. V., Vaniman, D. T., Blake, D. F., Gellert, R., Chipera, S. J., Rampe, E. B., Ming, D. W., Morrison, S. M., Downs, R. T., Treiman, A. H., Yen, A. S., Grotzinger, J. P., Achilles, C. N., Bristow, T. F., Crisp, J. A., Des Marais, D. J., Farmer, J. D., Fendrich, K. V., Frydenvang, J., Gradd, T. G., Morookian, J-M., Stolper, E. M. and Schwenzer, S. P.: Silicic volcanism on Mars evidenced by tridymite in high-SiO2 sedimentary rock at Gale crater. Proc. Natl. Acad. Sci. U.S.A., 113, 7071–7076, 2016.

Mutti, E.: Turbidite Sandstones. Agip Spe. Pub., 275 pp, 1992.

Nesbitt, H. W. and Young, G. M.: Early Proterozoic climates and plate motions inferred from major element chemistry of lutites. Nature, 199, 715–717, 1982.

Nomikou, P., Papanikolaou, D., Alexandri, M., Sakellariou, D., and Rousakis, G.: Submarine volcanoes along the Aegean volcanic arc. Tectonophysics, 597–598, 123–146, 2013.

Nomikou, P., Parks, M. M., Papanikolaou, D., Pyle, D. M., Mather, T. A., Carey, S., Watts, A. B., Paulatto, M., Kalnins, M.L., Livanos, I., and Bejelou, K.: The emergence and growth of a submarine volcano: The Kameni islands, Santorini (Greece). Geo. Res. J., 1, 8–18, 2014.

Ernest Chi Fru 23/2/2018 20:29
Deleted: Nijman, W., De Bruin, K., and Valkering, M.: Growth fault control of early Archean cherts, barite mounds, and chert-barite veins, North Pole Dome, Eastern Pilbara, Western Australia. Precam. Res., 88, 25–52, 1998. ... [3]

Ozawa, A., Ueda, A., Fantong, W. Y., Anazawa, K., Yoshida, Y., Kusakabe, M., Ohba, T., Tanyileke, G., and Hell, J.V. Rate of siderite precipitation in Lake Nyos, Cameroon. Geol. Soc. London Sp. Pub., 437, doi.org/10.1144/SP437.13, 2016.

Papanikolaou, D., Lekkas, E., and Syskakis, D.: Tectonic analysis of the geothermal field of Milos Island. Bull. Geol. Soc. Greece, 24, 27–46, 1990.

Papavassiliou, K., Voudouris, P., Kanellopoulos, C., Glasby, G., Alfieris, D., and Mitsis, I.: New geochemical and mineralogical constraints on the genesis of the Vani hydrothermal manganese deposit at NW Milos island, Greece: Comparison with the Aspro Gialoudi deposit and implications for the formation of the Milos manganese mineralization. Ore Geol., 80, 594–611, 2017.

Paulmier, A., Ruíz-Pino, D., and Garçon, V.: The oxygen minimum zone (OMZ) off Chile as intense source of CO2 and N2O, Cont. Shelf. Res., 28, 2746–2756, 2008.

Paulmier, A., Ruiz-Pino, D., and Gaçon, V.: CO_2 maximum in the oxygen minimum zone (OMZ). Biogeosciences, 8, 239–252. doi:10.5194/bg-8-239-2011, 2011.

Percoits, E., Gingras, M. K., Barley, M. E., Kapper, A., Posth, N. R., and Konhauser, K.O.: Petrography and geochemistry of the Dales Gorge banded iron formation: Paragenetic sequence, source and implications for palaeo-ocean chemistry. Pre. Res., 172, 2009.

Pichler, T. and Dix, G. R. Hydrothermal venting within a coral reef ecosystem, Ambitle Island, Papua New Guinea. Geology, 50, 435–438, 1996.

Pichler, T. and Veizer, J.: Precipitation of Fe(III) oxyhydroxide deposits from shallow-water hydrothermal fluids in Tutum Bay, Ambitle Island, Papua New Guinea. Chem. Geol., 162, 15–31, 1999.

Ernest Chi Fru 23/2/2018 20:30
Deleted: Ossa, F. O., Hofmann, A., Vidal, O., Kramers, J. D., Belyanin, G. and Cavalazzi, B.: Unusual manganese enrichment in the Mesoarchean Mozaan Group, Pongola Supergroup, South Africa. Pre. Res., 281, 414-433, 2016.

Ernest Chi Fru 23/2/2018 20:31
Deleted: Papike, J. J., Karner, J. M., Shearer, C. K. and Burger, P. V.: Silicate mineralogy of martian meteorites. Geochim. Cosmochim. Acta, 73, 7443–7485, 2009.

Pichler, T. and Veizer, J. The precipitation of aragonite from shallow-water hydrothermal fluids in a coral reef, Tutum Bay, Ambitle Island, Papua New Guinea. Chem. Geol., 207, 317–45, 2004.

Planavsky, N., Rouxel, O., Bekker, A., Shapiro, R., Fralick, P., and Knudsen, A.: Iron-oxidizing microbial ecosystems thrived in late Paleoproterozoic redox-stratified oceans. Earth Plan. Sci. Letts., 286, 2307–242, 2009.

Planavsky, N. J., Bekker, A., Rouxel, O. J., Kamber, B., Hofmann, A., Knudsen, A. and Lyons T. W.: Rare earth element and yttrium compositions of Archean and Paleoproterozoic Fe formations revisited: New perspectives on the significance and mechanisms of deposition. Geochim. Cosmo. Acta, 74, 6387–6405, 2010.

Plimer, I. Milos Geologic History. Koan Publishing House, Athens, Greece. 261 pp, 2000.

Poulton, S.W., and Canfield, D.E.: Development of a sequential iron extraction procedure for iron: implications for iron partitioning in continentally derived particles. Chem. Geol. 2014, 209–221, 2005.

Poulton, S.W. and Canfield, D.E.: Ferruginous conditions: A dominant feature of the ocean through Earth's history. Elements. 7, 107–112, 2011.

Preuß, A., Schauder, R., Fuchs, G., and Stichler W.: Carbon isotope fractionation by autototrophic bacteria with three different CO_2 fixation pathways. Zeitschrift für Naturforschung C., 44, 397–402, 1989.

Rancourt, D. G., Fortin, D., Pichler, T., and Lamarche, G.: Mineralogical characterization of a natural very As-rich hydrous ferric oxide coprecipitate formed by mixing of hydrothermal fluid and sea water. Am. Min., 86, 834–851, 2001.

Ernest Chi Fru 23/2/2018 20:38

Deleted: Ramos, E., Marzo, M., de Gibert, J. M., Tawengi, K. S., Khoja, A. A., and Bolatti, N. D.: Stratigraphy and sedimentology of the middle Ordovician Hawaz formation (Murzuq Basin, Libya). AAPG bull., 90, 1309-1336, 2006.

Rasmussen, B., Meier, D. B., Krapež. B., and Muhling, J. R.: Iron silicate microgranules as precursor sediments to 2.5-billion-year-old banded iron formations. Geology, 41, 435–438, 2013.

Rasmussen, B., Krapež, B., and Meier, D. B. Replacement origin for hematite in 2.5 Ga banded iron formation: Evidence for postdepositional oxidation of iron-bearing minerals. Geol. Soc. Am. Bull., 126, 438–446, 2014.

Riedel, T., Zak, D., Biester, H., and Dittmar, T.: Iron traps terrestrially derived dissolved organic matter at redox interfaces. Proc. Nat. Acad. Sci. U.S.A., 110, 10101–10105, 2013.

Robbins, E. I., Kourtidou-Papadeli, C., Iberall, A. S., Nord, Jr, G. L. and Sato, M.: From Precambrian Iron-Formation to Terraforming Mars: The JIMES Expedition to Santorini. Geomicrobiol. J., 33, 630–645, 2016.

Roy, S.: Manganese Mineralization: Geochemistry and mineralogy of terrestrial and marine deposits. Geol. Soc. Spe. Pub., 119, 5–27, 1997.

Roy, S.: Sedimentary manganese metallogenesis in response to the evolution of the Earth system. Earth-Sci. Rev., 77, 273–305, 2006.

Rudnick, R. and Gao, S. Composition of the continental crust. In: Treatise on Geochemistry, vol. 3. Elsevier–Pergamon, Oxford, 1–64 pp, 2003.

Shanmugam, G.: Submarine fans: a critical retrospective (1950–2015). J. Palaeogeogr., 5, 110-184, 2016.

Schwertmann, U. and Murad, E. Effect of pH on the formation of goethite and hematite from ferrihydrite. Clay Clay Min., 31, 277–284, 1983.

Shuster, D. L., Farley, K. A., Vasconcelos, P. M., Balco, G., Monteiro, H. S., Waltenberg, K., and Stone, J. O. Cosmogenic 3 He in hematite and goethite from

1590 Brazilian “canga” duricrust demonstrates the extreme stability of these surfaces.
1591 Earth Plan. Sci. Lett., 329, 41–50, 2012.
1592 Sigurdsson, H., Carey, S., Alexandri, M., Vougioukalakis, G., Croff, K., Roman, C.,
1593 Sakellariou, D., Anagnostou, C., Rousakis, G., Loakim, C., Goguo, A., Ballas, D.,
1594 Misaridis, T., and Nomikou, P. Marine investigations of Greece’s Santorini
1595 volcanic field. EOS Trans. Am. Geophy. Union, 87, 337–342, 2006.
1596 Simonson, B. M.: Sedimentological constraints on the origins of Precambrian iron-
1597 formations. Geol. Soc. Am. Bull., 96, 244–252, 1985.
1598 Simonson, B. M. and Hassler, S. W.: Was the deposition of large Precambrian iron
1599 formations linked to major marine transgressions? The J. Geol., 104, 665−676,
1600 1996.
1601 Skarpelis, N. and Koutles, T.: Geology of epithermal mineralization of the NW part of
1602 Milos Island, Greece. In Proceedings of the 5th International Symposium on
1603 Eastern Mediterranean Geology. (eds. Chatzipetros, A. & Pavlides S). School of
1604 Geology, Aristotelian University of Thessaloniki, Thessaloniki, Greece. pp. 1449–
1605 1452, 2004.
1606 Smith, A.J.B., Beukes, N.J., and Gutzmer, J.: The Composition and depositional environments of
1607 Mesoarchean Iron Formations of the West Rand Group of the Witwatersrand Supergroup, South
1608 Africa. Econ. Geol. 108, 111-134, 2013.
1609 Sperling, E.A., Wolock, C.J., Gill, B.C., Kunzmann, M., Halverson, G.P., Macdonald,
1610 F.A., Knoll, A.H., and Johnston D.T.: Statistical Analysis of Iron Geochemical
1611 Data Suggests Limited Late Proterozoic Oxygenation. Nature 523, 451–454, 2015.
1612 Stewart, A. L. and Mcphie, J.: Facies architecture and Late Ploicene – Pleistocene
1613 evolution of a felsic volcanic island, Milo, Greece. Bull. Volcanol. 68, 703–726,
1614 2006.

Ernest C 23/2/2018 15:28
Deleted: Simonson, B. M.: Origin and evolution of large Precambrian iron formations. Geol. Soc. Am., 370, 231−244, 2003. ... [4]

Ernest Chi Fru 26/2/2018 10:50
Formatted: EndNote Bibliography, Indent: Left: 0 cm, Hanging: 0,5 cm, Don't add space between paragraphs of the same style, Line spacing: double

Sun, S., Konhauser, K. O., Kappler, A., and Li, Y.-L.: Primary hematite in Neoarchean to Paleoproterozoic oceans. GSA Bull., 127, 850–861, 2015.

Stüben, D. and Glasby, G.P.: Geochemistry of shallow submarine hydrothermal fluids from Paleohori Bay, Milos, Aegean Sea. Exp. Min. Geol., 8, 273–287, 1999.

Swamy, V., Saxena, S. K., Sundman, B., and Zhang, J.: A thermodynamic assessment of silica phase diagram. J. Geophys. Res. Solid Earth, 99, 11787–11794, 1994.

Taylor, J., and Parkes, R. J.: The cellular fatty-acids of the sulfate-reducing bacteria, Desulfobacter sp., Desulfobulbus sp. and Desulfovibrio desulfuricans. J. Gen. Microbiol., 129, 3303–3309, 1983.

Tice, M. M. and Lowe, D. R.: The origin of carbonaceous matter in pre-3.0 Ga greenstone terrains: A review and new evidence from the 3.42 Ga Buck Reef Chert. Earth Sci. Rev., 76, 259–300, 2006.

Tiodjio, R. M., Sakatoku, A., Nakamura, A., Tanaka, A., Fantong, W. Y., Tchakam, K. B., Tanyileke, G., Ohba, T., Hell, V. J., Kusakabe, M., Nakamura, S., and Ueda, A.: Bacterial and archaeal communities in Lake Nyos (Cameroon, Central Africa). Sci. Rep., 4, 6151, DOI: 10.1038/srep06151, 2014.

Trendall, A.F.: The significance of iron-formation in the Precambrian stratigraphic record. Int. Assoc. Sed. Spe. Pub., 33, 33–66, 2002.

Tsikos, H., Mathews, A., Erel, Y., and Moore, J.M.: Iron isotopes constrain biogeochemical redox cycling of iron and manganese in a Palaeoproterozoic stratified basin. Earth Planet. Sci. Lett., 298, 125–134, 2010.

van Hinsbergen, D. J. J., Snel, E., Garstman, S. A., Mărunţeanu, M., Langereis, C. G., Wortel, M. J. R., and Meulenkamp, J. E.: Vertical motions in the Aegean volcanic arc: evidence for rapid subsidence preceding volcanic activity on Milos and Aegina. Mar. Geol., 209, 329–345, 2004.

Ernest Chi Fru 23/2/2018 20:46
Deleted: Stiegler, M. T., Lowe, D. R., and Byerly, G. R.: Abundant pyroclastic komatiitic volcanism in the 3.5-3.2 Ga Barberton greenstone belt, South Africa. Geology, 36, 779–782, 2008.

Ernest C 23/2/2018 13:20
Deleted: Trower, E. J. and Lowe, D. R.: Sedimentology of the ~3.3 Ga upper Mendon Formation, Barberton Greenstone Belt, South Africa. Pre. Res., 281, 473–494, 2016.

Varnavas, S. P. and Cronan, D. S.: Submarine hydrothermal activity off Santorini and Milos in the Central Hellenic Volcanic Arc: A synthesis. Chem. Geol., 224, 40–54, 2005.

Weber, K. A., Achenbach, L. A., and Coates, J. D.: Microorganisms pumping iron: anaerobic microbial iron oxidation and reduction. Nat. Rev. Microbiol., 4, 752–64, 2006.

Table 1. Table 1. Results of X-Ray Radiation (XRD) analysis showing major mineralogical compositions. NFIF (non-fossiliferous iron formation) and MFIF (microfossiliferous iron formation), respectively.

Mineral phase	MFIF1	MFIF2	MFIF3	Fe-rich NFIF2A	Si-rich NFIIF2B	Fe-rich NFIF2C	Si-rich NFIFD	Fe-rich NFIF2E	Fe-rich NFIF2F
Hematite	+	+	-	+	+	+	+	+	+
Quartz	+	+	+	-	-	-	-	-	-
Sanidine	-	-	-	+	+	+	+	+	+
Tridymite	-	-	-	-	+	+	+	+	+
Cristobalite	-	-	-	+	-	-	-	-	-
Cryptomelane	-	-	+	-	-	-	-	-	-

Table 2. Stable isotope results. Letters A-F on the NFIF samples represent respective bands of the sawn rock in Figure 7E.

Sample	$\delta^{13}C_{org}$ vs PDB (‰)	C_{org} (%)	$\delta^{15}N$ vs air (‰)	N (%)	$\delta^{34}S$ vs CDT (‰)	S (%)
Fe-rich NFIF2A	-25,63	0,061	nd	0,023	nd	0,01
Si-rich NFIF2B	-25,03	0,109	nd	0,017	nd	0,02
Fe-rich NFIF2C	-24,45	0,068	nd	0,013	nd	0,02
Si-rich NFIF2D	-25,04	0,076	nd	0,015	nd	0,02
Fe-rich NFIF2E	-25,19	0,042	nd	0,009	nd	0,01
Si-rich NFIF2F	-25,49	0,050	nd	0,012	nd	0,03
MFIF1	-25,49	0,087	nd	0,017	nd	0,01
MFIF2	-26,25	0,046	nd	0,005	nd	nd
MFIF3	-25,69	0,041	nd	0,006	nd	nd

ND, Not detected

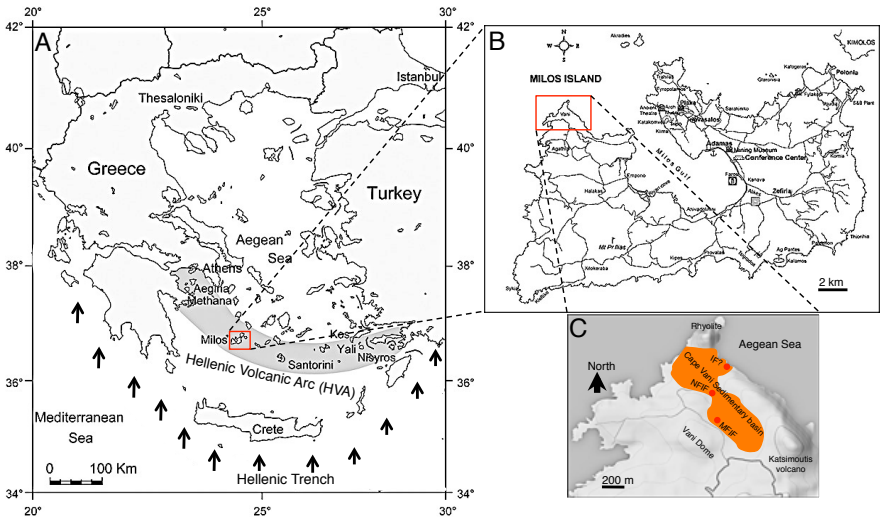

Fig. 1. Geological map of Milos (redrawn from Marschik et al., 2010). (A), Geotectonic map showing the position of Milos Island, along the Hellenic Volcanic

Arc (HVA). Arrows indicate the direction of subduction of the African plate underneath the Euroasian plate. (B) Milos Island. (C), The Milos iron formation is located in the 8-shaped Cape Vani sedimentary basin (CVSB). At least two IFs are present in the CVSB. These are made up of a non-fossiliferous IF (NFIF) at the juncture between the two large sedimentary basins and a microfossiliferous iron formation (MFIF) located at the SW margin in the second basin. A potential third IF (IF?) is located NE, close to the present day Aegean Sea. It is however not certain if this deposit is part of the NFIF or not, because of the open mining pit separating the two.

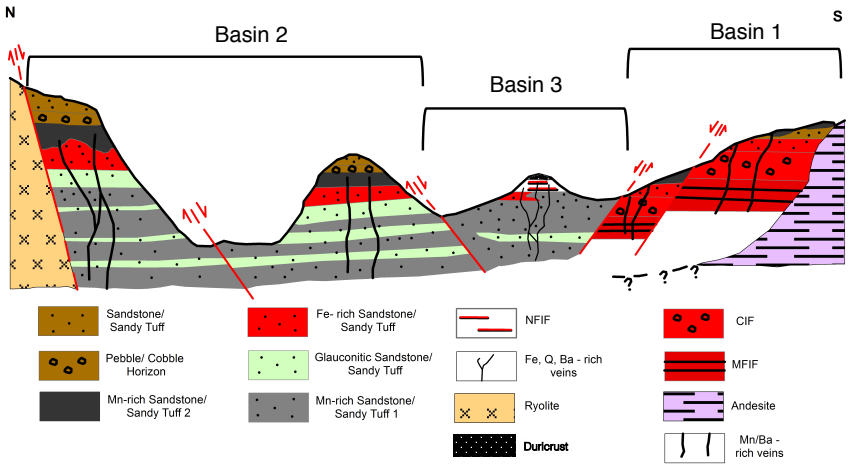

Fig. 2. Generalized schematic north-south geologic cross section through the ~1 km long CVSB showing interpreted geology, relationships between the main lithofacies, main fault locations, the iron and manganese formations, in support of a proposed three-basin hypothesis. Not drawn to scale. Four types of iron-rich sedimentary rocks occur in the CVSB. These include the iron-rich sandstones, the iron-Mn-rich sandstones, the conglomerate hosted iron formation (CIF) and the MFIF and NFIF formations that are depositionally and chemically distinct from the sandstone deposits.

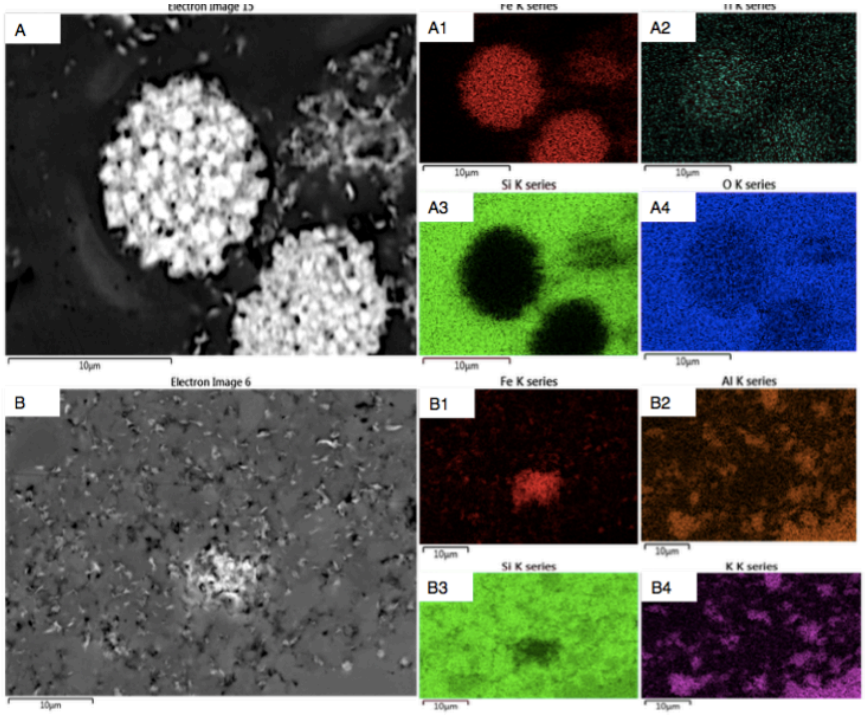

Fig. 3. EDS-electron image showing different Fe-rich mineral phases in a Si-rich matrix from the MFIF. The bright colours correspond to the analysed elements. (A), framboidal hematite particles. A1-A4, different element compositions associated with framboidal particles in panel A. (B), Dispersed fluffy Fe-rich mineral grains. B1-B4, corresponding elements associated with the micrograph in panel A.

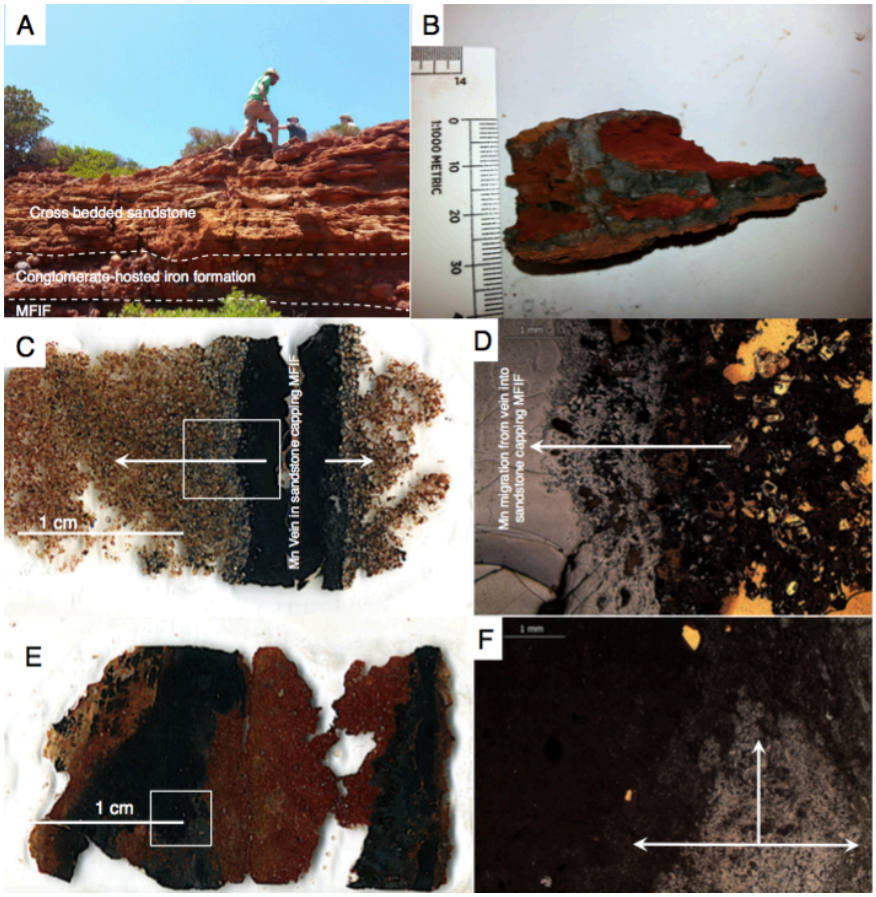

1761

1762 Fig. 4. Sedimentary profile, thin section scans and optical microscope images of the
1763 MFIF. (A), Field photo showing the sedimentary profile of the MFIF chacterized by
1764 the overlying sandstone cap. (B), Photograph showing black diffused Mn-rich bands
1765 near the base of the MFIF. (C), Scanned image of thin section showing a black Mn-
1766 rich vein in the overlying MFIF sandstone showing a gradient of Mn migrating into
1767 the sandstone matrix (white arrows). (D), Light microscopy images showing details in
1768 panel C. (E), Scanned image of an MFIF thin section showing black Mn bands
1769 migration into a red iron-rich background. (F), Amplified light microscope image
1770 showing gray Mn layers migrating into a black Fe-rich matrix. White arrows show
1771 direction of movement. Boxes in C and E are amplified in D and F.
1772

1773

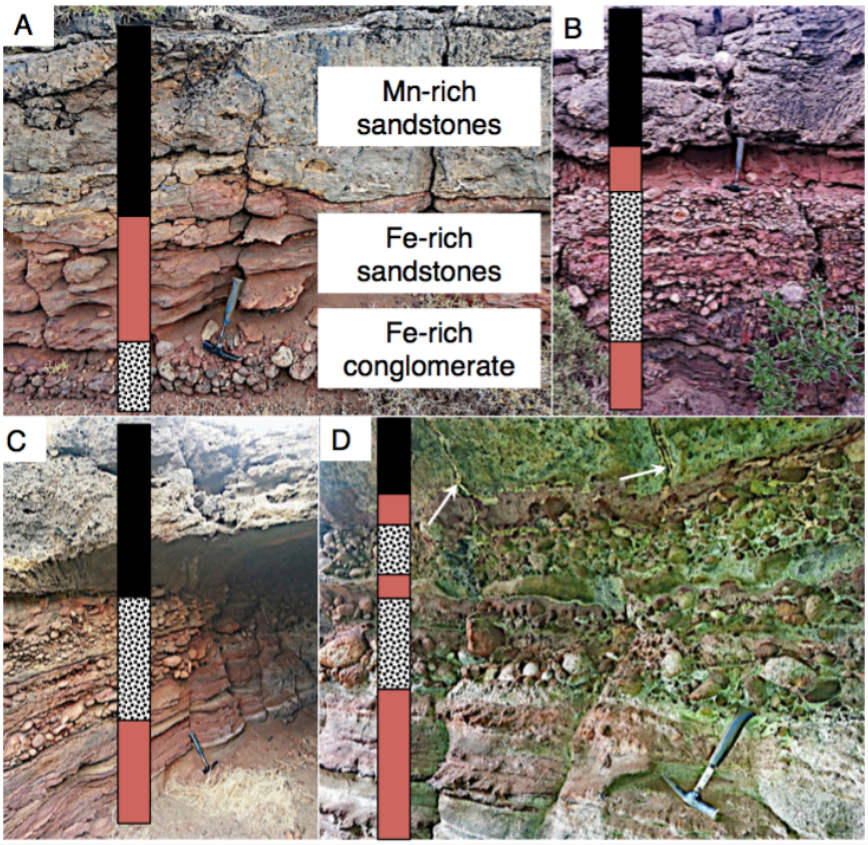

Fig. 5. Sedimentary sequence overlying the MFIF, consisting of thin (< 0.5 m) polymictic andesite-dacite cobble-pebble, and sandstone-sandy tuff pebble, and Fe-rich conglomerate facies overlain by thinly laminated Fe-rich sandstone beds. This vertical sequence is interpreted to represent a progressively deeper water environment deepening-upward sequence (A) as a result of sea level rise due to tectonic subsidence. The multiple cycles shown in panels B-D signify several potential episodes or sea level rise. Arrows in panel D showing hydrothermal feeder veins feeding the overlying layers. The sequence is overlain by a thin package of parallel and cross-bedded Mn-sandstone cap.

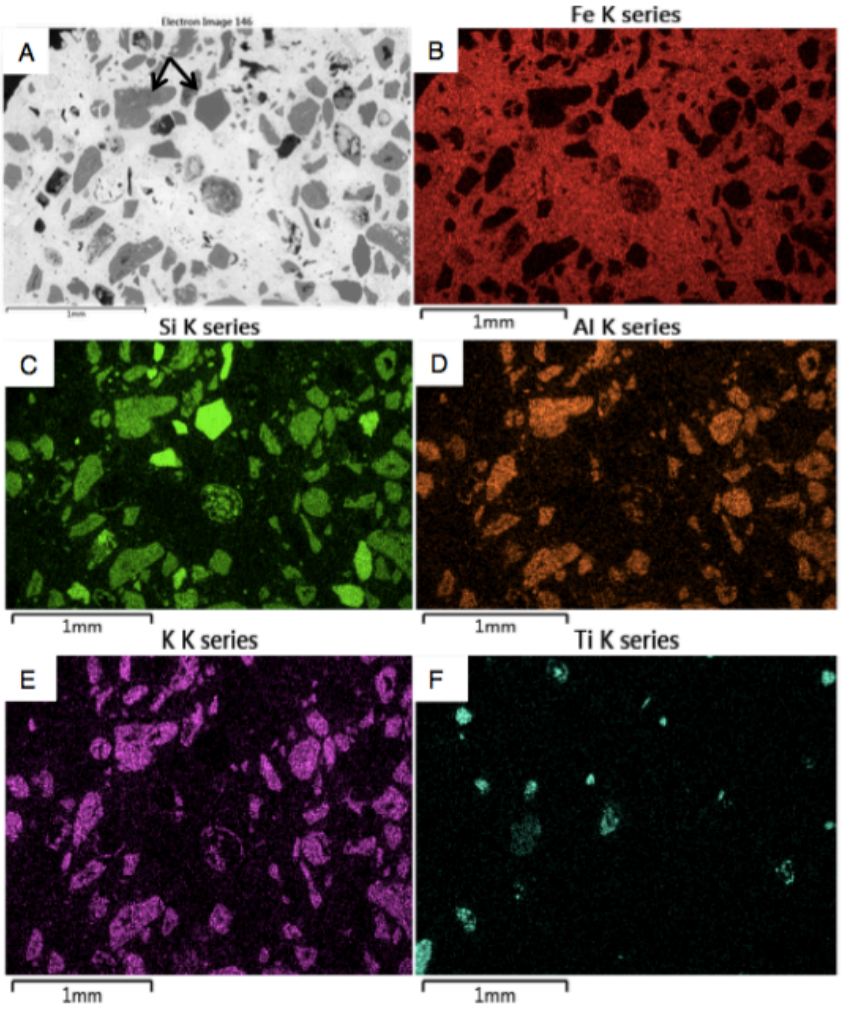

1786

1787 Fig. 6. Scanning electron microscope electron image of the volcaniclastic (K-
1788 feldspar)/ iron-rich sandstone conglomerate overlying the MFIF.
1789

1790

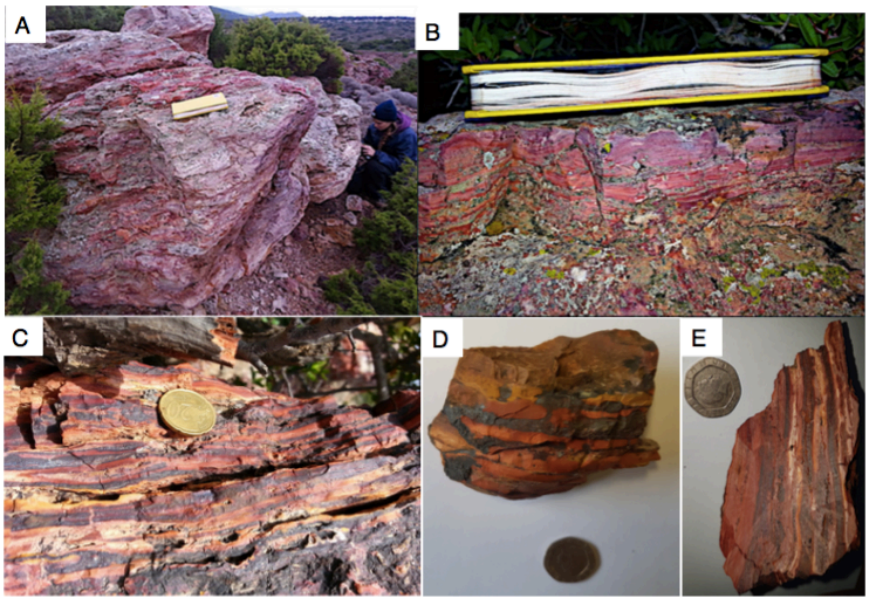

Fig. 7. Typical NFIF banded iron rocks. (A-C), Field photographs. (D), Handheld banded Fe sample. (E), Sawn NFIF sample with laminated Fe-rich bands alternating with Si-rich bands.

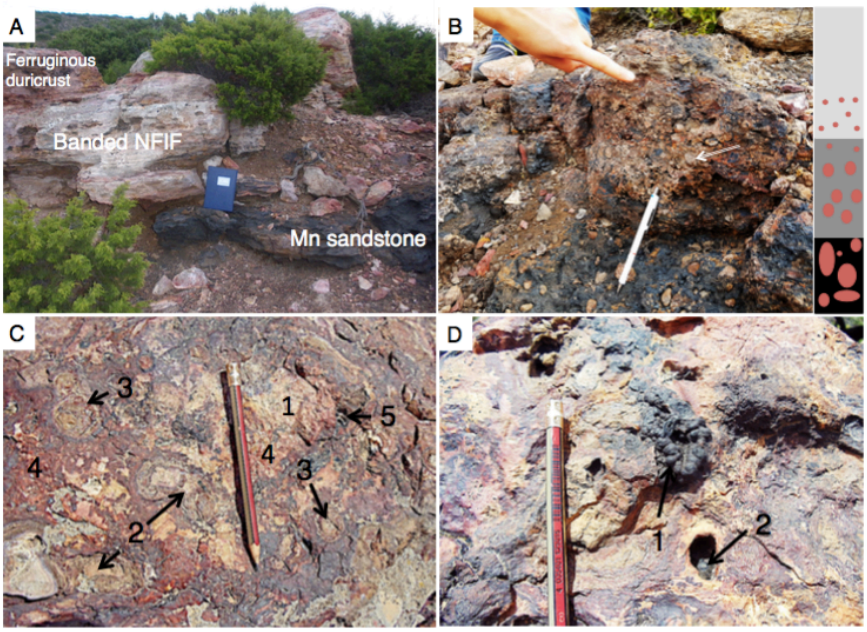

Fig. 8. Field sedimentology and stratigraphy of Section B sequence containing the NFIF. (A), Sharp boundary between lower Mn sandstone and unconformably overlying NFIF capped by a ferruginous duricrust. (B), Sandstone-sandy tuff pebble to gravel conglomerate lag facies, showing an upward fining character and bored clasts (black), locally overlies the Mn sandstone and capped by a sharp erosional contact with the overlying NFIF. The tip of the pen (7 cm long) rests on late blue-black Mn oxide overprint. (C), Ferruginous duricrust that comprises lithic fragments composed of (1) Fe-nodules (2) and Fe-concretions (3) in a hematite-rich matrix (4). (D), Matrix dissolution resulting in vermiform Mn nodules (1) and cavity black Mn oxide (2) infillings, post-dating the ferruginous duricrust formation.

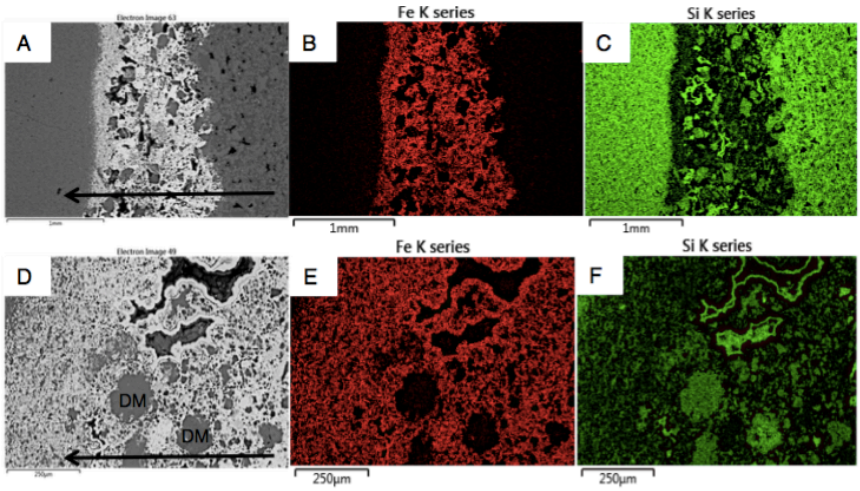

Fig. 9. EDS-electron image showing major elemental composition of typical Fe bands alternating with Si-rich layers in the NFIF. Volcaniclastic detritus mostly present in the Fe-rich bands, suggests precipitation during active submarine volcanism. To the contrary, the Si-rich bands are composed of more fine-grain, signifying deposition during periods of minimal volcanic activity. Arrows in panels (A) and (B) depict the direction of sedimentation, which was often seen to proceed from an Fe-rich matrix mixed with large grains of volcaniclastic detritus (DM) to one composed essentially of very fine-grained Fe particles before transitioning into the very fine-grained Si-rich layer. An upward fining of the volcaniclastic particles in the Fe-rich layers transitions from one made up of volcaniclastic debris and hematite, to a mainly thin hematite-rich horizon at the top of this mixed layer (see supplementary Figs 8-11 for details). This concurrent occurrence of volcaniclast and Fe oxides and the upward fining nature of the Fe-rich layers, suggest the release and oxidation of Fe(II) coincided with the settling of hydrothermal debris resulting from the introduction of enormous amount of reduced materials into the water column (Bekker et al., 2010). The iron-rich layer ceased forming as hydrothermal/volcanic release of Fe subsided, followed by deposition of the Si-rich layer. This repetitive cycle of events is observed for tens of metres laterally and vertically, stressing that the layers are not single isolated or post-depositional replacement events, but chemical precipitates that sequentially sedimented out of the water column. Red colour in Panels (B) and (C) depict Fe and green in panels (C) and (F), Si.

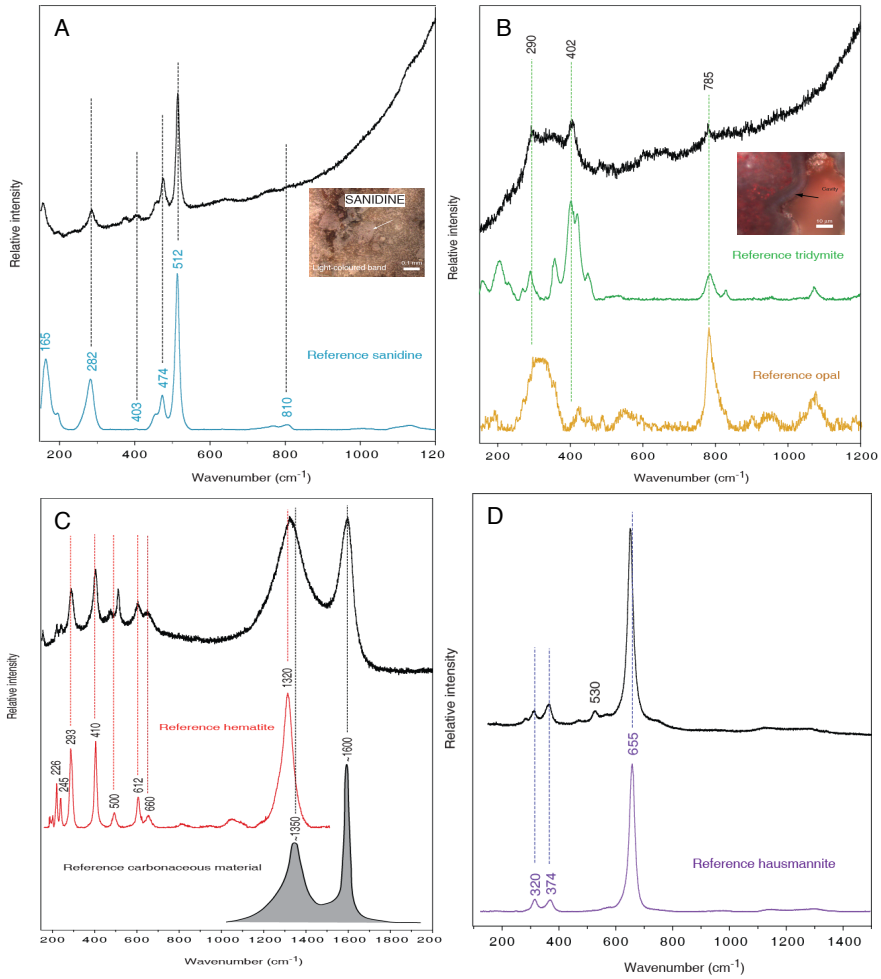

1834

1835 Fig. 10. Raman spectroscopy of the Fe- and/or Si-rich bands from NFIF.

1836

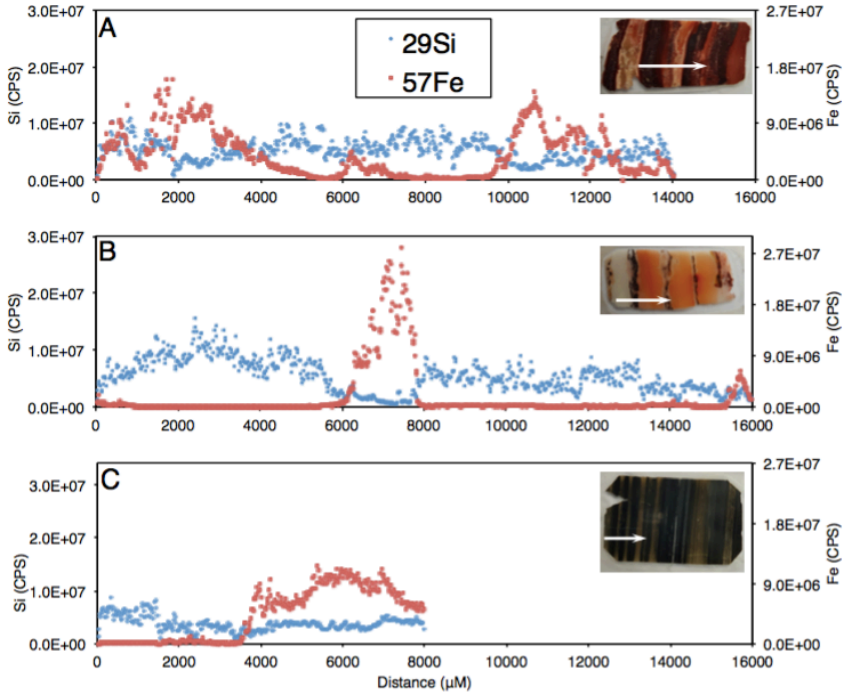

1837

1838 Fig. 11. Fluctuation in Si and Fe content measured by in situ laser ablation ICP-MS
1839 analysis. (A), Milos BIF-type rock with evenly distributed Si and iron rich bands. (B),
1840 Milos BIF type rock with large Si bands (whitish-brownish strips) and narrow Fe-rich
1841 bands (dark strips). (C), An example for the 2.5 Ga Kuruman BIF. Insets are analyzed
1842 thin sections. For scale, each thin section is ≈3.3 cm long. White arrow on thin section
1843 indicates analyzed area.
1844

1845

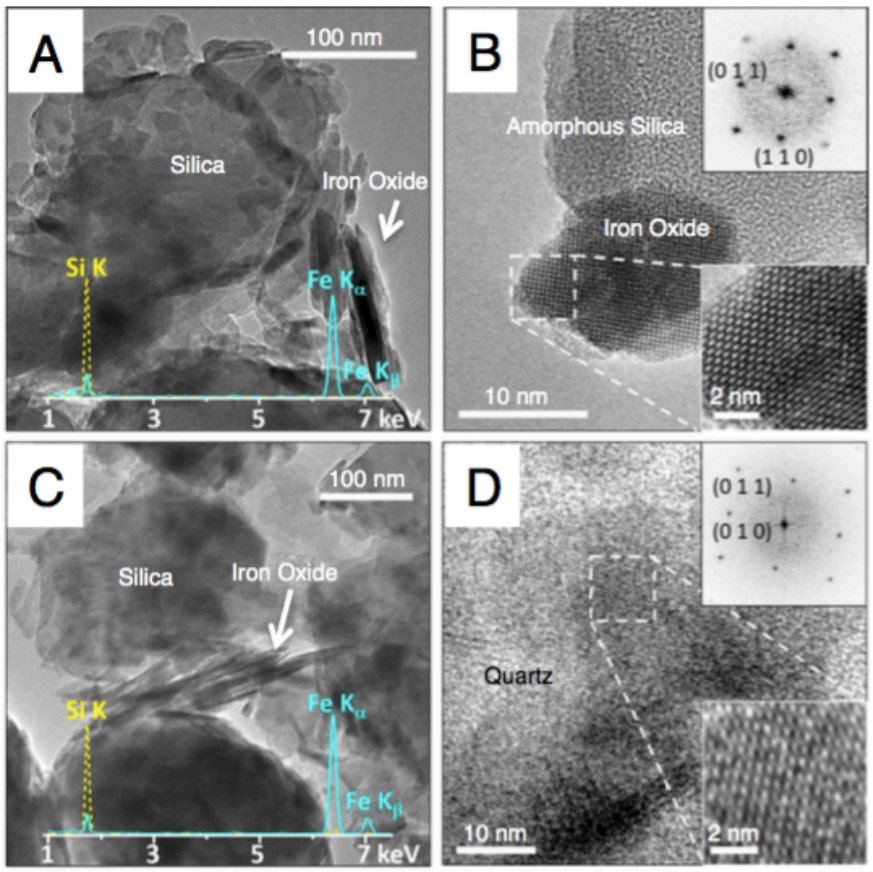

Fig. 12. TEM characterization of an NFIF and MFIF specimen. (A) lower magnification MFIF TEM-BF image. (B) High resolution images of NFIF showing amorphous Si and iron oxide crystallline lattice structures. Insets highlight a hematite particle viewed from the [1-11] axis (Rhombohedral lattice). (C) Lower magnification MFIF TEM-BF image. (D) High resolution images of MFIF showing crystalline quartz and iron oxide crystallline lattice structures. Insets in (D) show a quartz crystal viewed from the [100] axis. Both samples contain silica with a few hundred nm particle size, and smaller needle-like iron oxide particles. Spectral lines in panels (A) and (C) are X-ray Energy Dispersive elemental profiles of the individual Fe and Si mineral phases.

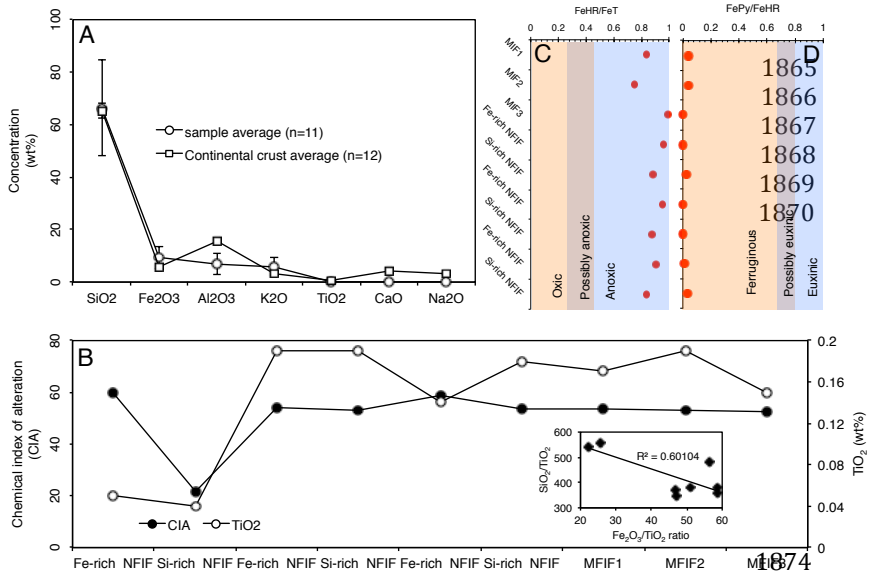

Fig. 13. Bulk average concentrations of major trace elements, chemical weathering indices and reconstructed redox depositional conditions for typical MFIF and the Fe/Si-rich NFIF ands for the sawn rock sample in Figure 7E. (A), Relationship between average major trace element content and average continental crust (Rudnick and Gao, 2003). (B), Chemical Index of Alteration (CIA). Inset, relationship between SiO_2 and Fe_2O_3. (C) Highly reactive Fe (FeHR) to Total Fe ratio (FeT). (D) Pyrite to FeHR ratio.

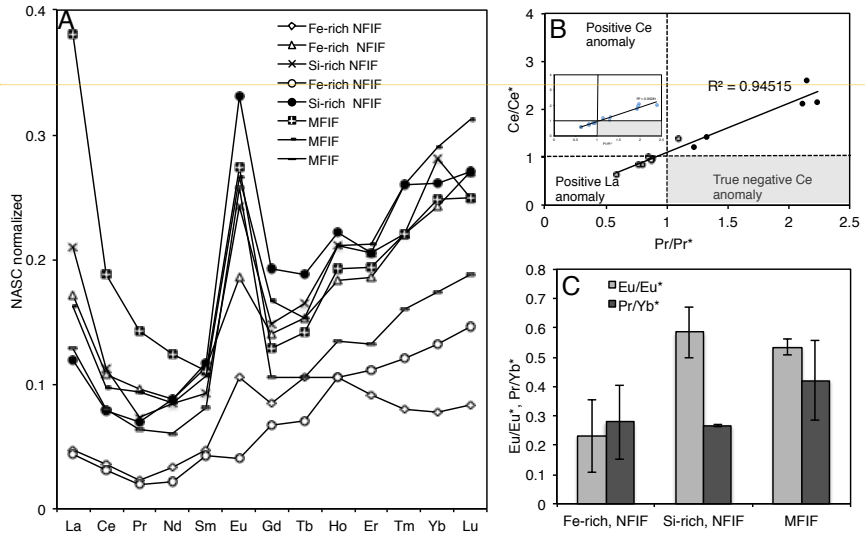

Fig. 14. Rare earth element (REE) distribution in samples and calculated Ce and Eu anomalies. (A), NASC normalized REE distribution in various rock facies. (B), Ce and Eu anomalies. (C), Eu anomalies and light REE (LREE) vs. heavy REE (HREE). Similar trends were reproduced when REE data were normalized with the Post Archean Australian Shale standard (McLennan, 1989; Bau and Dulski, 1986). This is exemplified by the insert in B.

Unknown
Formatted: Font:(Default) Times New Roman, Font color: Text 1

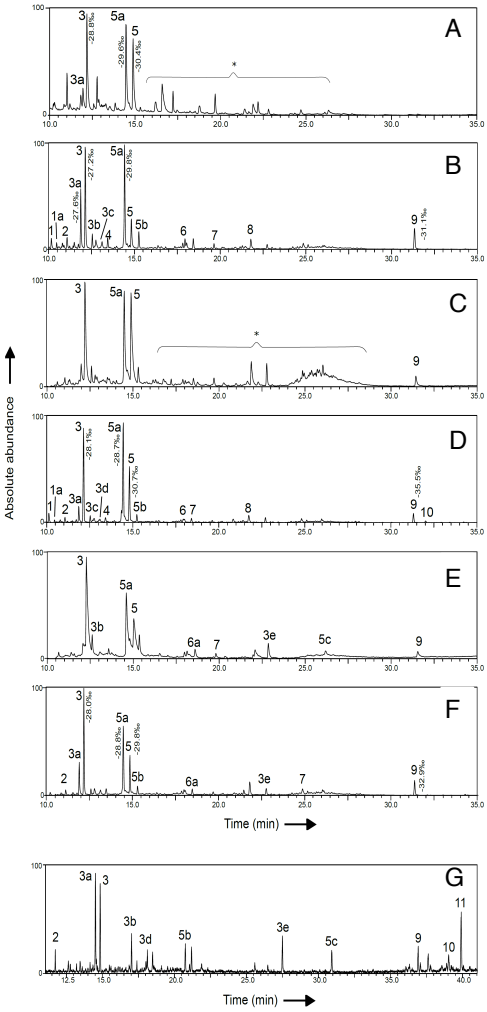

Fig. 15. GC/MS chromatogram sections of total lipid extracts of the BIF (A-F) for bands excised from the sawn rock in Figure 7E. Panel G illustrates a total lipid extract of modern sediment from the Milos basin. Values beside peaks indicate the lipid-specific $\delta^{13}C$ values in per mil. Because of the low intensity of the lipids recovered, it was not possible to obtain $\delta^{13}C$ values specific for all peaks. Peaks are annotated as; FAME = fatty acid methyl ester; Me = methyl group; TMS = trimethylsilyl; TMSE = trimethylsilyl ester. (1) $C_{14:0}$ FAME, (1a) $C_{14:0}$ 13Me FAME, (2) $C_{15:0}$ FAME, (3) $C_{16:0}$ FAME, (3a) $C_{16:9}$ FAME, (3b) C16:0 TMS, (3c) 10Me $C_{16:0}$ FAME, (3d) $C_{16:9}$ FAME, (3e) $C_{16:0}$ TMSE, (4) $C_{17:0}$ TMS, (5) $C_{18:0}$ FAME, (5a) $C_{18:9}$ FAME, (5b) $C_{18:0}$ TMS, (5c) $C_{18:0}$ TMSE, (6) $C_{19:0}$ FAME, (6a) $C_{19:0}$ 18Me TMS, (7) $C_{21:0}$ TMS, (8)

$C_{22:0}$ TMS, (9) Cholesterol TMS, (10) Stigmasterol TMS, (11) beta-Sitosterol (*) contaminants (e.g., phthalates).

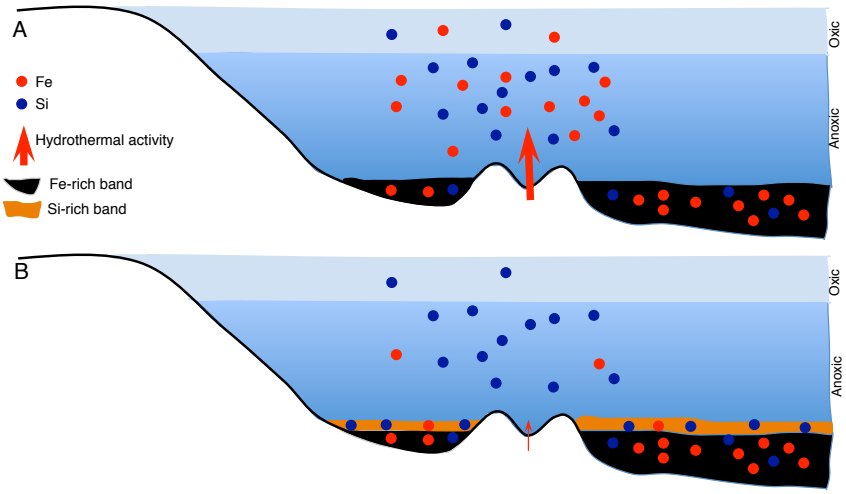

1933

1934 Fig. 16. Conceptual model showing the mechanism of band formation in the NFIF
1935 related to changes in the intensity of hydrothermal activity and chemical oxidation of
1936 Fe(II) to Fe(III) in the water column, inferred directly from our data. See Chi Fru et
1937 al. (2013) for a biological model for the formation of the MFIF.